A Numerical Study of the Stability of a Stratified Mixing Layer

by

David A. Collins

A thesis submitted to the Faculty of Graduate Studies and Research in partial fulfillment of the requirements for the degree of Doctor of Philosophy.

Department of Mathematics
McGill University
Montreal, Canada

September, 1982

ABSTRACT

Using a two-dimensional nonlinear numerical simulation of a (viscous) stratified shear layer, strong instabilities resulted from the resonant interaction of a long linearly neutrally stable wave and the corresponding fastest growing wave. This linearly fastest growing wave, with optimal initial conditions, grows initially at a rate five times that predicted by linear theory. With other initial conditions, the linearly fastest growing wave may actually decay. The possibility of this type of interaction is suggested by the weakly nonlinear theory (cf. Maslowe, 1977). This coupled system of fourth order nonlinear partial differential equations was solved using a modified pseudo-spectral scheme for the spatial variables, incorporating the use of fast Fourier transforms to calculate spatial derivatives, and a second order Adams-Bashforth scheme for the temporal derivatives.

RÉSUMÉ

Dans cette étude, en utilisant une simulation numérique nonlinéaire à deux dimensions d'une couche stratifiée, décollée et visqueuse, on obtint des résultats intéressants à partir des cas correspondant à l'interaction résonnante d'une onde longue à stabilité neutre et d'une onde courte qui croît la plus rapidement selon la théorie linéaire. En utilisant certaines conditions initiales, l'onde courte croît initialement à un taux cinq fois supérieur à celui prédit par la théorie linéaire. Avec d'autres conditions initiales l'onde courte décroît. La possibilité de ce genre d'interaction est prédite par la théorie faiblement nonlinéaire (voir Maslowe, 1977). Ce système couplé aux equations nonlinéaires du quatrième ordre aux derivées partielles, est résolu par une mèthode pseudo-spectrale modifiée, pour les variables spatiales, et une mèthode Adams-Bashforth du second ordre pour les dérivées temporelles.

TABLE OF CONTENTS

ACKNOWLEDGEMENTS

The author wishes to express his sincere gratitude to Professor Sherwin A. Maslowe who has not only provided guidance and arranged financial support but also provided much encouragement. The author would also like to express his thanks to Dr. R. Metcalfe and Professor S. Orszag for information regarding pseudo-spectral schemes, and Professor T. Warn for helpful discussions.

The author would like to extend his thanks to Professor W.D. Thorpe of the McGill Computing centre for additional computing funds.

This work was supported in part by NSERC grants.

1.0 INTRODUCTION

Mixing layers develop in regions where the velocity varies (shear) and/or the density varies (stratification). In particular, many articles have appeared dealing with free shear layers, i.e. where the domain is assumed to be of infinite extent in the positive and negative vertical directions. This domain is used to approximate what happens in the atmosphere, ocean and in some large scale laboratory experiments away from the boundaries. The physical problems for which such models are used include what happens at the boundary between a warm and cold front, mixing in the ocean, and combustion. Among other concerns, these problems are important in weather prediction, the distribution of nutrients in the sea, and aviation.

Turbulence, sometimes defined as random eddy motion, is an important phenomenon because drag forces and heat transfer rates are much higher in turbulent fluids. Thus the ability to predict transition from a laminar to turbulent flow is the most important goal in hydrodynamic stability theory.

One method of studying the stability of two-dimensional fluid flow problems is the normal mode approach. This is the traditional approach to studying the linear stability of a fluid. When using this method, one assumes a mean flow with horizontal velocity $\bar{u}(y)$ and stratification $\bar{\rho}(y)$, where y is the vertical coordinate. A perturbation, proportional to $\exp(i\alpha(x-ct))$, is then added to the stream function and hence to the density. The governing equations are linearized and an eigenvalue problem arises in terms of the wavenumber α, which is real, $c=c_r+ic_i$, which is complex and other parameters depending on the flow being considered.

Thus c_r is the phase speed of the wavelike perturbation and αc_i is termed the amplification factor. Instability corresponds to $c_i > 0$ and hence linear instability implies that a specified infinitesimal perturbation will grow exponentially. This prediction is a consequence of the linearization and is valid only as long as the perturbation remains small. Ultimately, nonlinear effects become significant. Initial growth rates, for small perturbations, however, agree well with laboratory experiments. Also, weakly nonlinear theories using perturbation methods use linear theory as a starting point.

A second approach to studying the stability of fluid flows is to use large computer models to solve nonlinear viscous initial value problems corresponding to the Navier-Stokes Equations. These models require large amounts of computer time but their validity, in general, is for longer periods of time than perturbation methods. They also can be a convenient way to study the stability of flows corresponding initially to a flow given by the normal mode approach. Subsequent growth rates obtained by these models agree very well initially with linear theory. This type of approach is a logical method to study ideas and theories based on the normal mode approach.

A third approach to studying the stability of fluid flows is the use of vortex methods. These are used to simulate incompressible flows at high Reynolds numbers which, as often happens, are characterized by regions of concentrated vorticity imbedded in irrotational fluid. This is done by discretizing the regions containing vorticity and tracking this discretization in a Lagrangian reference frame. The traditional method of doing this is to use point vortices, i.e. the vorticity is assumed to be a finite linear combination of Dirac delta functions.

This method works well for solving the Euler (inviscid) equations but is often inadequate to represent physically interesting vorticity fields. The problem is that point vortices are singular (cf. Leonard, 1980). To overcome this difficulty investigators have used vortices with finite cores, otherwise known as vortex blobs (Leonard, 1980), in their simulations, as first done by Chorin (1973). Vortex blobs yield more realistic vorticity distributions and bounded induced velocities. Also, unlike point vortices, they can be extended to three-dimensional models where they are called vortex filaments.

In this study we wish to consider initial conditions which could create large horizontally periodic vortical structures which have been observed in the laboratory, in the ocean, and, at high altitudes in the atmosphere by radar where none are observed visually (see Figure 1). These structures involve large temperature gradients. It is the temperature gradients which the radar observes. It has been suggested that these types of structures are an important component of clear air turbulence (cf. Maslowe, 1972).

If we consider the normal mode approach with a Holmboe mean flow,

$\bar{u} = \tanh y$ and

$\bar{\rho} = \exp(-\beta \tanh y)$

linear theory predicts that instability will occur only if the minimum local Richardson number is less than ¼. The local Richardson number Ri is given by $Ri = -g\bar{\rho}'/(\bar{\rho}\bar{u}'^2)$ and $J_0 = g\beta L/V^2$ denotes the overall Richardson number. Note that typically J_0 is greater than one for the atmosphere and rarely is it less than 0.25. In fact, in order for such large scale structures to grow within a reasonable time, linear theory would require J_0 to be less than 0.15. Therefore a nonlinear

theory is needed to explain the existence of large scale vortical structures in the atmosphere. One mechanism which could create such large scale structures is the process of subharmonic resonance of linearly neutral waves where one wave of wavelength λ and another of wavelength 2λ interact. This process can be viewed as a model for vortex pairing which has been observed in laminar and turbulent stratified and unstratified flows.

Vortex pairing is the process where pairs of vortices coalesce to form single vortical structures (see Figure 2). Note that in Figure 2, as in most laboratory experiments, including the ones described below, the waves are spatially growing. Figure 1 appears to depict a disturbance formed by temporally growing waves. Vortex pairing occurs with both spatially growing and temporally growing waves. This process has been recognized as a very important large scale feature of mixing layers. It was first observed in laboratory experiments by Sato (1959). Kelly (1967) gave the first analytical treatment of this phenomenon. In laboratory experiments, Winant and Browand (1974) injected dye between two streams, each travelling at a different velocity, just before they came together after a splitter plate. Unstable waves were observed to grow and coalesce into discrete vortical structures. Vortex pairing occurred repeatedly and according to Winant and Browand was the most important factor controlling the growth of the mixing layer during its transitional and later turbulent stages. The initial formation of eddies is similar to the cat's eye structures that have been observed in numerical studies of stratified shear layers with low Richardson numbers in regions of nonlinear critical layers.

Maslowe (1977) considered the weakly nonlinear theory of a Holmboe

flow with a perturbation consisting of a single neutral wave:

$$\psi = \int^y \bar{u}(s)ds + \varepsilon(A(\tau)\phi(y)\exp(i\alpha(x-ct))+*) + o(\varepsilon^2)$$

Thus ϕ is an eigenfunction of the linearized viscous stratified two-dimensional Boussinesq equations. Then by taking τ to be the slow time variable $\tau = \alpha\varepsilon^2 t$ and solving to $o(\varepsilon)$, a secularity condition then implies

$$\frac{dA}{d\tau} = c_i A/\varepsilon^2 + a_2|A|^2 A + o(\varepsilon^2) \tag{1.1}$$

where a_2 is known as the Landau constant and c_i corresponds to the c_i calculated according to linear theory. Maslowe calculated a_2 for various values of α with Re = 100 and Pr = 0.72. He found that a_2 became unbounded when α tended to a value of about 0.31. This is due to a second order resonance, which will be denoted by the term of subharmonic resonance, consisting of two linearly neutral waves. For a given Reynolds number there is a J_0 such that the corresponding neutral waves are given by α and 2α with the same c. Thus Maslowe was led to consider

$$\psi = \int^y \bar{u}(s)ds + \varepsilon(A_1(\tau)\phi_1(y)\exp i\theta + A_2(\tau)\phi_2(y)\exp 2i\theta + *) + o(\varepsilon^2) \tag{1.2}$$

where $\theta = \alpha(x-ct)$. Here $\tau = \alpha\varepsilon t$ as opposed to $\tau = \alpha\varepsilon^2 t$ for a single wave and hence the instability occurs at a much faster rate. Variables can be separated if

$$dA_1/d\tau = \gamma_1 A_1^* A_2 \text{ and } dA_2/d\tau = \gamma_2 A_1^2 \tag{1.3}$$

where γ_1 and γ_2 are determined by imposing orthogonality conditions on the $o(\varepsilon^2)$ terms. After some manipulation we find

$$a_1^2 - (\gamma_1/\gamma_2)a_2^2 = E \tag{1.4}$$

where a_1, a_2 are half the absolute value of the amplitude of the long

and short waves respectively as a function of τ and E is a constant. Maslowe solved numerically for γ_1, γ_2 and found $\gamma_1/\gamma_2 >> 0$. Hence under certain initial conditions, the amplitudes of both waves grow simultaneously by taking energy from the mean flow. This may seem surprising as second order triad resonance usually results in $\gamma_1/\gamma_2 < 0$ and hence involving a simple exchange of energy between the waves (cf. McGoldrick, J.F.M., 1970). Furthermore, since this theory holds for neutral disturbances, J_0 is much larger than what linear theory would require in order for large growth rates.

This thesis is the first numerical study of the fully nonlinear, stratified, viscous, initial value problem using linearly neutral waves as initial conditions. Previously, numerical studies of a Holmboe or similar flow have used inviscid eigenfunctions as initial conditions. For this reason only waves with large linear growth rates have been previously considered as initial conditions.

Patnaik, Sherman and Corcos (1976) considered a number of initial and boundary value problems for stably stratified, viscous, free shear layers. To basic laminar shear and stratification profiles consisting of error functions, which result in a flow very close to Holmboe flow, perturbations of unstable eigensolutions to the Taylor-Goldstein equation, which are the corresponding linearized inviscid equation, were added. The x and y components of the Boussinesq equations were considered. Along with these equations, the equation for the temperature state with density a linear function of temperature, which is consistent with the Boussinesq approximation, was considered. The above equations were solved using a finite difference scheme to numerically simulate the growth of the disturbances. Initial growth rates compared favorably

with linear growth rates predicted using the linear viscous eigenvalue problem (Maslowe and Thompson, 1971). A subharmonic resonant interaction was investigated by introducing two unstable perturbations corresponding to the fastest growing wave and its first subharmonic for a Reynolds number of 50, an overall Richardson number of 0.07, a Prandtl number of 0.72 and hence wavenumbers of 0.215 and 0.43. The qualitative behavior of the interaction depended on the initial relative positions of the waves but, regardless, the disturbance decayed after maximum amplitude was reached with the long wave eventually decaying but at a slower rate than that of the short wave. Woods (1969) found in measurements of the ocean in the presence of a thermocline that only disturbances that grew from a background Reynolds number greater than about 300 had turbulent final states. Patnaik, Sherman and Corcos, due to problems with their numerical scheme, obtained results only for Reynolds numbers of 200 or less.

A similar problem has been studied by Peltier and Davis (1979). A finite difference scheme was used to study a stratified two-dimensional shear layer which was semi-infinite in the vertical direction with a tanh y background horizontal velocity and a ρ_0 - βtanh y background density profile. The model used a numerical domain with length in the x coordinate corresponding to the horizontal wavelength of the fastest growing wave. All runs mentioned were made with $J_0 = 0.07$ except for a resonant case with $J_0 = 0.01$. In this case, resonance was due to the "ground" being an integral number of half-wavelengths $n\lambda_z$, where λ_z was the vertical wavelength of the eigenfunction, from the region of small local Richardson number. This is a completely different type of resonant interaction from that discussed above.

In this study, the two-dimensional Boussinesq equations with heat conduction were approximated numerically in a domain which is infinite in the vertical direction. A pseudo-spectral scheme was used consisting of double Fourier trigonometric series in space and finite difference in time. Fast Fourier transforms were used to transfer back and forth between physical and Fourier space. It was anticipated that a pseudo-spectral scheme would resolve higher Reynolds number cases than a comparable finite difference scheme as suggested by S. Orszag (private communication). Such a scheme, it was considered, would be more accurate and more efficient than a comparable finite difference scheme for modelling wave phenomena as suggested by Abe and Inoue (1980). Abe and Inoue solved the Korteweg-de Vries equation by a pseudo-spectral scheme, finite difference schemes and by other methods. Each method was applied to a common initial value problem and compared with the other methods. The Fourier expansion (pseudo-spectral) method was found to be the most accurate and most efficient. The present study was initiated primarily in order to attempt to determine whether the mechanism suggested by weakly nonlinear theory of subharmonic resonance of neutral or nearly neutral waves could result in much higher growth rates than linear theory predicts and hence be a mechanism which could create large scale vortical structures. The effect of flows having initial background Reynolds numbers greater than 300 was thought to be of interest as suggested by Woods' measurements and the calculations of Peltier and Davis. Comparisons with the linear theory and the results of previous fully nonlinear numerical calculations were used as a check for the numerical scheme.

The results obtained are most dramatic for cases corresponding to

the subharmonic resonant interaction between linearly neutral and fastest growing waves at the same Richardson number. For example if Re = 200 and Pr = 0.72, then α = 0.225, 0.45 and J_0 = 0.174. With suitable initial amplitudes and relative positioning the "fastest growing" wave grows at an initial rate five times that predicted by linear theory. Thus while linear theory predicts that this wave will grow like exp(0.06t), initially it grows like exp(0.29t). For the same case but with a different initial relative positioning the wave, which linear theory predicts to be the fastest growing, for J_0 = 0.174, decays initially like exp(-0.22t).

2.0 MATHEMATICAL MODEL

In this chapter the mathematical model used for this study is described. The governing equations are given in section 2.1. In the second section, the mean flows used are considered and the concept of a body force, which was used for some test cases, is explained. In the third section the various initial conditions considered are described.

2.1 Governing Equations

The basic equations governing the time dependent motion in two dimensions of an incompressible, viscous, heat-conducting fluid in a gravitational field are

$$\frac{Du}{Dt} + \frac{1}{\rho_0}\frac{\partial p}{\partial x} = \nu\left(\frac{\partial^2 u}{\partial x^2} + \frac{\partial^2 u}{\partial y^2}\right) \tag{2.1.1}$$

$$\frac{Dv}{Dt} + \frac{1}{\rho_0}\frac{\partial p}{\partial y} = \nu\left(\frac{\partial^2 v}{\partial x^2} + \frac{\partial^2 v}{\partial y^2}\right) - \frac{\rho g}{\rho_0} \tag{2.1.2}$$

$$\partial u/\partial x + \partial v/\partial y = 0 \tag{2.1.3}$$

$$\frac{DT}{Dt} = \hat{\beta}\left(\frac{\partial^2 T}{\partial x^2} + \frac{\partial^2 T}{\partial y^2}\right) \tag{2.1.4}$$

$$\rho = 1 - a_0 T_0 (T-1) \tag{2.1.5}$$

where u, v are the x and y components of velocity, ρ the density, p the pressure, ν the kinematic viscosity, g the gravitational acceleration, T the temperature, $\hat{\beta}$ the coefficient of thermal conductivity,

$$\frac{D}{Dt} = \frac{\partial}{\partial t} + u\frac{\partial}{\partial x} + v\frac{\partial}{\partial y},$$

T_0 is a reference temperature, ρ_0 is a reference density and a_0 the coefficient of thermal expansion. Viscosity and thermal conductivity are

assumed to be constant. The density variations of the fluid particles are attributed to thermal diffusion and expansion alone and are neglected except in the calculation of the buoyancy force (Boussinesq approximation). The equations were non-dimensionalized by setting

$$x = x^*\delta_0$$

$$y = y^*\delta_0$$

$$u = u^*U_0$$

$$v = v^*U_0$$

$$t = t^*\delta_0/U_0$$

$$\rho = \rho^*\rho_0$$

$$p = p^*\rho_0 U_0^2$$

where U_0 is one-half of the total change in the mean flow and δ_0 is one-half the initial shear layer thickness.

These were substituted into equations (2.1.1) to (2.1.5) and converted into non-dimensional vorticity and density equations using equation (2.1.5) which, consistent with the Boussinesq approximation, gives the density as a linear function of temperature. Hereafter we drop the superscript "*". Thus in terms of ζ, ρ, ψ, u, v, and g the non-dimensional vorticity, density, stream function, x and y components of velocity, and gravity, respectively, we have

$$\frac{D\zeta}{Dt} + \frac{J_0 \partial\rho}{\beta \partial x} = \frac{1}{Re}\left(\frac{\partial^2\zeta}{\partial x^2} + \frac{\partial^2\zeta}{\partial y^2}\right) \tag{2.1.6}$$

$$\frac{D\rho}{Dt} = \frac{1}{RePr}\left(\frac{\partial^2\rho}{\partial x^2} + \frac{\partial^2\rho}{\partial y^2}\right) \tag{2.1.7}$$

$$\zeta = -\nabla^2\psi, \quad u = \frac{\partial\psi}{\partial y}, \quad v = -\frac{\partial\psi}{\partial x} \tag{2.1.8}$$

The Reynolds number and the Prandtl number have the definitions $Re = \rho_0 U_0 \delta_0/\mu_0$ and $Pr = c_p \mu_0/k$ where μ_0 is the molecular viscosity, c_p the specific heat at constant pressure and k the coefficient of heat conduction and U_0 and δ_0 are as defined above (note that $\nu = \mu_0/\rho_0$).

Equations (2.1.6) to (2.1.8) are solved in a rectangular domain with prescribed initial and boundary conditions.

2.2 Mean Flow

The mean flow velocity and density in dimensionless form, for the most part, were chosen to be

$$\bar{u}(y) = \tanh y \tag{2.2.1}$$

$$\bar{\rho}(y) = \exp(-\beta \tanh y) \tag{2.2.2}$$

which represent the flow resulting from molecular diffusion of earlier coincident discontinuities (see Figure 3). Runs were also made with

$$\bar{u}(y) = \mathrm{erf}(y) \tag{2.2.3}$$

$$\bar{\rho}(y) = 1 - \beta \mathrm{erf}(\sqrt{Pr}\, y)/\sqrt{Pr} \tag{2.2.4}$$

to compare with results obtained by Patnaik (1973) and Patnaik, Sherman and Corcos (1976). These profiles are similarity solutions of the Boussinesq equations. However, as similarity solutions, they are time dependent. Furthermore, results using these profiles differed very little from using (2.2.1) and (2.2.2). Also weakly nonlinear theory has not been developed for error function profiles for stratified free shear layers while it has been for hyperbolic tangent profiles as the latter are much more tractable to analytical analysis.

Frequently in perturbation analysis of fluid flows, a body force is added explicitly or implicitly to the Navier-Stokes equations in order

to make a background flow an exact steady solution of the corresponding time dependent equations. Hence if we consider the case of a mean flow $\bar{u}(y)$ and mean stratification $\bar{\rho}(y)$ and equations (2.1.6) to (2.1.8) $\bar{u}''/Re$ and $-\bar{\rho}''/(RePr)$ would be added to the right hand sides of equations (2.1.6) and (2.1.7) respectively. This is very easy to implement in the fully nonlinear calculations with the scheme used for this study as will be explained in the next chapter. Thus this was done for particular cases in order to make comparisons with previous results.

2.3 Initial Conditions

To a basic laminar flow perturbations were added whose y-dependent component consists of viscous eigensolutions to the steady linear problem with heat conduction (cf. Maslowe and Thompson, 1971). Previous studies have used the corresponding inviscid equation, the Taylor-Goldstein equation

$$\frac{d^2\phi}{dy^2} - \left(\frac{\bar{u}''}{\bar{u}-c} - \frac{g\bar{\rho}'}{\bar{\rho}(\bar{u}-c)^2} + \alpha^2\right)\phi = 0 \qquad (2.3.1)$$

with asymptotic boundary conditions

$$\begin{aligned} &\phi \sim a\exp(-\alpha y) \text{ as } y \to \infty \\ &\phi \sim b\exp(\alpha y) \text{ as } y \to -\infty \end{aligned} \qquad (2.3.2)$$

where ϕ is the perturbation stream function vertical eigenfunction, i.e.

$$\psi = \int^y \bar{u}dy + \varepsilon(\phi\exp(i\alpha(x-ct)) + *) \qquad (2.3.3)$$

However, this approach will not work if neutral waves or nearly neutral waves are to be used as initial conditions since the eigenfunctions corresponding to neutral waves of the Taylor-Goldstein equation are singular. Even for waves away from the neutral curve, this method in-

troduces large initial errors for Reynolds numbers less than 600.

The computer program used by Maslowe and Thompson solves the corresponding problem with viscosity and heat conduction. This involves solving the following sixth order ordinary differential equation boundary value problem:

$$(\bar{u}-c)^2\nabla^2\phi + (\bar{u}-c)\bar{u}''\phi + \frac{i}{\alpha Re}(\bar{u}-c)(1+\frac{1}{Pr})\nabla^4\phi - \frac{g\bar{\rho}'\phi}{\rho}$$

$$= \frac{1}{Pr(\alpha Re)}\nabla^6\phi - \frac{i}{Pr(Re)}(2\bar{u}'\nabla^2\phi' - 2\bar{u}''\phi' - \bar{u}^{iv}\phi) \qquad (2.3.4)$$

where the operator $\nabla^2 = d^2/dy^2 - \alpha^2$. The boundary conditions are as follows

$$\phi \sim a\exp(\alpha y) + b\exp(ry) + C\exp(qy) \text{ as } y \to -\infty \qquad (2.3.5)$$

$$\phi_r'(0) = \phi_r'''(0) = \phi_r^v(0) = 0 \qquad (2.3.6)$$

and

$$\phi_i(0) = \phi_i''(0) = \phi_i^{iv}(0) = 0 \qquad (2.3.7)$$

where

$$r = \alpha\left(1 - \frac{icRe}{\alpha}\right)^{\frac{1}{2}} \qquad (2.3.8)$$

$$q = \alpha\left(1 - \frac{icRePr}{\alpha}\right)^{\frac{1}{2}} \qquad (2.3.9)$$

and ϕ_r, ϕ_i are the real and imaginary parts of ϕ respectively. This boundary value problem was solved using a shooting method with a fourth order Runge-Kutta scheme.

The initial perturbation vorticity $\hat{\zeta}$ is then given by

$$\hat{\zeta} = -(\phi'' - \alpha^2\phi)\exp i\alpha x \qquad (2.3.10)$$

and the initial perturbation density $\hat{\rho}$ is given by

$$\hat{\rho} = \left[(\bar{u}-c)(\phi'' - \alpha^2\phi) - \bar{u}''\phi + \frac{i}{\alpha Re}(\phi^{iv} - 2\alpha^2\phi'' + \alpha^4\phi)\right]\frac{\beta}{J_0}\exp i\alpha x \qquad (2.3.11)$$

Thus this program was modified to set up the initial conditions, changed to error function profiles for some test runs and changed to run in extended precision for high Reynolds number cases. The eigenfunction ϕ, as was done by Maslowe (1977), was normalized by referring it to the "standard solution" $\alpha = 1$, $\phi = \text{sech } y$ corresponds to the case $J_0 = 0$ and $Re = \infty$. Thus ϕ was adjusted so that

$$\int_{-\infty}^{\infty} (|\phi'|^2 + \alpha^2|\phi|^2)_{dy} = 8/3 \tag{2.3.12}$$

$A(0)$ was taken to be $\sqrt{3/8}$. Hence the perturbation kinetic energy in the fundamental, $E(t)$, is given by

$$E(t) = \varepsilon^2 A^2 \int_{-\infty}^{\infty} (|\phi'|^2 + \alpha^2|\phi|^2)_{dy} \tag{2.3.13}$$

As the phenomenon of most interest in this study was resonant interaction, for most runs ψ was initially of the form

$$\psi = \int^y \bar{u}(s)ds + \varepsilon(A_1 \phi_1 \exp(i\alpha x) + A_2 \phi_2 \exp(i2\alpha x) + *) \tag{2.3.14}$$

where ϕ, ϕ are eigenfunctions of (2.3.4) corresponding to α and 2α respectively. Thus the initial conditions become

$$\zeta = -\bar{u}' + (\hat{\zeta} + \hat{\zeta}^*) \tag{2.3.15}$$

$$\rho = \bar{\rho} + (\hat{\rho} + \hat{\rho}^*) \tag{2.3.16}$$

where

$$\hat{\zeta} = -((\phi_1'' - \alpha^2\phi_1) \exp(i\alpha x) + (\phi_2'' - 4\alpha^2\phi_2) \exp(i2\alpha x)) \tag{2.3.17}$$

$$\begin{aligned}\hat{\rho} = {} & ((\bar{u}-c)(\phi_1'' - \alpha^2\phi_1) - \bar{u}''\phi_1 + \frac{i}{\alpha Re}(\phi_1^{iv} - 2\alpha^2\phi_1'' + \alpha^4\phi_1)) \frac{\beta}{J_0} \exp i\alpha x \\ & + ((\bar{u}-c)(\phi_2'' - 4\alpha^2\phi_2) - \bar{u}''\phi_2 + \frac{i}{\alpha Re}(\phi_2^{iv} - 8\alpha^2\phi_2'' \\ & + 16\alpha^4\phi_2)) \frac{\beta}{J_0} \exp i2\alpha x\end{aligned} \tag{2.3.18}$$

Note that ϕ_1 and A_1 and ϕ_2 and A_2 were normalized as in the single wave case mentioned above.

3.0 NUMERICAL MODEL

In this chapter the numerical model used to approximate the mathematical model described in the second chapter is examined. In the first section the actual pseudo-spectral scheme used in this study is described and its differences, advantages and disadvantages are considered. Comparisons with linear theory made with this numerical model are described in the third section. In the final section of this chapter the ranges of the various parameters used in the different numerical simulations are given.

3.1 Numerical Method

Equations (2.1.1 to 2.1.5) have generally been solved by other investigators with finite difference methods. However, there are various other possibilities for calculating the spatial derivatives. One is the Galerkin method where n convenient, linearly independent functions (ϕ_j) are chosen and if the differential equation is given by $L(G) = 0$ in a region A, then we determine c_j such that

$$\int_A L\left(\sum_{j=1}^{n} c_j \phi_j\right)\phi_k \, dA = 0, \quad k=1,2,\ldots,n \tag{3.1.1}$$

Thus, in terms of the L^2 inner product, the c_j are determined so that the error is orthogonal to all of the ϕ_k, $k = 1,\ldots,n$. Hence the error is minimized with respect to the L^2 norm.

Another method, called collocation or the pseudo-spectral method, involves choosing n linearly independent functions (ϕ_j) as above and determining c_j by setting

$$L\left(\sum_{j=1}^{n} c_j \phi_j\right) = 0 \qquad (3.1.2)$$

at the n points $x_1, x_2, \ldots, x_n$. Hence, in a collocation scheme, the error is minimized pointwise on a finite number of points.

In Galerkin schemes nonlinear terms are more difficult to handle than in pseudo-spectral schemes. For instance, a simple quadratic nonlinearity involves calculating convolution sums in a Galerkin scheme while in a pseudo-spectral scheme nonlinear terms are just calculated pointwise in physical space making even very complicated nonlinear terms easy to calculate. However, pseudo-spectral schemes generate aliasing errors in the nonlinear terms. For example, in a quadratic nonlinear term, the n-k spectral mode (for $k < n/2$), includes the energy from the n+k mode as well as that from the n-k mode. The convolution sums used in a corresponding Galerkin scheme avoid this. The importance of aliasing errors can be monitored by graphing the energy spectrum as a function of wavenumber. This was done as a part of all runs that were made.

A popular choice for the ϕ_j is a set of trigonometric polynomials. These have the advantage of ease of calculation of derivatives and result in practically no phase errors, i.e. if a system has a dominant frequency as a solution, this solution will retain its shape and phase using trigonometric polynomials while with finite difference methods the solution may have its phase shifted, and in nonlinear problems, the solution may lose its sharpness and form a wake. A trigonometric series approximating a function f will converge at least as fast as $1/n^k$ if the first (k-1) derivatives of f are continuous (including at the end points). Thus, this type of approximation converges very quickly for "smoothly" periodic or almost periodic functions. Finally, what makes

using trigonometric series economical is that fast Fourier transform (FFT) methods may be employed.

Fast Fourier transforms consist of efficient algorithms for calculating the n sums

$$c_j = \sum_{k=0}^{n-1} f_k \exp(i2\pi kj/n) \qquad j=0,1,2,\ldots,n-1 \tag{3.1.3}$$

If f_k is $f(x_0 + dx*k)$, for instance, then the above n sums c_j under suitable manipulation result in the coefficients d_j such that

$$f_k = \sum_{j=-n/2}^{n/2-1} d_j \exp(i2\pi jk/n) \qquad k=0,1,\ldots,n-1 \tag{3.1.4}$$

i.e. d_j are the coefficients of a trigonometric polynomial t such that $t(x_0 + k*dx) = f(x_0 + k*dx)$ and thus this is a pseudo-spectral scheme. Similarly, the sums c_j can be viewed as approximations to the integrals involved in a Galerkin scheme. The FFT, by the use of judicious bookkeeping, calculates these sums in o(nlogn) steps as compared to the "naive" approach taking $o(n^2)$ steps. An FFT is most efficient when n is a power of a small prime number or the product of powers of several small prime numbers. Thus $n = 2^k$ would take o(nk) steps while if n was a prime number there would be no saving at all. By suitable manipulations the finite Fourier transform of a multi-dimensional array can be calculated using a one-dimensional fast Fourier transform. In summary, for smoothly periodic solutions, a pseudo-spectral scheme gives better accuracy at a fraction of the cost for a corresponding finite difference scheme (cf. Abe and Inoue, 1980).

Numerically, the following representation was used

$$\zeta = \bar{\zeta} + \sum_m \sum_n a_{mn} \exp(i(m\alpha x + \mu_n y)) \tag{3.1.5}$$

$$\rho = \bar{\rho} + \sum_m \sum_n b_{mn} \exp(i(m\alpha x + \mu_n y)) \tag{3.1.6}$$

where ζ is the vorticity and ρ is the density. Also $\bar{\zeta}(y) = -\bar{u}'(y)$ where $\bar{u}$ is the initial laminar velocity (tanh y) and $\bar{\rho}(y) = \exp(-\beta\tanh(y))$, the initial laminar density (Holmboe's flow), $\alpha = \pi/L_x$, $\mu_n = n\pi/L_y$ where L_x and L_y are half of the box size in the horizontal and vertical directions respectively. Thus if the wavelength of the initial disturbance was λ, L_x was chosen to be $\lambda/2$. This is a collocation scheme with n1 points in the horizontal and n2 points in the vertical. Hence $-n1/2 \leq n < n1/2$ and $-n2/2 \leq m < n2/2$ and $0 \leq x \leq \lambda$, $-L_y \leq y \leq L_y$. Some cases, for comparison purposes were run with $\bar{u} = \mathrm{erf}(y)$, $\bar{\rho} = 1 - \beta\,\mathrm{erf}(\sqrt{Pr}\,y)/\sqrt{Pr}$ (see section 3.1).

This method of handling ζ, ρ is used in order to avoid Gibbs phenomenon by separating these functions into non-periodic and nearly periodic parts. The idea is that for the integration times involved, the mean flow distortion and the disturbance remain small close to the $y = \pm L_y$. With this method the boundary conditions are periodic in both the x and y directions.

An alternate method would be to take

$$\zeta = \sum_m \sum_n a_{mn} \exp(m\alpha x)\cos(\mu_n y) \qquad (3.1.7)$$

$$\rho = \sum_m \sum_n b_{mn} \exp(m\alpha x)\sin(\mu_n y) \qquad (3.1.8)$$

(cf. Riley and Metcalfe, 1980). This method is equivalent to imposing asymptotic boundary conditions $u = \pm 1$, $v = 0$ at $y = \pm\infty$, at the finite distances of $y = \pm L_y$ and hence free slip boundary conditions are being used. Finite difference schemes, as used by Patnaik, Sherman and Corcus (1976) and by Peltier and Davis (1979) also use free slip boundary conditions.

The above two types of boundary conditions, for short enough times

and large enough L_y give the same results to reasonable accuracy. However some problems are to be expected in that the boundary conditions for the initial conditions do not match those used for the time stepping part of the scheme. Again, this along with the resolution problems can be improved by using an appropriate y domain. See section 3.2 for more details. Work is in progress to use asymptotic boundary conditions for the whole scheme (Orszag and Metcalfe, private communication) which appears promising. This method involves using the linearized equations to obtain the asymptotic behavior and attempting to subtract out, near the vertical boundaries, the part of the solution which does not act like the asymptotic solution.

Spatial derivatives were calculated using term-by-term differentiation. Taking ζ as in (3.1.5), we then have

$$\frac{\partial \zeta}{\partial y} = \bar{\zeta}' + \sum_m \sum_n a_{mn}\, i\mu_n \exp(i(m\alpha x + \mu_n y)) \qquad (3.1.9)$$

ψ was considered to be given as follows:

$$\psi = \int_0^y \bar{u}(s)ds + \sum_m \sum_n c_{mn} \exp(i(m\alpha x + \mu_n y))$$

where

$$c_{mn} = \begin{cases} \dfrac{1}{\alpha^2 m^2 + \mu_n^2}\, a_{mn}, & m^2 + n^2 \neq 0 \\ c_{00}, & m = n = 0 \end{cases}$$

and where a_{mn} are the coefficients of $\zeta - \bar{\zeta}$ (equation 3.1.5) and c_{00} is an arbitrary constant of integration. This is consistent with $\zeta = -\nabla^2\psi$ and $(\partial\psi/\partial y - \bar{u}) \sim \exp(-\alpha|y|)$ for y large. Differentiating with respect to y (term-by-term) we obtain,

$$u = \bar{u} + \sum_{\substack{m \\ m^2+n^2\neq 0}} \sum_{n} a_{mn} \frac{i}{\mu_n^2+\alpha^2 m^2} \exp(i(m\alpha x + \mu_n y)) \qquad (3.1.10)$$

The various other partial derivatives of ζ, ρ, ψ, u and v were calculated in a similar fashion. These terms were calculated in Fourier space and then transformed into physical space where nonlinear terms were calculated pointwise and where time differencing was done.

Time differencing was accomplished using a second order Adams-Bashforth scheme which was started using Euler's method. Nystrom's method was also tested but required smaller time steps than the Adams-Bashforth scheme in order to be numerically stable. These methods are common explicit finite difference methods. Their stability has been analysed with respect to various linear mixed problems as time differencing methods for schemes using spectral methods in space, by Gottlieb and Orszag (1977), with stability depending on the exact problem and method being considered. It is likely that a semi-implicit scheme would have less severe stability restrictions. However it is not clear how that should be done nor what the overall improvement in efficiency would be. Time differencing in a pseudo-spectral scheme can be done either in physical space or in the transform space. In this study the time differencing was done in physical space. Thus, if

$$NL1(\zeta,\rho,\psi) = -\frac{\partial\psi}{\partial y}\frac{\partial\zeta}{\partial x} + \frac{\partial\psi}{\partial x}\frac{\partial\zeta}{\partial y} - \frac{J0}{\beta}\frac{\partial\rho}{\partial x} + \frac{1}{Re}\nabla^2\zeta \qquad (3.1.11)$$

$$NL2(\rho,\psi) = -\frac{\partial\psi}{\partial y}\frac{\partial\rho}{\partial x} + \frac{\partial\psi}{\partial x}\frac{\partial\rho}{\partial y} + \frac{1}{RePr}\nabla^2\rho \qquad (3.1.12)$$

where $\nabla^2 = \partial^2/\partial x^2 + \partial^2/\partial y^2$ and if $\zeta - \bar{\zeta}$ and $\rho - \bar{\rho}$ are denoted by $\hat{\zeta}$ and $\hat{\rho}$ respectively (note $\bar{\zeta} = -u'$) then

$$NL1(\zeta,\rho,\psi) = NL1(\hat{\zeta},\hat{\rho},\hat{\psi},\bar{u}) = -(\bar{u} + \frac{\partial\hat{\psi}}{\partial y})\frac{\partial\hat{\zeta}}{\partial x} + \frac{\partial\hat{\psi}}{\partial x}(-\bar{u}'' + \frac{\partial\hat{\zeta}}{\partial y})$$

$$- \frac{J_0}{\beta} \frac{\partial \hat{\rho}}{\partial x} + \frac{1}{Re} (\nabla^2 \hat{\zeta} - \bar{u}'') \tag{3.1.13}$$

$$NL2(\rho,\psi) = NL2(\hat{\rho},\hat{\psi},\bar{u},\bar{\rho}) = - (\bar{u} + \frac{\partial \hat{\psi}}{\partial y}) \frac{\partial \hat{\rho}}{\partial x} \frac{\partial \hat{\psi}}{\partial x} (\bar{\rho}' + \frac{\partial \hat{\rho}}{\partial y})$$

$$+ \frac{1}{RePr} (\nabla^2 \hat{\rho} + \bar{\rho}'') \tag{3.1.14}$$

Note, from (3.1.5) and (3.1.6) that, for the scheme used, ζ and ρ are separated into $\hat{\zeta}$, $\bar{\zeta}$ and $\hat{\rho}$, $\bar{\rho}$ where

$$\hat{\zeta} = \sum_m \sum_n a_{mn} \exp(i(m\alpha x + \mu_n y)) \tag{3.1.15}$$

$$\hat{\rho} = \sum_m \sum_n b_{mn} \exp(i(m\alpha x + \mu_n y)) \tag{3.1.16}$$

respectively. The nonlinear operators NL1, NL2 were evaluated at each time step and every spatial grid point. NL1(r,j,k) and NL2(r,j,k) will denote NL1, NL2 respectively, evaluated at time $t = t_0 + r*dt$ and at the grid point $(x,y) = (x_0 + j*dx, y_0 + k*dy)$. Hence, if $\zeta(r,j,k)$ denotes the approximation to $\zeta(t_0 + rdt, x_0 + jdx, y_0 + kdy)$ and similarly for $\rho(r,j,k)$, $\hat{\zeta}(r,j,k)$, $\hat{\rho}(r,j,k)$, $\psi(r,j,k)$, $\bar{u}(k)$, $\bar{\rho}(k)$ then using an Adams-Bashforth second order scheme would imply

$$\zeta(r+1,j,k) = \zeta(r,j,k) + dt(3*NL1(r,j,k) - NL1(r-1,j,k)) \tag{3.1.17}$$

$$\rho(r+1,j,k) = \rho(r,j,k) + dt(3*NL2(r,j,k) - NL2(r-1,j,k)) \tag{3.1.18}$$

Adding a body force to make $\bar{u}$, $\bar{\rho}$ an exact steady solution of the resulting equations in terms of this numerical scheme is done simply by dropping the $\bar{u}''$ term and the $\bar{\rho}''$ term from NL1 and NL2 respectively (i.e. equations (3.1.13) and (3.1.14) respectively). Note that the ease of adding this body force is due to the method of splitting ζ, ρ and helped by the fact that the time stepping was done in physical space.

Two factors would have resulted in savings of CPU time. The code could have been run in IBM single precision instead of IBM double precision. This, however, would have degraded the results at a saving of

only about ten percent. The other factor is that the FFT routines could have been written in IBM Assembler. The routines used were modified versions of FORTRAN subroutines written at MIT (by Greenberg). They were switched to IBM double precision and compiled using an optimizing compiler (FORTRAN H extended with opt = 2). At present there are no FFT routines written in IBM Assembler. Writing such routines would require an enormous effort. The resulting savings are estimated at only about forty percent per time step (S. Orszag, private communication).

There are other methods which would provide a closer approximation to the vertical boundary conditions. One such method would be to use Laguerre polynomials in the vertical coordinate. However this would increase the amount of computation enormously. A less ambitious method would be to use a finite element method in the vertical. However, this would still involve much more computation and has given disappointing results. Haidvogel, Robinson and Schulman (1980) considered several inviscid barotropic vorticity initial value problems and found that, for these particular test problems, a finite element model and a pseudo-spectral model, despite their complexity, were on the average 4 and 15 times more accurate, respectively, than a finite difference model. Thus the pseudo-spectral scheme was almost 4 times more accurate than the finite element model.

Tests were made to check the scheme. Aliasing was monitored, as explained earlier in this section. The perturbation kinetic energy and wave amplitudes were monitored (see sections 3.2, 4.1 and 4.2). The Reynolds stress term was computed for several runs in order to check conservation of energy. Also, vertical and temporal mesh sizes were varied as a check of numerical convergence and stability. Furthermore,

comparisons were made with results obtained in linear and weakly nonlinear theory (see the next section and section 4.1 respectively).

3.2 Comparisons with Linear Theory

Viscous linear theory (see Maslowe and Thompson, 1971) for a tanh y velocity profile and an exp(-βtanh y) density profile (Holmboe flow) results in a sixth order ordinary differential equation eigenvalue problem. According to inviscid theory, J_0 (the overall Richardson number) has to fall to less than 0.25 in order for instability to occur. In fact, for Holmboe flow $J_0 = \alpha(1-\alpha)$, $0 \leq \alpha \leq 1$, defines the neutral curve (see Figure 4). The viscous case shrinks the unstable region according to Re the Reynolds number and Pr the Prandtl number. Since the linear theory quoted above is a steady state theory, the best comparisons with a nonlinear initial value problem numerical simulation would be expected to occur for values of Re, Pr, J_0 and α away from the neutral curve, with ϵ not too large.

The perturbation kinetic energy, E(t), given by

$$E(t) = \frac{\int_{\infty}^{\infty} \int_{0}^{\lambda} ((u-\bar{u}_t)^2 + v^2)dx\, dy}{2\lambda} \tag{3.2.1}$$

where

$$\bar{u}_t(y) = (1/\lambda) \int_{0}^{\lambda} u(x,y,t)dx \tag{3.2.2}$$

was used to estimate the growth of the eigenfunction (cf. Patnaik, Sherman and Corcos, 1976) where these integrals were approximated by sums over mesh points. This method does not give the energy of a single wave as it includes the energy of excited harmonics. Moreover, to com-

pare with weakly nonlinear theory, we need to take $\bar{u}_t = \bar{u} = \bar{u}_0$. However, then E(t) includes a cross term

$$1/(2\lambda) \int_0^{\lambda} 2\bar{u}(u-\bar{u})dxdy \tag{3.2.3}$$

due to $\bar{u}$ not being a steady state solution. This introduces a large error when ε is small and/or Re is small.

When ε was very small, the growth rate, calculated using the perturbation kinetic energy (E(t)) with $\bar{u}_t = \bar{u}$, increased as the cross term became of the same order as ε. Even if the system is forced such that the laminar flow is an exact steady solution of the Boussinesq form of the Navier-Stokes equations, the mean flow is distorted by the disturbance so the cross term remains non-zero. This can be improved by taking $\bar{u}_t$ instead of u_t as in (3.2.1). A more satisfactory method consists of the following. Suppose ψ is initially of the form

$$\psi = \int^y \bar{u}(s)ds + \varepsilon(A(t)\exp(i\alpha x)\phi(y) + *) \tag{3.2.4}$$

Then the perturbation kinetic energy to $o(\varepsilon^2)$ becomes

$$E(t) = \varepsilon^2|A|^2 \int_{-\infty}^{\infty} (|\phi'|^2 + \alpha^2|\phi|^2)dy \tag{3.2.5}$$

Thus if

$$\phi \sim \sum_{n=-N2/2}^{N2/2-1} p_n \exp(i\mu_n y) \tag{3.2.6}$$

and

$$\psi = \int^y \bar{u}(s)ds + \sum_{m=-N1/2}^{N1/2-1} \sum_{n=-N2/2}^{N2/2-1} d_{mn}(t) \exp(i(\alpha m x + \mu_n y)) \tag{3.2.7}$$

then

$$A(t)\phi(y) \sim \sum_{n=-N2/2}^{N2/2-1} d_{1n}(t) \exp(i\mu_n y) \tag{3.2.8}$$

This is extremely easy to implement in a finite Fourier series pseudo-

spectral scheme. We find that

$$A(t) \sim \sum_{n=-N2/2}^{N2/2-1} d_{1n}(t)p^* \Big/ \sum_{n=-N2/2}^{N2/2-1} |p_n|^2 \qquad (3.2.9)$$

The growth of A(t) was then used to compare with the linear growth rates. This method gives the amplitude of the excited wave as a function of time which is the quantity for which linear theory makes its predictions. However, it does not include distortion of the eigenfunction and includes higher order terms. As some runs were made with a body force so that $\bar{u}$ and $\bar{\rho}$ are a steady state solution of the resulting equations (see preceding section for more details) comparisons were made between linear growth rates and those obtained from the (numerical) nonlinear initial value problem both with and without a body force. Amplitudes of single waves with linear growth rates of about 0.1 or more and for a wide range of ε had growth rates, calculated in this manner, within one percent of those predicted by the linear viscous theory even for small ε and small Re. Figures 5 and 6 compare the nonlinear growth of the wave which is the fastest growing according to linear theory for $J_0 = 0.07$, with and without a body force; $\varepsilon = 0.01, 0.05$; and with Re = 200 and Re = 50. Figure 5A depicts A(t) compared with linear theory with and without a body force where $\varepsilon = 0.01$, $J_0 = 0.07$, $\alpha = 0.45$, Re = 200 and Pr = 0.72. In Figure 5B all the parameters are the same except $\varepsilon = 0.05$. In Figure 6A and 6B cases with and without a body force are again depicted for $\varepsilon = 0.01, 0.05$ respectively. For these cases Re = 50, $\alpha = 0.43$, $J_0 = 0.07$ and Pr = 0.72. Other test runs were made for a range of J_0 and a wider range of α, ε, Re and Pr. Away from the neutral curves, the results were close to the linear viscous theory. Near the neutral curve, of course, higher order effects become important

and thus it is not surprising that growth rates in this region, even for these single wave cases, differ from what linear theory predicts. All of these results were dependent on an appropriate choice of the vertical coordinate domain. When y ranged at least from -3 to +3 the linear viscous eigenfunction routine would still converge to essentially the same eigenvalues but the initial perturbation kinetic energy and A(t), calculated using fast Fourier transforms, had substantial errors when the y domain ranged only from -3 to +3. By increasing the domain these errors decreased to a minimum and then started increasing. It would seem that the errors with a smaller domain are due to the different boundary conditions in the y direction, i.e. whereas they are asymptotic for the initial conditions (linear eigenfunctions), they are periodic for the numerical model of the nonlinear initial value problem. For y large the dominant term in the asymptotic expansion of the linear eigenfunctions is an o(1) complex constant times $\exp(-\alpha y)$. If, for instance, $\alpha = 0.5$ the eigenfunction routine will converge to the correct eigenfunction for, say, $y = 3.2$. Then $|\phi(3.2)|$ would be of the order of 0.27; similarly, for $|\phi(-3.2)|$. Hence, representing ϕ by a Fourier series on this interval would result generally in poor convergence of the series and significant Gibbs phenomenon at the end points. Increasing the y domain decreases this jump and improves the convergence. If too large a domain is taken, then dy, the grid spacing in the y direction, becomes large. However, for α around 0.5, Reynolds numbers around 100, and Prandtl numbers of around 1.0, the eigenfunction routine would not converge for a domain extending beyond 5.5. Thus, typically, the domain would be calculated using the linear eigenfunction routine to $\alpha y = 2.4$ and extended to $\alpha y = 3.2$ by using the asymptotic expansion for the

eigenfunction and its derivatives.

In conclusion, it should also be noted that this method of calculating A(t) facilitates comparison with weakly nonlinear theory since much of the information given by this theory is in terms of the wave amplitude(s).

3.3 Numerical Parameters

The computing region was limited to one wavelength in x and roughly one wavelength in y for the single mode runs. For the resonant interaction runs the length was the long wave's length and the height was slightly less than that. For most runs 32 points were used in the x direction and 64 in the y direction. For some resonant interaction cases at high Reynolds numbers, a grid of 32 by 128 was used and for large initial amplitude high Reynolds number cases, a grid of 64 by 128 was used. The time step size was usually 0.125. However for some runs and parts of others 0.0625 was used. For single wave runs with α close to 1.0 a time step of 0.03125 was generally used. In order to calculate the initial conditions, typically eight times as many grid points were used.

The Reynolds numbers used varied between 50 and 600. J_0 varied between about 0.01 and 0.25 except for the homogeneous runs which were approximated by taking J_0 and β very small. For the resonant cases J_0 was always greater than or equal to 0.07. ε varied between 0.00001 and 0.2. The Prandtl number was varied only for the single mode cases (0.72 to 4.0). It was 0.72 for all the resonant cases; α varied between 0.215 and 1.0.

The computer time involved was about 30 seconds on an Amdahl 470 V7 for every 64 time steps. This included calculation of the amplitude(s) of the wave(s) at each time step and various line printer graphs which were produced every 64 time steps (or sometimes more frequently). These graphs included energy versus wavenumber in the x and y directions for the vorticity and density; disturbance amplitudes and E (see equation 4.2.8) versus time; and mean flow distortion versus y. Also line printer contour graphs of the stream function, vorticity and density were included.

4.0 COMPARISONS WITH OTHER NONLINEAR STUDIES AND RESULTS

This study presented an opportunity to compare fully nonlinear initial value problem simulations with existing weakly nonlinear theory. In section 4.1 of this chapter, the single wave weakly nonlinear theory is reviewed in terms of the Landau constant. The method used to compare the present study with this theory is then presented along with the results obtained. In the second section subharmonic interactions are considered. Again, the theory is first reviewed and then the results of this study are presented. Finally, comparisons are made between this and previous numerical simulations.

4.1 Calculation of the Equivalent Landau Constant

In weakly nonlinear or finite amplitude theory, ψ is assumed to be of the form

$$\psi = \int^y \bar{u}(s)ds + \epsilon(A\phi(y)\ \exp(i\alpha x) + *) \qquad (4.1.1)$$

where ϵ is small, ϕ is a neutral or nearly neutral eigenfunction of the corresponding linear problem and A is a function of τ, some slow time scale. Thus ϕ is an eigenfunction of an ordinary differential equation which depends on the exact problem being considered. In this study eigenfunctions of the linear viscous problem were generally used. A few runs with inviscid eigenfunctions were made for comparison purposes. In previous studies neutral or nearly neutral waves were not considered as initial conditions because the inviscid eigenfunctions used were singular. On the other hand, the neutral eigenfunctions for the viscous problems are nonsingular. If for instance $\tau = \alpha\epsilon^2 t$, then we are

actually approximating an amplitude equation of the form

$$(1/A)dA/dt = \alpha c_i + a_2\,\alpha\varepsilon^2|A|^2 + a_4\,\alpha^2\varepsilon^4|A|^4 + o(\varepsilon^6), \qquad (4.1.2)$$

where αc_i is the linear growth rate which is assumed to be small. Weakly nonlinear theory has been developed (cf. Brown, Rosen and Maslowe, 1981) for the case of a single wave solution to a two-dimensional tanh y shear layer with exp(-βtanh y) density profile. It was found that a_2, known as the Landau constant, was dependent on the Prandtl number as well as the wavenumber. However, these results have strong constraints on the range of their validity due to the parallel flow approximation. These conditions are

$$\varepsilon^{-5/3} \ll Re \ll \varepsilon^{-12/7}$$

and

$$(Re)^{1/3} \ll t \ll \varepsilon\, Re.$$

Included in these asymptotic conditions is the condition that $\lambda_c = 1/(\alpha Re\varepsilon^{3p}) \gg 1$ where $p = 1/(1.75 - J(y_c))$ if $J(y_c) < 0.25$ and $p = 2/3$ if $J(y_c) > 0.25$ where J(y) is the local Richardson number and y_c is the critical point. Note that for this case $J(y_c) = J(0) = J_0$. (The quantity λ_c is often denoted by λ in the literature, and in order not to confuse it with the wavelength λ we adopt the notation λ_c used by some researchers. The condition $\lambda_c \ll 1$ implies that the nonlinear critical layer is much thicker than the diffusive critical layer (cf. Maslowe, 1973), whereas linear diffusive theory requires that $\lambda_c \gg 1$. For example, if $\varepsilon = 1/16$ then $101.6 \ll Re \ll 115.9$, and if $Re = 110$ then $4.79 \ll t \ll 6.88$.

Thus, it was not surprising that the calculated equivalent for the Landau constant in the fully nonlinear simulations was not constant. In these runs the Landau constant was approximated by using the values of

A(t) at two adjacent time steps. This was done by considering (4.1.2) to $o(\varepsilon^2)$. Integration of both sides yields

$$|A|^2 = (c_i/\varepsilon^2 + a_2|A|^2)c_0^2 \exp(2\alpha c_i t) \tag{4.1.3}$$

where c_0 is an arbitrary constant. From this two cases arise: $c_i = 0$ and $c_i \neq 0$. If $c_i = 0$ then

$$a_2 = \left[\frac{1}{|A(t_1)|^2} - \frac{1}{|A(t_2)|^2}\right] / (2\alpha\varepsilon^2(t_2 - t_1)) \tag{4.1.4}$$

where A was calculated using equation (3.2.9). Similarly, if $c_i \neq 0$, we have

$$a_2 = \frac{c_i}{\varepsilon^2}\left[\frac{1}{|A(t_1)|^2} - \frac{\exp 2\alpha c_i(t_2 - t_1)}{|A(t_2)|^2}\right] / (\exp 2\alpha c_i(t_2 - t_1)) \tag{4.1.5}$$

However, further runs were made using a body force so that $\bar{u} = \tanh y$, $\bar{\rho} = \exp(-\beta \tanh y)$ were exact solutions of the resulting equations (see the preceding chapter for details). For these simulations, it was found that the calculated equivalent to the Landau constant was close to being a constant. Hence for Re = 110, Pr = 0.72, $\varepsilon = 1/16$, $c_i = 0$, $\alpha = 0.46$, a_2 was calculated to be approximately 4, while Brown, Rosen and Maslowe found $a_2 < 0$. For the same case without a body force, a_2 initially was about 4 but quickly became negative and continued to decrease.

Comparisons were also made with Huerre's results (1980). Huerre considered an unstratified flow with such a body force. For $\varepsilon = o(1/Re)$ $\alpha - \alpha_0 = o(\varepsilon^2)$, where α_0 is the wavenumber of the linearly neutral wave, he found a_2 to be approximately $28.2/\alpha$. This would imply for Re = 100 that a_2 is about 29.9 and for Re = 200 that a_2 is approximately 29.1. In this study, for $\varepsilon = 0.005$, $\alpha = \alpha_0$, and for both Re = 100 ($2\varepsilon = 1/Re$) and Re = 200 ($\varepsilon = 1/Re$) a good comparison with this result was obtained, as shown in Figure 7. The value for a_2 calculated from the fully non-linear initial value problem is sensitive to ε. For example, for Re =

100 a higher value of a_2 was found for $\varepsilon = 0.0025$, a lower value for $\varepsilon = 0.01$ and a negative value for $\varepsilon = 0.04$. However, if $\varepsilon = 0.0025$ it would take a long time for the wave to double in amplitude, even if initial growth rates were maintained. Huerre's results are for a steady state theory while the present results are for the initial value problem. In addition, Huerre's results are valid only for $\varepsilon = o(1/Re)$. Furthermore, higher order nonlinear and viscous effects distort ϕ which in this study is taken to be the initial viscous eigenfunction, while Huerre assumes ϕ to be the inviscid eigenfunction (sech y). Higher order effects may become important in the amplitude equation as well.

The mean flow distortion was also monitored. For the case of the unstratified neutral wave with body force (Re = 100), the mean flow distortion $(\overline{u}(t,y) - \overline{u}(0,y))/\varepsilon^2$ for all cases was antisymmetric within the mixing layer and zero outside the mixing layer. The maximum value of the distortion grows with time in agreement with weakly nonlinear theory. For $\varepsilon = 0.005$ the maximum value is 0, 0.40, 0.61 and 0.73 at the non-dimensional times t = 0, 4, 8 and 12, respectively. Huerre also obtained an antisymmetric mean flow distortion. It is a consequence of the model employed in his theory that the mean flow distortion remains non-zero outside the mixing layer. His maximum distortion of about 1.2 is in reasonable agreement with our results.

4.2 Subharmonic Resonant Interaction

In this section, the weakly nonlinear theory for subharmonic resonant interaction (Maslowe, 1977) will first be reviewed. Consider ψ of the form

$$\psi = \int^y (u(s)ds + (A_1(\tau)\phi_{11}(y)\ \exp(i\alpha(x-ct)) + A_2(\tau)\phi_{21}(y)\ \exp(2i\alpha(x-ct)) + *) \qquad (4.2.1)$$

where α, 2α are the wavenumbers of waves which are neutrally stable according to linear theory. Note that $\tau = \alpha\varepsilon t$ instead of the value $\alpha\varepsilon^2 t$ obtained for the single wave case, implying that changes in the amplitudes occur on a much faster time scale. For this problem c = 0.0. At the next order in ε, secular terms will arise due to the interactions

$$\exp(i\alpha x)\ \exp(i\alpha x) = \exp(2i\alpha x)$$
$$\exp(2i\alpha x)\ \exp(-i\alpha x) = \exp(i\alpha x) \qquad (4.2.2)$$

Variables can be separated if A_1 and A_2 satisfy the equations

$$dA_1/d\tau = \gamma_1 A_1^* A_2 \text{ and } dA_2/d\tau = \gamma_2 A_1^2 \qquad (4.2.3)$$

where γ_1 and γ_2 are constants consisting of ratios of integrals determined by imposing orthogonality conditions on the $o(\varepsilon^2)$ terms. After detailed analysis and computational work, Maslowe found that both γ_1 and γ_2 are real and have the same sign (negative). By setting $A = \frac{1}{2}a\exp(-i\phi)$, a and ϕ real functions, the above system becomes

$$da_1/d\tau = \tfrac{1}{2}\gamma_1 a_1 a_2 \cos\theta \qquad (4.2.4)$$

$$da_2/d\tau = \tfrac{1}{2}\gamma_2 a_1^2 \cos\theta \qquad (4.2.5)$$

$$d\phi_1/d\tau = -\tfrac{1}{2}\gamma_1 a_2 \sin\theta \qquad (4.2.6)$$

$$a_2 d\phi_2/d\tau = \tfrac{1}{2}\gamma_2 a_1^2 \sin\theta \qquad (4.2.7)$$

where $\theta = 2\phi_1 - \phi_2$ is sometimes called the relative phase. This terminology will be employed here. Note that from now on, a_2 refers to twice the absolute value of the amplitude of the short wave in a subharmonic interaction and not the Landau constant, as is obvious from its context.

From equations (4.2.4) and (4.2.5), one can derive the energy integral

$$a_1^2 - (\gamma_1/\gamma_2)a_2^2 = E \tag{4.2.8}$$

where E is a constant. Thus a_1 and a_2 may both grow at the same time by extracting energy from the mean flow if γ_1 and γ_2 have the same sign, as they do in this case.

From the above equations,

$$d^2a_1^2/d\tau^2 - \tfrac{1}{2}\gamma_1\,\gamma_2\,a_1^2(3a_1^2 - 2E) = 0 \tag{4.2.9}$$

By multiplying both sides of this equation by $da_1^2/d\tau$ and then integrating we obtain

$$(da_1^2/d\tau)^2 = \gamma_1\,\gamma_2\,a_1^4(a_1^2 - E) + C \tag{4.2.10}$$

where C is a constant of integration. From this, the phase plane for a_1^2 was plotted (Figure 8). For the case Re = 200 and Pr = 0.72 Maslowe calculated $\gamma_1 = -35.9$ and $\gamma_2 = -0.54$. The phase plane depicted is for this case with E = 1.1 which corresponds to $a_1(0) = 8.3$ $a_2(0) = 8.3(2\sqrt{0.375})$. Note that the only possible trajectories correspond to the ones where C is less than or equal to zero. Since the direction of increasing τ along these trajectories corresponds to the direction of increasing $da_1/d\tau$, the weakly nonlinear theory predicts that if the initial relative phase $\theta(0)$ is in the range $\pi/2 < (0) < 3\pi/2$ then, to this order, a_1 (and a_2) can become unbounded in time. Note that since

$$d^2a_1^2/d\tau^2 = \tfrac{1}{2}\gamma_1\,\gamma_2(a_1^2 + 2\gamma_1/\gamma_2 a_2^2) \tag{4.2.11}$$

the second derivative of a_1^2 is always greater than zero if at least one of a_1, a_2 is non-zero. Thus, even though $da_1/d\tau < 0$ for some initial relative phases, eventually $da_1/d\tau$ becomes greater than zero.

I have worked out the governing equations when these are not neutral modes. Assuming $a = a(t,\tau)$ and that αc_i is the linear growth rate,

$$da_1/dt = \alpha c_{i_1} a_1 + \tfrac{1}{2}\varepsilon\alpha \gamma_1 a_1 a_2 \cos\theta + o(\varepsilon^2) \tag{4.2.12}$$

$$da_2/dt = 2\alpha c_{i_2} a_2 + \tfrac{1}{2}\varepsilon\alpha \gamma_2 a_1^2 \cos\theta + o(\varepsilon^2) \tag{4.2.13}$$

with the equations for ϕ_1, ϕ_2 remaining unchanged. We then obtain the following equations

$$d^2 a_1^2/dt^2 = 4\alpha^2 c_{i_1}^2 a_1^2 + 4\varepsilon \alpha^2 c_{i_1} \gamma_1 a_1^2 a_2 \cos\theta + 2\varepsilon \alpha^2 c_{i_2} \gamma_1 a_1^2 a_2 \cos\theta + \varepsilon^2 \alpha^2 \gamma_1 a_1^2 (\tfrac{1}{2}\gamma_2 a_1^2 + \gamma_1 a_2^2) + o(\varepsilon^3) \tag{4.2.14}$$

$$d^2 a_2^2/dt^2 = 16\alpha^2 c_{i_2}^2 a_2^2 + 2\varepsilon\alpha^2 \gamma_2 a_1^2 a_2 \cos\theta(c_{i_1} + 3c_{i_2}) + \varepsilon^2 \alpha^2 \gamma_2 a_1^2 \cos\theta(\cos\theta + \sin\theta)(\gamma_1 a_2^2 + \tfrac{1}{2}\gamma_2 a_1^2) + o(\varepsilon^3) \tag{4.2.15}$$

Numerical simulations were conducted with initial conditions consisting of subharmonic pairs of linearly neutral or nearly neutral waves as suggested by the weakly nonlinear theory. Along with the single neutral wave runs mentioned in the preceding section, these are the main new results of this study.

For the numerical simulations of subharmonic resonant interactions $|A_2(0)| = \sqrt{0.375}$, matching the normalization of $A(0)$ in the single wave case. Some of the results obtained from these simulations are presented in the three pairs of Figures 9&10, 11&12 and 13&14. Of each pair, one figure is a plot of $a_1/2$ versus t for the cases $\theta(0) = 0$, $\pi/2$ and π; $|A|$ versus t for a single wave is shown for comparison. The other figure is a corresponding plot of $a_2/2$, with $|A|$ for some single wave cases.

In Figures 9 to 12 are found the amplitudes of the waves from two groups of runs consisting of the resonant interactions of waves which are neutral according to linear theory, along with comparison runs of (initially) single wave cases. Plotted in these figures are $a_1/2$, $a_2/2$, the absolute values of the waves, with wavenumbers 0.321461, 0.642992 respectively, versus the non-dimensional time t with the one exception in Figure 12. For these cases Re = 200, Pr = 0.72 and $J_0 = 0.216516$.

Figures 9 and 10 demonstrate the effect of varying the initial relative phase when $a_2(0) = a_1(0)$ $(= 2\sqrt{0.375})$ and $\epsilon = 0.01$ and also compares these cases with initially just one of the waves. Thus in Figure 9, a_1 versus t is plotted for the cases when $\theta(0) = 0, \pi/2, \pi$ and also when the long wave is initially alone (with the same initial amplitude). Note that initially the $a_1(t)$ corresponding to $\theta(0) = \pi$ grows fastest and $\theta(0) = 0$ the slowest; however, after about 3.5 non-dimensional time units the opposite is true. In fact, for $\theta(0) = \pi$ the amplitude decays. For $\theta(0) = \pi/2$ $a_1(t)/2$ is very close to the amplitude obtained when this wave is started by itself. Thus, qualitatively, Figure 9 would imply that the amplitude behaves as if $\gamma_1 < 0$ initially, then at a later time as if γ_1 has become greater than zero. This is quite different from the weakly nonlinear theory in which $\gamma_1 < 0$ and is constant. However, the weakly nonlinear theory predicts the importance of $\theta(0)$. It also predicts that cases with $\theta(0) = \pi/2$ and with initially just the short wave alone should result in amplitudes which remain close (for $t < o(1/\epsilon^2)$), as found in this study.

In Figure 10, $a_2/2$ versus t was plotted for the cases corresponding to Figure 9, $\theta(0) = 0, \pi/2, \pi$, and also for initially the short wave alone (with the same initial amplitude). Note that $a_2(t)$ for the short

wave alone and the resonant case with $\theta(0) = \pi/2$ are almost exactly the same. In fact there is little variation in $a_2(t)$ among all four cases. An interesting point is that initially a_2 increases slightly except for the case $\theta(0) = \pi$.

Figures 11 and 12 demonstrate that the initial relative phase is much more important when $a_1(0) = 30a_2(0)$ ($\epsilon = 0.004$) than for the case $a_1(0) = a_2(0)$, which is reflected in the change in the scaling of the graphs. In Figures 9 and 10 the $a_1/2$, $a_2/2$ axes have a total range of 0.025 while in Figures 11 and 12 the range is 1.2. For all four figures the time t varies between 0 and 8.

In Figure 11 the cases depicted consist of $a_1/2$ for the resonant interaction cases with $\theta(0) = 0$, $\pi/2$ and π and a reference case of initially just the long wave (same initial amplitude). These results are similar to those obtained when $a_1(0) = a_2(0)$ (Figure 9). However, the interaction is stronger for $a_2(t)$ when $a_1(0) >> a_2(0)$ as can be seen by comparing Figure 12 with Figure 10. The results qualitatively correspond to a weakly nonlinear theory with γ_2 small and positive. The function $a_2(t)$ is plotted in Figure 12 for the resonant interaction cases with $\theta(0) = 0$, $\pi/2$, π, and for the three initially single wave cases corresponding to $a_2(0) = 0$, $a_1(0) = 0$ and $a_1(0) = a_2(0) = 0$ along with the corresponding linearly fastest growing wave. The last two have the same initial amplitude as a_2 in the resonant cases. For comparison purposes, growth rates estimated by $\ln(a(t)/a(t-dt))/dt$, where dt is the time step, were calculated for the initial value problems at various times t for $a(t) = a_1(t)$ and $a_2(t)$. For this fastest growing wave, linear theory gives a growth rate αc_i of about 0.025. The computed growth rate for the first time step of this initial value problem for ϵ

= 0.004 was 0.026, and at t = 8 it was 0.020. The initial growth rate for a_2 when $\theta(0) = 0$ was 0.222; for $\theta(0) = \pi/2$, 0.003; for $\theta(0) = \pi$, -0.277. These rates, however, change quite rapidly. At t = 8 the growth rate for a_2 when $\theta(0) = 0$ is -0.072; for $\theta(0) = \pi/2$, -0.051; and for $\theta(0) = \pi$, 0.248. Although it is not clear whether $a_2(t)$ for $\theta(0) = \pi$ will eventually become larger than $a_2(t)$ for $\theta(0) = 0$, it does seem likely from Figure 12, that despite its large initial growth rate $a_2(t)$ for $\theta(0) = 0$ will eventually be overtaken by the wave which was initially the fastest growing of linear theory.

Various other resonant pairs were tried as initial conditions. As well, variations in ε, the initial amplitudes and the relative phase were investigated. The greatest initial growth rates occurred when $a_1(0) >> a_2(0)$, and the behavior was qualitatively similar to that shown in Figures 11 and 12. The cases tried included the fastest growing wave according to linear theory and a damped wave (α = 0.46, 0.23 respectively, Re = 200, Pr = 0.72, J_0 = 0.20), two almost neutral but linearly unstable waves, one neutral and one almost neutral but linearly unstable wave, and a stable wave with the fastest growing wave at J_0 = 0.20. The fastest initial growth (and decay) rates and most sustained growth for $a_2(t)$ were obtained at lower Richardson numbers. These rates were quite impressive for the case of a neutral wave and the linearly fastest growing wave. For example, cases for which α = 0.225, 0.45, Re = 200, Pr = 0.72, J_0 = 0.174154 are shown in Figures 13 and 14. Note that longer times are involved, and except for one case with a maximum of 40, all extend to t = 32. Also the $a_1/2$ and $a_2/2$ axes have a total range of 4.0.

In Figure 13 $a_1(t)/2$ and $|A|$ are plotted for the four cases $\theta(0)$ = 0, $\pi/2$, π and initially just the neutral wave. As found for the two

neutral wave cases in Figures 9 and 11, there is a cross over in the amplitudes. Although the $\theta(0) = \pi$ cases begin by growing the fastest, the $a_1(t)$ corresponding to $\theta(0) = 0$ cases eventually have the largest amplitudes. Also for $\theta(0) = \pi/2$ and initially the (long) neutral wave alone $a_1(t)$ is almost the same. Initial growth rates are of the order of 0.001. These increase with time and then decrease. A maximum growth rate of about 0.007 is obtained when $\theta(0) = 0$ at about $t = 7$.

In Figure 14 $a_2(t)$ is plotted for the four cases in Figure 13, as well as $|A|$ of initially the short (fastest growing) wave alone. Initial growth rates were 0.294 for $\theta(0) = 0$; 0.004 for $\theta(0) = \pi/2$; -0.179 for $\theta(0) = \pi$. However, by $t = 32$ the amplitude of the fastest growing wave alone, with an initial growth rate of 0.061, appears to be overtaking that of the corresponding wave for $\theta(0) = 0$ which has an initial growth rate approximately five times greater. Note also that for $\theta(0) = \pi$, the wave which is the one that linear theory predicts will grow the fastest actually decays initially. Eventually it does start growing, as predicted by equation (4.2.15), assuming γ_1 small.

Figures 15 to 18 are contour graphs for two of the cases whose amplitudes are depicted in Figures 13 and 14. Figures 15 and 16 are density contour graphs for the cases $\theta(0) = 0$ and $\theta(0) = \pi$ respectively and Figures 17 and 18 are vorticity contour graphs for the same cases. With such a great difference between $a_1(0)$ and $a_2(0)$, there is not much of a change in the contour graphs.

Other runs were made with higher Reynolds numbers with the fastest growing wave and corresponding (long) neutral wave. It was found that a lower Richardson number had a greater effect on initial growth rates

than using the exact fastest growing wave. Thus for $\theta(0) = 0$, $\alpha = 0.225, 0.45$, $Re = 400$, the initial growth rate for the short wave was 0.3142 while for $\alpha = 0.2275, 0.455$ and $Re = 400$ the initial growth rate for the neutral (short) wave was 0.3201. Note from these results that no sudden change in growth rates was found with increasing Re.

Patnaik, Sherman and Corcos (1976) found that the relative phase was important although their runs did not consist of neutral waves but of two unstable waves ($\alpha = 0.215$ and 0.43, $Re = 50$, $Pr = 0.72$, $J_0 = 0.07$). As a test for the resonant interaction scheme, runs were made with initial conditions similar to those used by Patnaik (1973) and to those used by Patnaik, Sherman and Corcos (1976). Figures 19, 20 and 21 consist of density contour graphs where the density is shown evolving for three different initial conditions. These runs used viscous eigenfunctions at a smaller initial amplitude than those used by Patnaik who used inviscid eigenfunctions. Other conditions (e.g. the initial ratio of amplitudes) were identical. Other runs were made duplicating Patnaik's runs, i.e. using error function profiles, inviscid eigenfunctions, and the equivalent initial amplitudes. However these runs were not taken out to maximum amplitude as it was felt the CPU time could be better used for other cases. Figure 19 shows the development of the density when $Re = 50$, $Pr = 0.72$, $\alpha = 0.215$, $J_0 = 0.07$, $\epsilon = 0.0616$ with the disturbance centred at $x = \lambda/4$. Figures 20 and 21 illustrate the case when the same wave interacts with a wave having twice its wavelength, which in this case is the fastest growing wave of linear theory. This wave has a wavenumber of 0.43 and its initial amplitude was taken to be $\epsilon = 0.0326$. In Figure 20 the long wave is initially centred at $x = \lambda/4$ as in Figure 19 and thus $\theta(0) = \pi$. In Figure 21 it is initially

centred at $x = \lambda/2$ and hence $\theta(0) = 0$ initially. Note that the development at first varies quite a bit among the cases corresponding to Figures 20 and 21 while for large dimensionless times t a "final" state consisting of the long wave alone was the general result. Of course, eventually the long wave disturbance will dissipate as well.

In Figures 22 and 23, a_1 and a_2, respectively, are given as a function of time for the three cases corresponding to Figures 19, 20, 21. The linear growth rates for these two waves are 0.086 for the long wave and 0.119 for the short wave. Initial growth rates for the short wave are 0.093 for $\theta(0) = \pi$; 0.091 for initially just the short wave; and 0.090 for $\theta(0) = 0$. For the long wave these become 0.116 for $\theta(0) = \pi$ and 0.120 for $\theta(0) = 0$.

As in the other cases closer to the neutral curve, the graphs of the amplitudes of the short wave cross over at a later time and the wave for which $\theta(0) = 0$ becomes the fastest growing and eventually the one with the largest amplitude. For the case $\theta(0) = 0$ the short wave goes to zero, then θ changes to π and the short wave grows, that is, there is a time t where θ jumps from 0 to π. However, considering the amplitude A_2 itself as a complex function, we see that A_2 is continuous at this value of t, i.e. the real and imaginary parts of A_2 are continuous but change sign while the phase is discontinuous.

The fact that a_2 becomes zero and then grows larger than its initial value could be explained by the weakly nonlinear theory, equation (4.2.15), which implies that the second derivative of a_2 is much greater than zero. Thus, this behavior can be explained if $\gamma_2 < 0$. However, the sign change in the real and imaginary parts of A_2 implies that there is a jump discontinuity in ϕ_2 and in the first derivative of a_2.

A run was also made with two neutral waves, with Re = 200, Pr = 0.72 (J_0 = 0.174154), $\theta(0) = 0$, $\varepsilon = 0.08$ and $a_1(0) = 1.5\ a_2(0)$. This case resulted in oscillatory behavior in A_2 as well. For this case A_2 oscillated between positive and negative real values. This suggests that, at least for some cases, it is not completely valid to consider A_1, A_2 in terms of their phases and amplitudes, and that perhaps A_1, A_2 should be considered in terms of their real and imaginary parts.

5. SUMMARY AND CONCLUSIONS

In this study the fully nonlinear, time dependent, two dimensional, Boussinesq equations were solved for various initial conditions. The primary motivation of this study was to investigate the subharmonic resonance of two linearly neutral or nearly neutral waves. The weakly nonlinear theory of Maslowe (1977) suggests that, under suitable initial conditions (the initial relative phase $\theta(0)$ equal to π), that the subharmonic resonant interaction of two neutral waves will result in the growth of both of their amplitudes at the same time. The simultaneous growth of both of these amplitudes also occurred in this study for initial periods of time (see Figures 11 and 12) but for a different relative phase ($\theta(0) = 0$) than predicted by the theory. Large growth rates could result from this type of two wave interaction. This was supported, in part, by the present study.

Large initial growth rates were obtained for the short wave when its amplitude was initially much smaller than the long wave with these growth rates dependent on the initial relative phase as predicted by the theory. However, growth rates obtained for the long neutral wave were not as great as those predicted by the theory and the growth rates for the short wave quickly dropped off. In general the long neutral or nearly neutral wave continued to grow after the short wave reached maximum amplitude. A possible explanation for this phenomenon is that it is due to the growth of the shear layer. The non-dimensional wavenumber of the disturbance is inversely proportional to the shear layer thickness. Hence this has the effect of increasing the non-dimensional wavenumber. A long neutral wave becomes stable while a short neutral wave becomes

unstable before eventually becoming stable.

For example, for the cases with initial conditions consisting of a short neutral wave and the fastest growing wave with $\epsilon = 0.004$, $a_1(0) = 30\ a_2(0)$, Re = 200, Pr = 0.72 and $J_0 = 0.174$, after 8 non-dimensional time steps, i.e. at t = 8, the shear layer had increased in thickness by 9 percent. At t = 32, the shear layer thickness had increased by 24 percent for $\theta(0) = 0, \pi/2$ and 23 percent for $\theta(0) = \pi$. The $\theta(0) = 0$ case was taken out to t = 40, at which time the shear layer thickness had increased by 28 percent.

Similar results were obtained for cases corresponding to initially two linearly neutral waves. At t = 8 for two neutral waves with Re = 200 ($J_0 = 0.174154$), Pr = 0.72, $\epsilon = 0.004$ and $a_1(0) = 30\ a_2(0)$ the shear layer increased by about 12 percent. For a similar case only with $\epsilon = 0.08$, $a_1(0) = 1.5\ a_2(0)$ and $\theta(0) = 0$, implying the long wave has the same initial amplitude as in the preceding case, at t = 8 there was a 19 percent increase in the shear layer. For this case, at t = 56, the shear layer had increased by 47 percent. Figure 24 depicts the distortion of the mean flow from its original profile, i.e. $(\bar{u}(40,y) - \bar{u}(o,y))/\epsilon^2$, for this case at this time (t = 56).

Thus, as could be expected from these results, for $a_1(0)$, $a_2(0)$ having approximately the same magnitude there was even less resemblance with the theory. For these cases, for large enough ϵ, the amplitude of the short wave oscillated and that of the long wave grew to maximum amplitude and then decreased. For smaller values of ϵ, e.g. $\epsilon = 0.025$, the growth rates of the amplitudes of both the long and short waves oscillated. An oscillating amplitude with changes in the signs of its

real and imaginary parts, as occurred for certain cases, would seem difficult, if not impossible, to model in terms of phase and amplitude as done in the theory of Maslowe (1977).

When $a_1(0)$ was much smaller than $a_2(0)$ the results also were very different from the theory. In general, small oscillations in the growth rates of the amplitudes occurred.

Two effects control the growth of a shear layer. These are the viscosity and the Reynolds stress. Without a disturbance, the shear layer grows like $\sqrt{1+t/(2Re)}$. A single wave disturbance causes an $o(\varepsilon^2)$ distortion. It is possible that with much larger Reynolds numbers and small enough ε closer agreement, at least for some cases, could be attained with the resonant interaction theory of Maslowe (1977). Alternatively, if a theory could be developed which includes mean flow distortion and is derived in terms of the real and imaginary parts of the amplitudes, perhaps it would predict results in closer agreement to those of this study.

Comparisons were also made with the single wave theory. In unstratified flows linearly neutral waves with a body force grew at rates which agree very well with Huerre's (1980) calculations of the corresponding Landau constant within a small range of ε. In these numerical simulations the mean flow distortion was in satisfactory agreement with Huerre's results. Comparisons were also made with the low J_0 subharmonic resonant interaction numerical simulations of Patnaik (1973) and Patnaik, Sherman and Corcos (1976). These runs resulted in interactions similar to vortex pairing; the outcome was a strong function of the initial relative phase as found by Patnaik and Patnaik et al. For these cases there were large increases in the shear layer thickness, as

would be expected from the preceding remarks. At $t = 64$, for example, with $\theta(0) = 0$, $\varepsilon = 0.0326$, $a_1(0) = 1.89\ a_2(0)$, $Re = 50$, $\alpha = 0.215, 0.43$, $J_0 = 0.07$, it had increased 80 percent. The mean flow distortion for these cases was qualitatively the same as those for the cases closer to the neutral curve. This and the fact that the real and imaginary parts of A_2 changed sign in this case under similar conditions for which they changed sign with two neutral waves is remarkable.

Finally, it should be reiterated, as mentioned indirectly in the preceding chapter, for the cases considered, results were qualitatively similar with no sudden changes for $Re = 50$ up to $Re = 600$. Thus, the observations of Woods (1969) and the calculations of Peltier and Davis (1979) are not supported by the present results.

BIBLIOGRAPHY

Abe, K. and Inoue, O. 1980 Fourier expansion solution of the Korteweg-de Vries equation. J. Comp. Phys. 34, 202-210.

Brown, S.N., Rosen, A.S. and Maslowe, S.A. 1981 The evolution of a quasi-steady critical layer in a stratified viscous shear layer. Proc. Roy. Soc. Lond. A 375, 271-293.

Browning, K.A. 1971 Structure of the atmosphere in the vicinity of large-amplitude Kelvin-Helmholtz billows. Quart. J. Roy. Met. Soc. 97, 283-289.

Chorin, A.J. 1973 Numerical study of slightly viscous flow. J. Fluid Mech. 57, 785-796.

Freymuth, P. 1966 On transition in a separated laminar boundary layer. J. Fluid Mech. 25, 683-704.

Gottlieb, D. and Orszag, S.A. 1977 Numerical analysis of spectral methods: theory and applications. SIAM Regional Conference Series in Appl. Math. 26.

Haidvogel, S.N., Robinson, A.R. and Schulman, E.E. 1980 The accuracy, efficiency, and stability of three numerical models with applications to open ocean problems. J. Comp. Phys. 34, 1-53.

Huerre, P. 1980 The nonlinear stability of a free shear layer in the viscous critical layer regime. Phil. Trans. Roy. Soc. Lond. A 293, 643-675.

Kelly, R.E. 1967 On the stability of an inviscid shear layer which is periodic in space and time. J. Fluid Mech. 27, 657-689.

Leonard, A. 1980 Review: Vortex methods for flow simulation. J. Comp. Phys. 37, 289-335.

Maslowe, S.A. 1973 Finite-amplitude Kelvin-Helmholtz billows. Bound. Layer Met. 5, 43-52.

Maslowe, S.A. 1977 Weakly nonlinear stability theory of stratified shear flows. Quart. J. Roy. Met. Soc. 103, 769-783.

Maslowe, S.A. and Thompson, J.M. 1971 Stability of a stratified free shear layer. Phys. Fluids 14, 453-458.

McGoldrick, L.F. 1970 On Wilton's ripples: a special case of resonant interactions. J. Fluid Mech. 42, 193-200.

Patnaik, P.C. 1973 A numerical study of finite amplitude Kelvin-Helmholtz waves. Ph.D. thesis, Fluid Mechanics Division, University of California, Berkeley.

Patnaik, P.C., Sherman, F.S. and Corcos, G.M. 1976 A numerical simulation of Kelvin-Helmholtz waves of finite amplitude. J. Fluid Mech. 73, 215-240.

Peltier, W.R. and Davis, P.A. 1979 Some characteristics of the Kelvin-Helmholtz and resonant overreflection modes of shear flow instability through vortex pairing. J. Atmo. Sci. 36, 2394-2412.

Riley, J.J. and Metcalfe, R.W. 1980 Direct numerical simulation of a perturbed, turbulent mixing layer. AIAA Paper, no. 80-0274.

Sato, H. 1959 Further investigation on the transition of two-dimensional separated layer at subsonic speeds. J. Phys. Soc. Japan 14, 1797-1810.

Winant, C.D. and Browand, F.K. 1974 Vortex pairing: the mechanism of turbulent mixing layer growth at moderate Reynolds number. J. Fluid Mech. 63, 237-355.

Woods, J.D. 1969 On Richardson's number as a criterion for laminar-turbulent-laminar transition in the ocean and atmosphere. Rad. Sci. 4, 1289-1298.

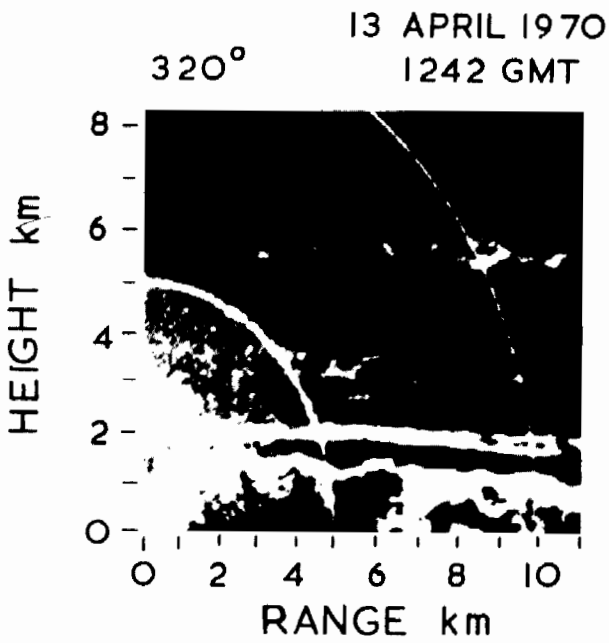

Figure 1: Radar picture showing clear air turbulence centred at an altitude of 5.6 km. Note the sinusoidal structure (Browning, 1971)

Figure 2: Vortex pairing in a transitional free shear layer as observed in smoke-flow experiments (Freymuth, 1966)

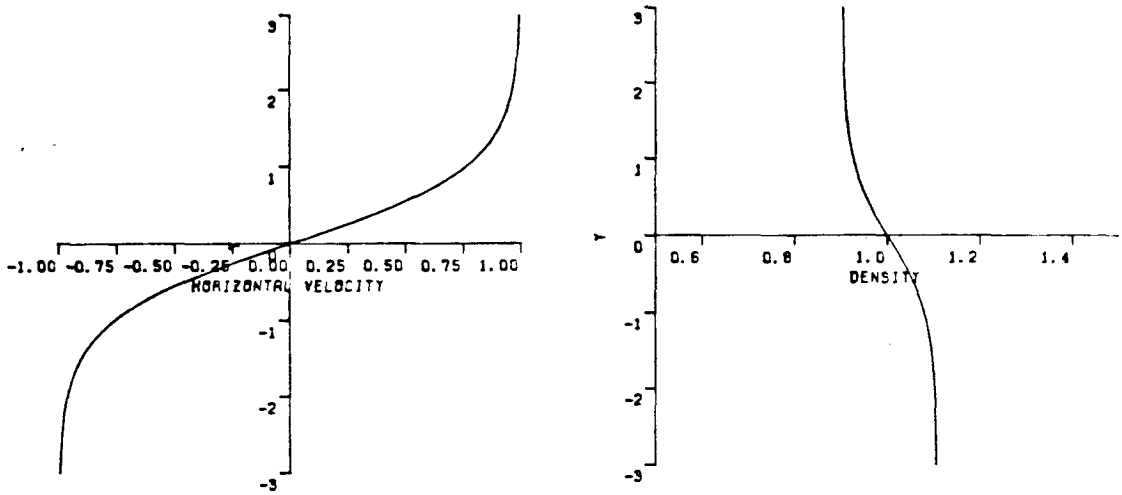

FIGURE 3: HOLMBOE FLOW

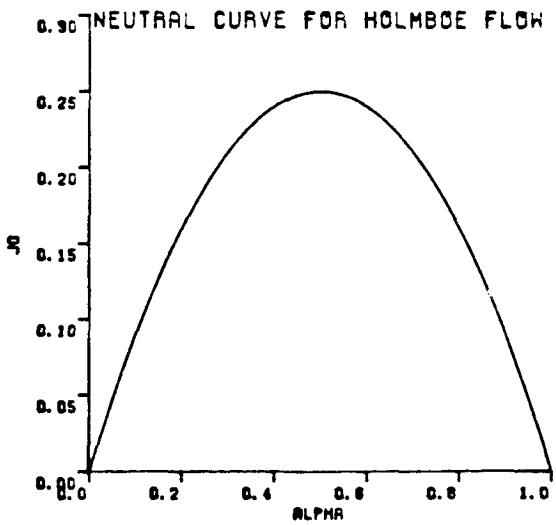

FIGURE 4

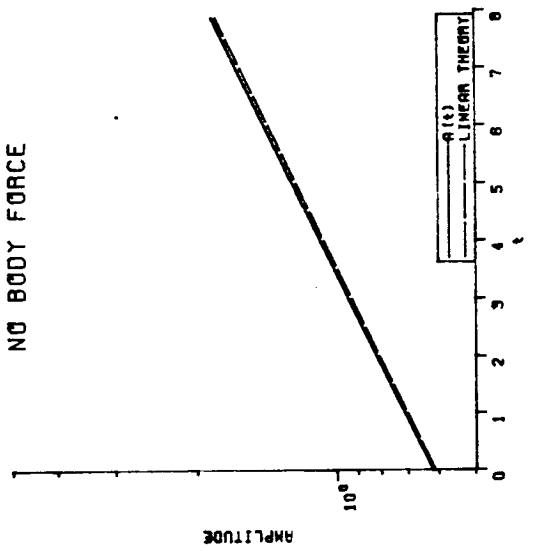

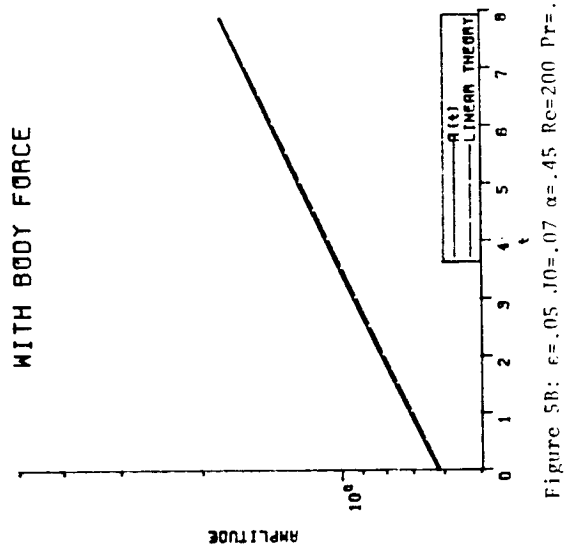

Figure 5B: ε=.05 .10=.07 α=.45 Re=200 Pr=.72

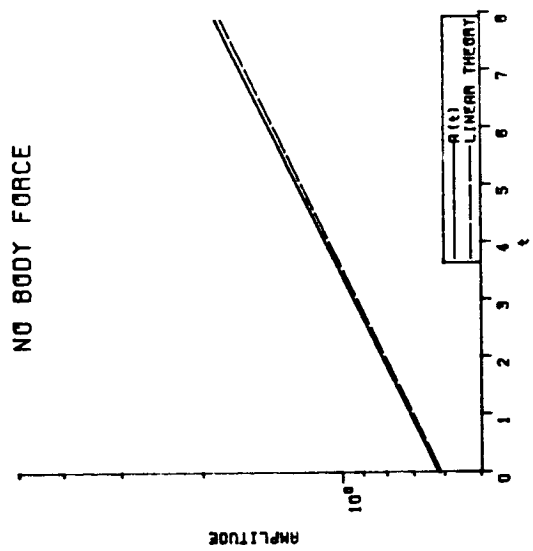

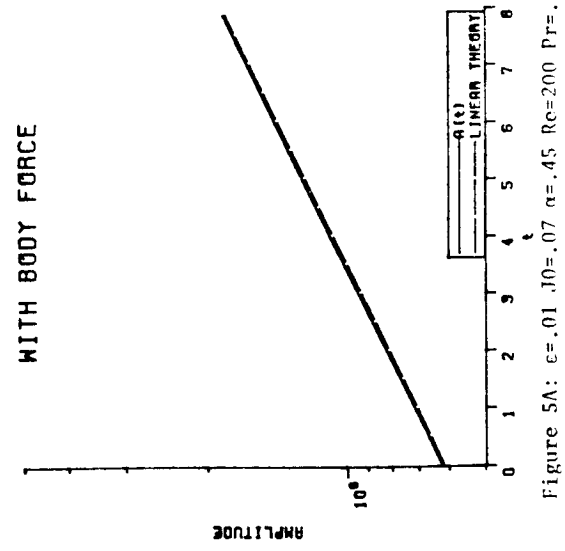

Figure 5A: ε=.01 .10=.07 α=.45 Re=200 Pr=.72

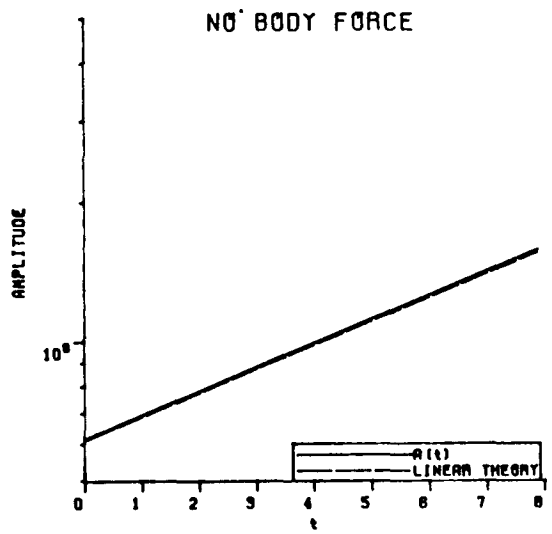

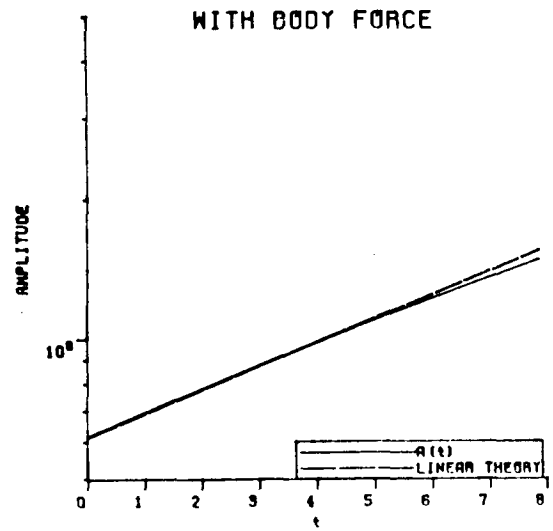

Figure 6A: ε=.01 J0=.07 α=.43 Re=50 Pr=.72

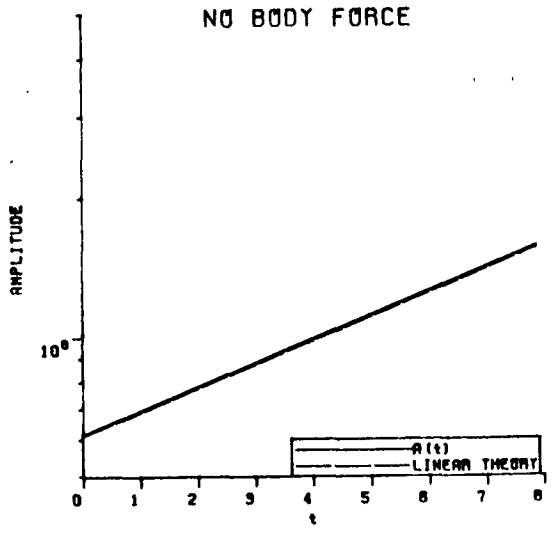

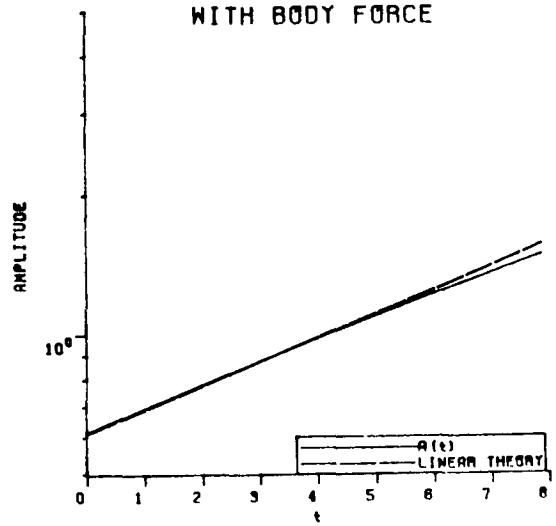

Figure 6B: ε=.05 J0=.07 α=.43 Re=200 Pr=.72

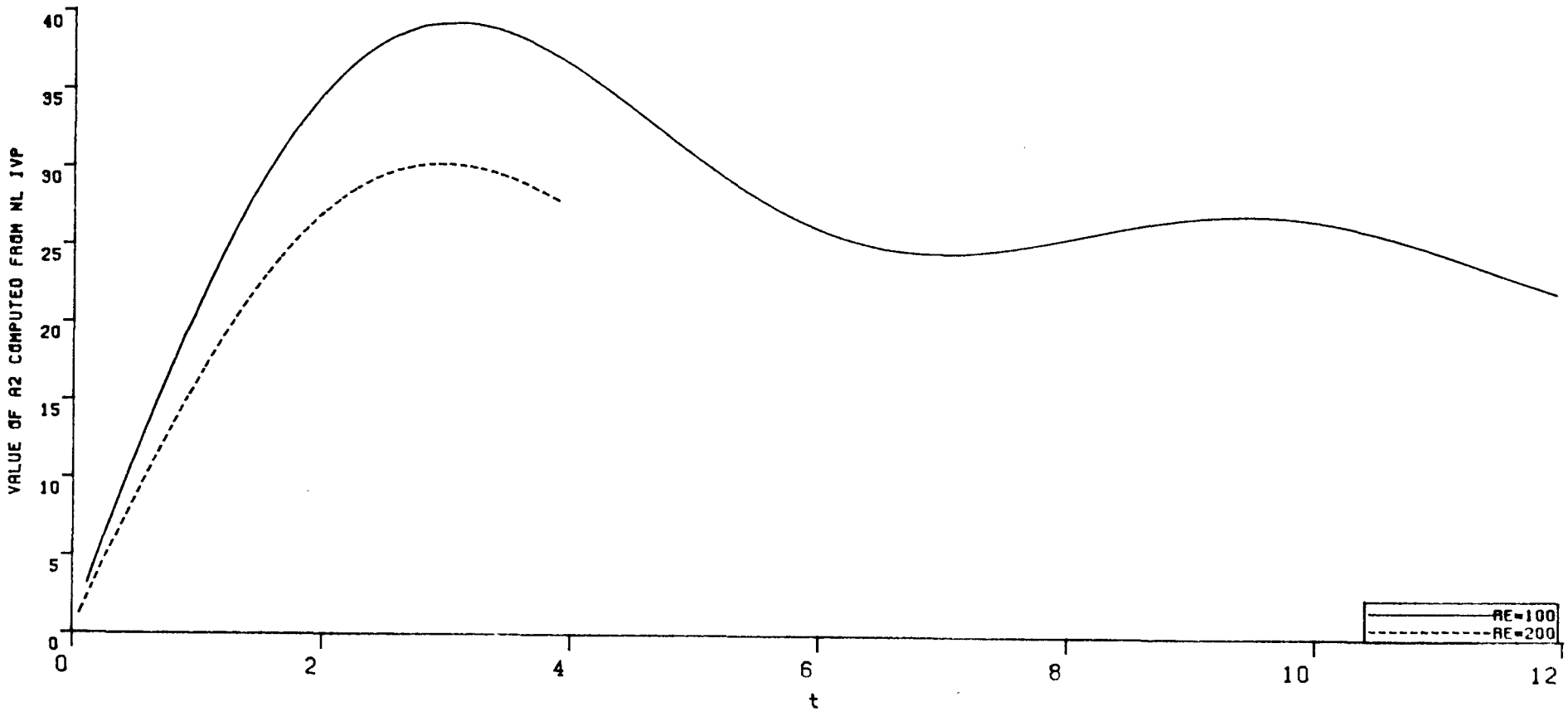

FIGURE 7: J0=0 CI=0.0 EPS=.005 WITH BODY FORCE
HUERRE'S RESULT: A2=29.9 FOR RE=100, A2=29.1 FOR RE=200

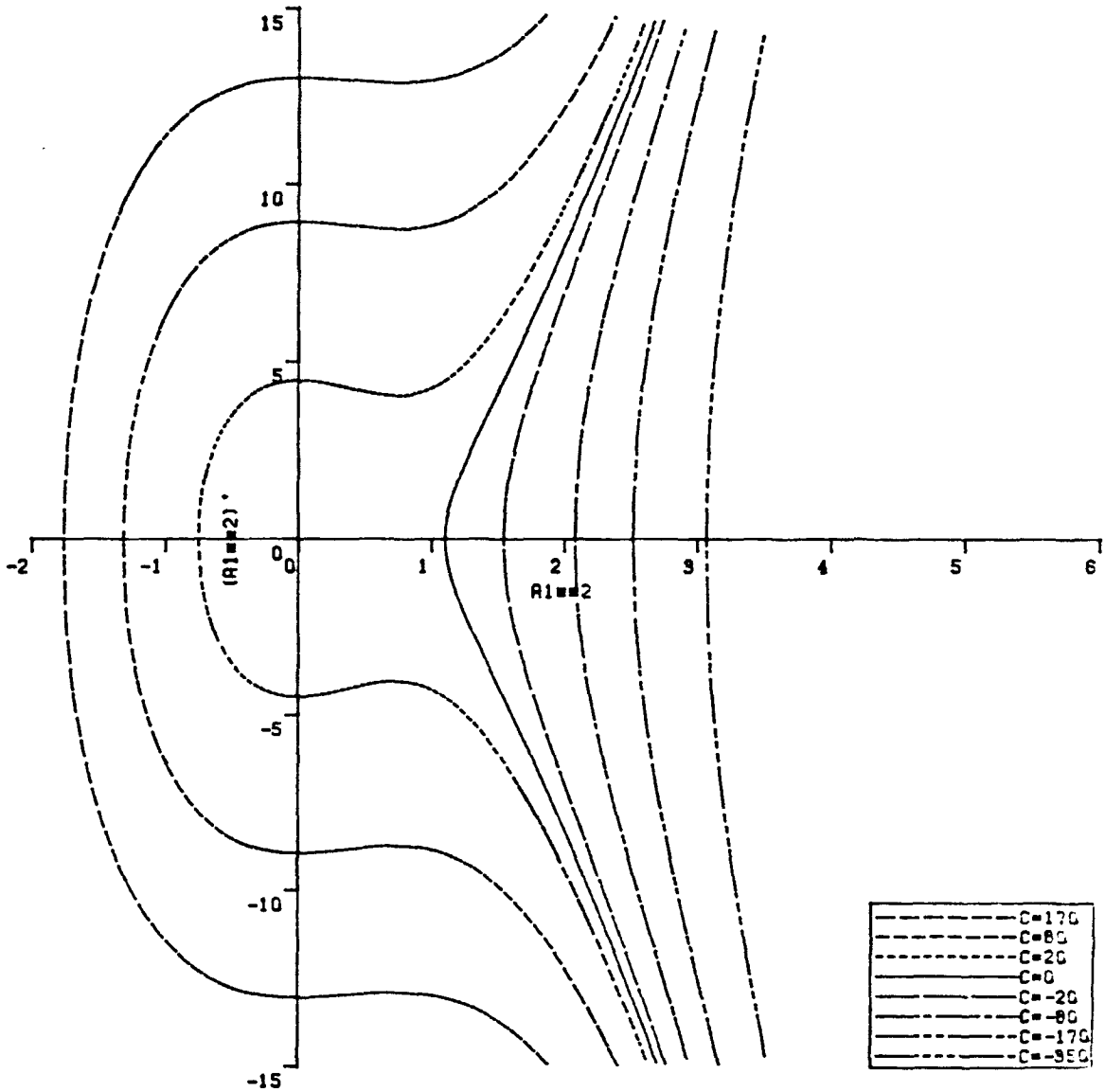

FIGURE 8: PHASE PLANE FOR A1**2 WITH G1=-35.9 G2=-.54
E=1.1 CORRESPONDING TO RE=200 PR=.72 A1(0)=(8.3)A2(0)

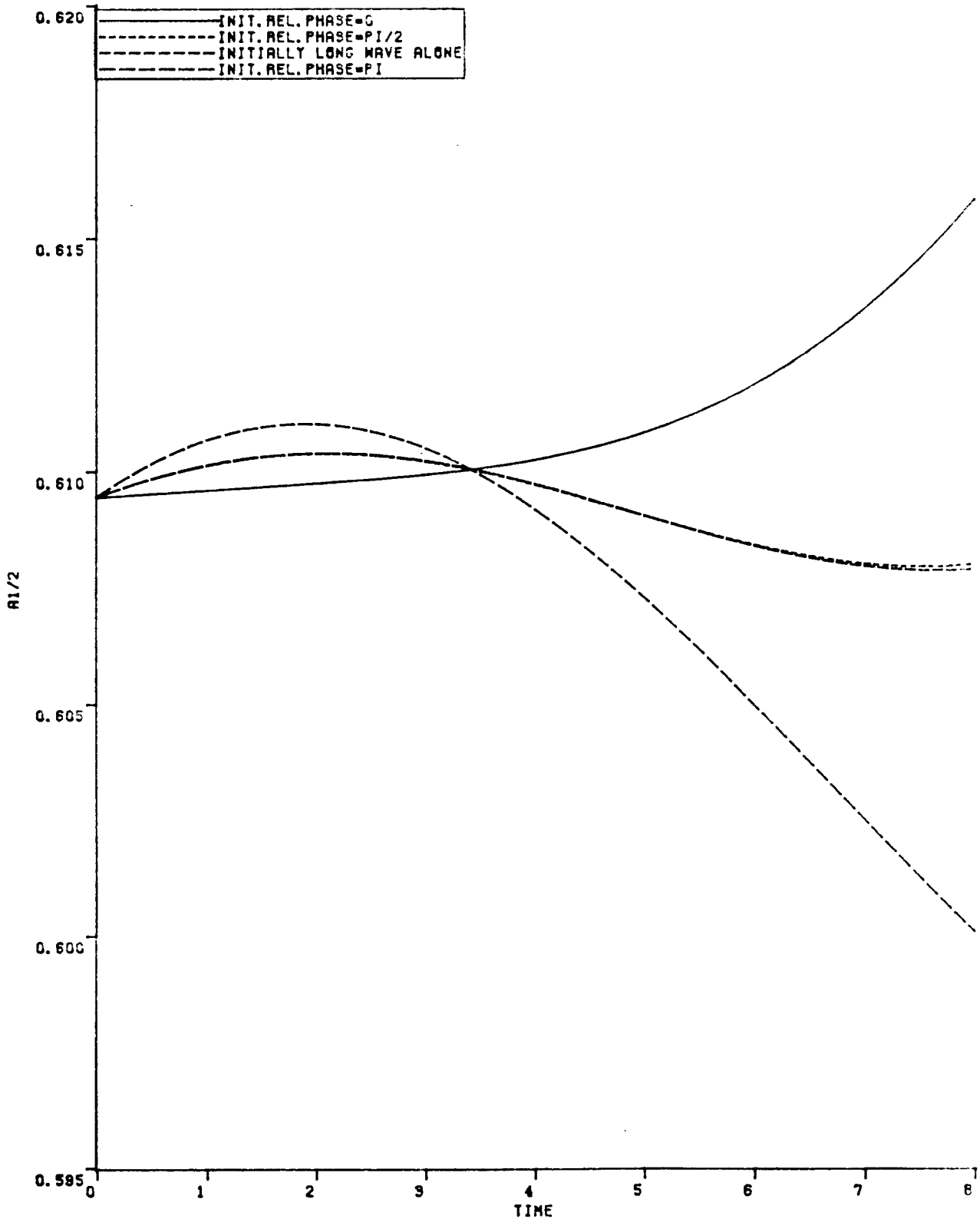

FIGURE 9: LONG WAVE OF TWO NEUTRAL WAVES, A1(0)=A2(0)
RE=200 PR=.72 JO=.217 ALPHA=.321,.642 EPS=.01

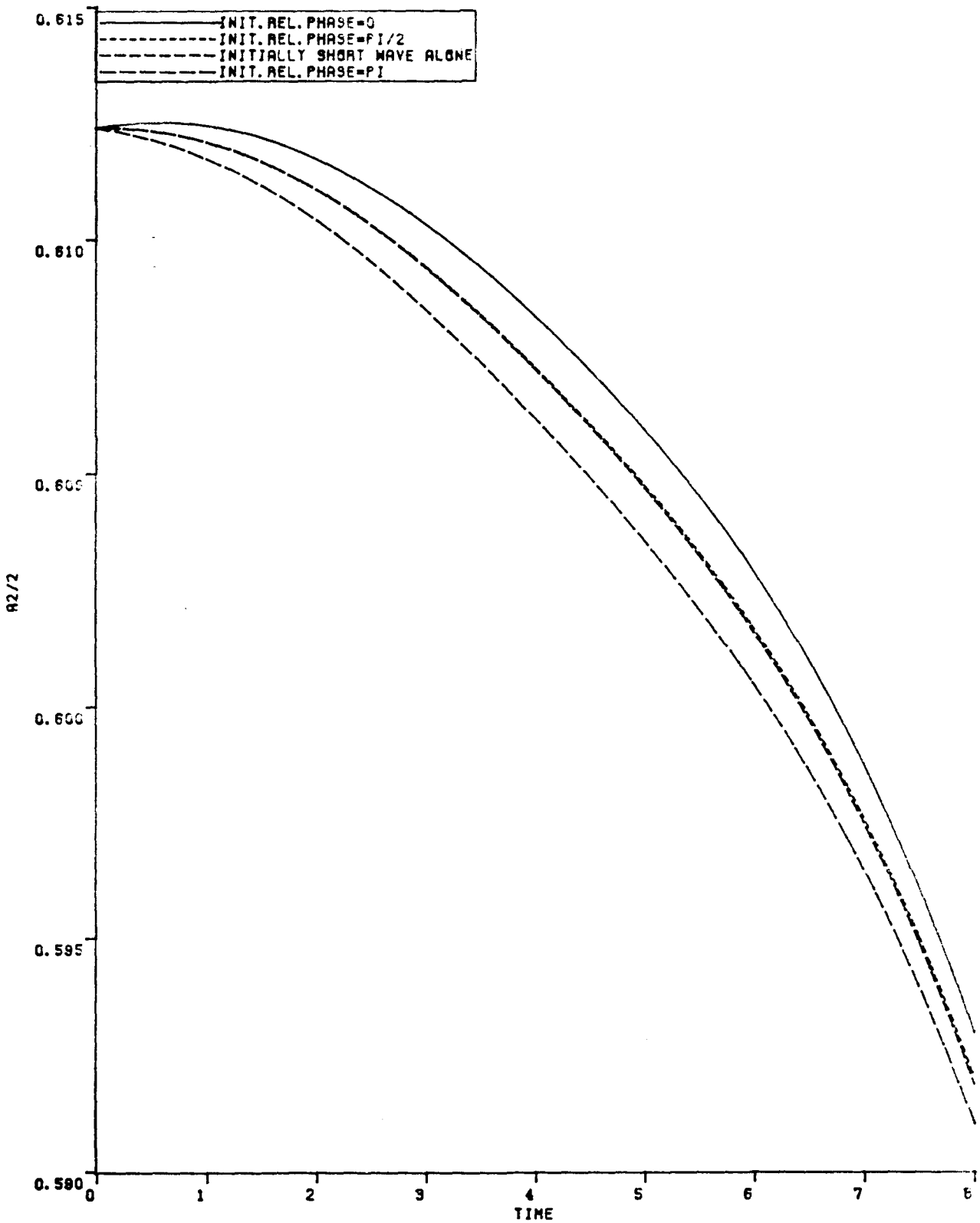

FIGURE 10: SHORT WAVE OF TWO NEUTRAL WAVES, A1(0)=A2(0)
RE=200 PR=.72 JO=.217 ALPHA=.321,.642 EPS=.01

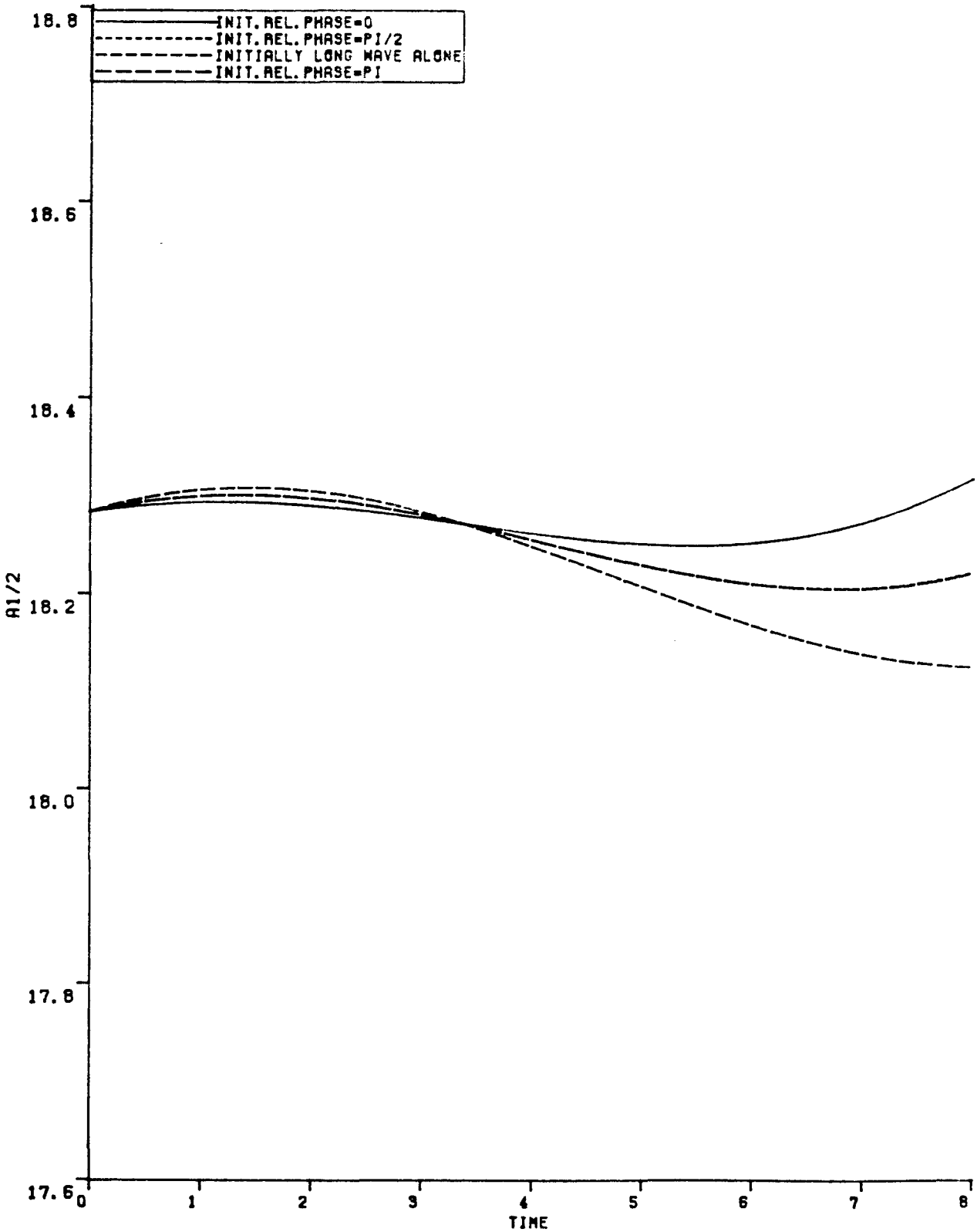

FIGURE 11: LONG WAVE OF TWO NEUTRAL WAVES, A1(0)=30A2(0)
RE=200 PR=.72 JO=.217 ALPHA=.321,.642 EPS=.004

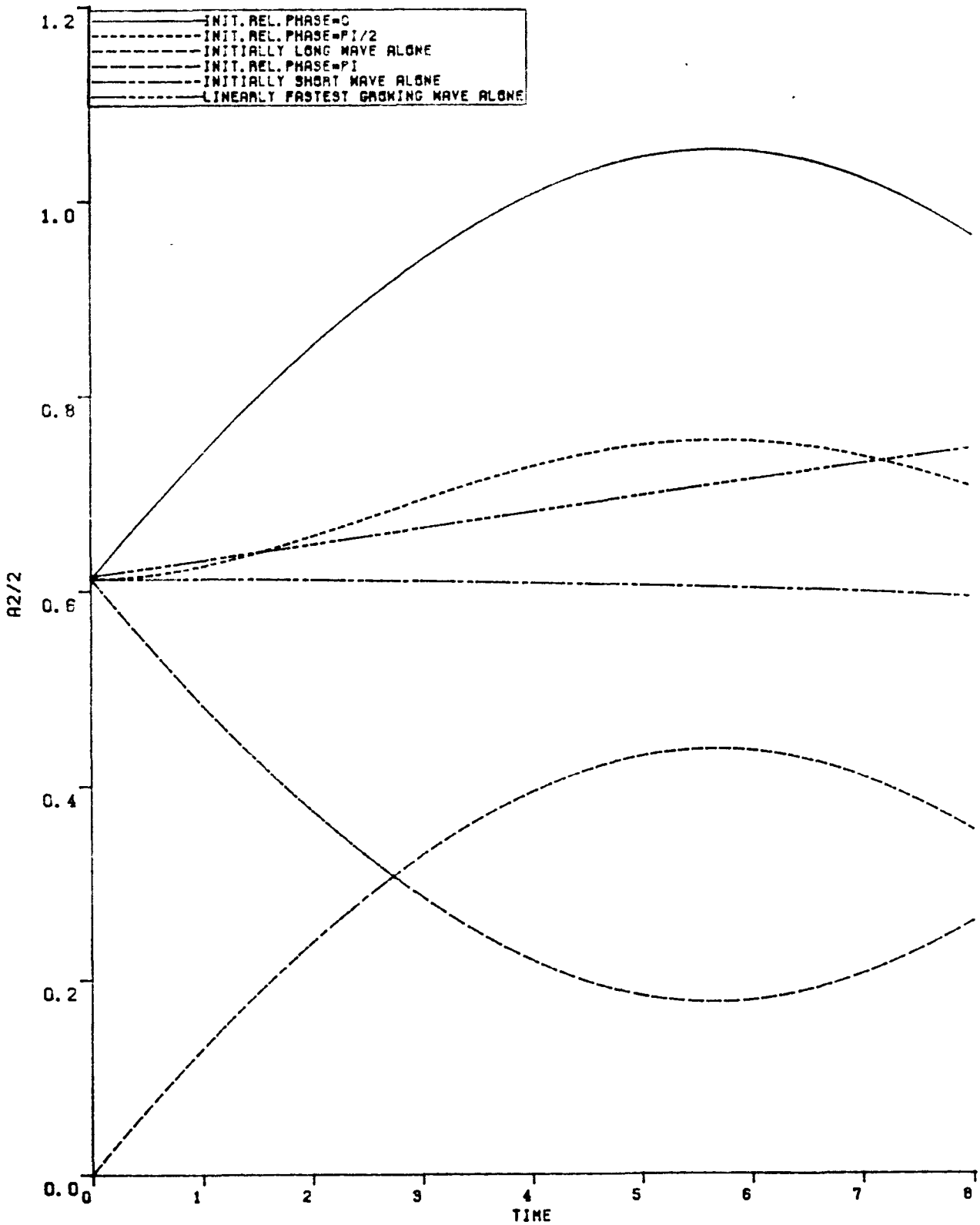

FIGURE 12: SHORT WAVE OF TWO NEUTRAL WAVES, A1(0)=30A2(0)
RE=200 PR=.72 JO=.217 ALPHA=.321,.642 EPS=.004

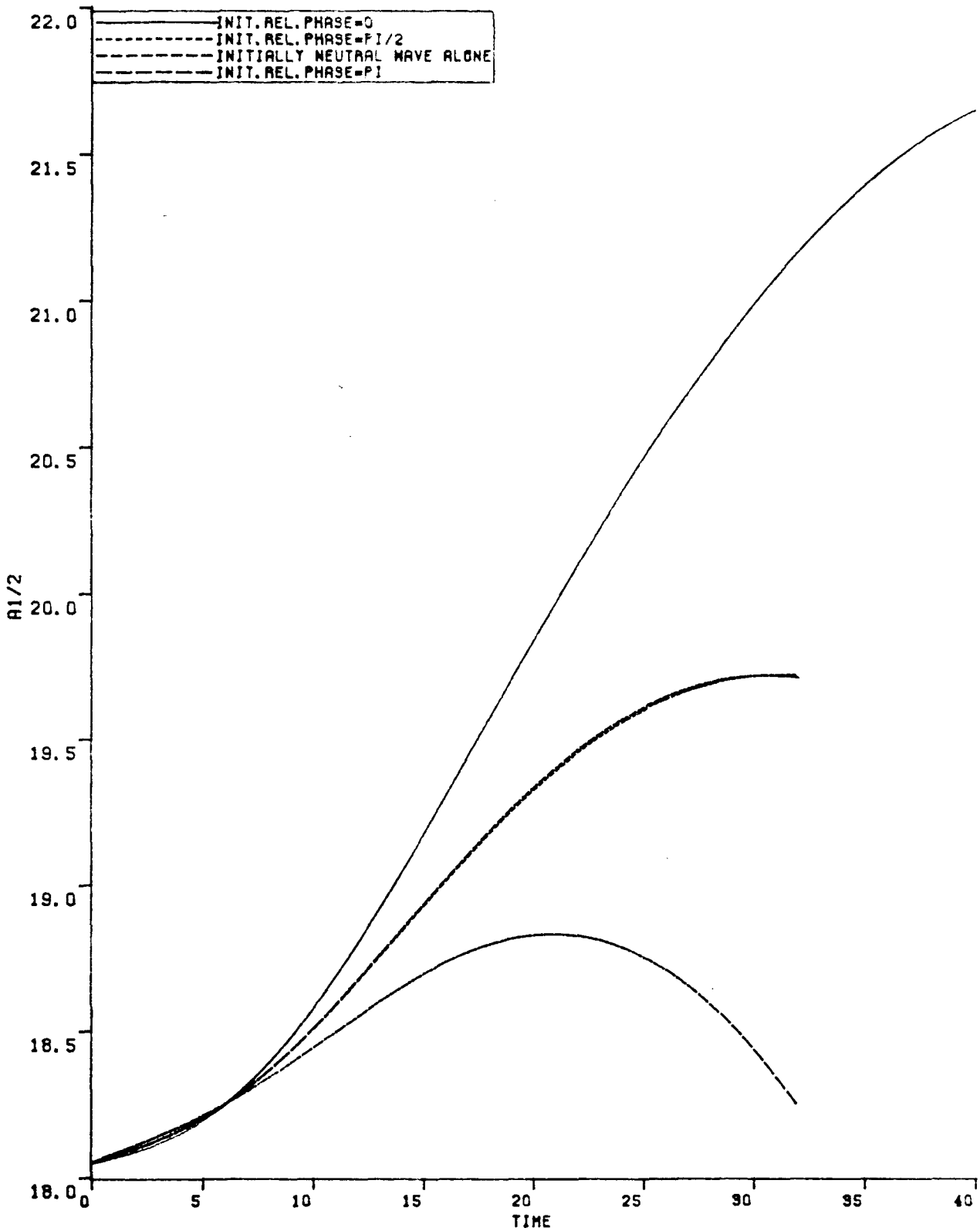

FIGURE 13: NEUTRAL WAVE OF LINEARLY NEUTRAL AND FASTEST GROWING WAVES, A1(0)=30A2(0) RE=200 PR=.72 JO=.174 ALPHA=.225,.45 EPS=.004

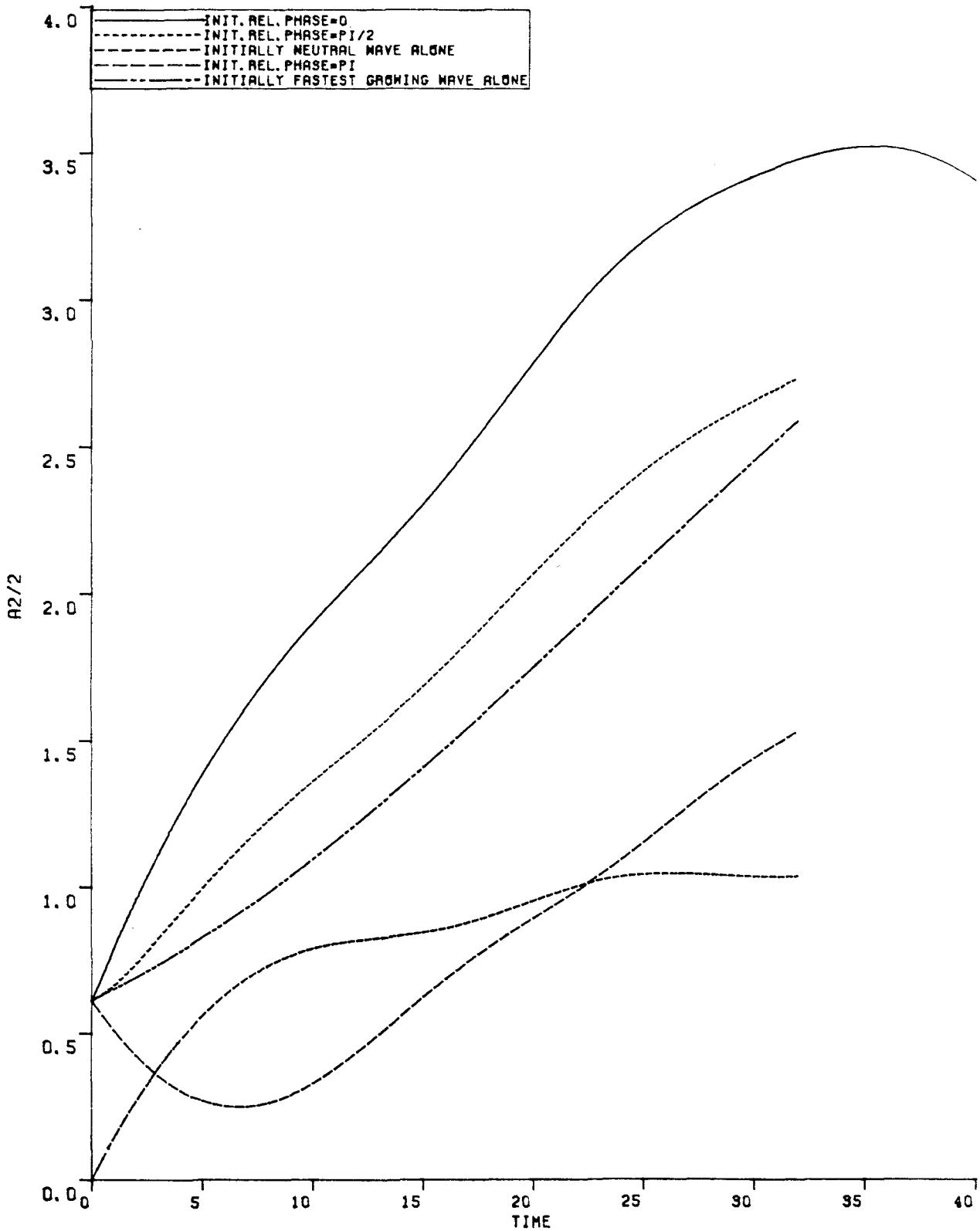

FIGURE 14: FASTEST GROWING WAVE OF LINEARLY NEUTRAL AND FASTEST GROWING WAVES, A1(0)=30A2(0) RE=200 PR=.72 JO=.174 ALPHA=.225,.45 EPS=.004

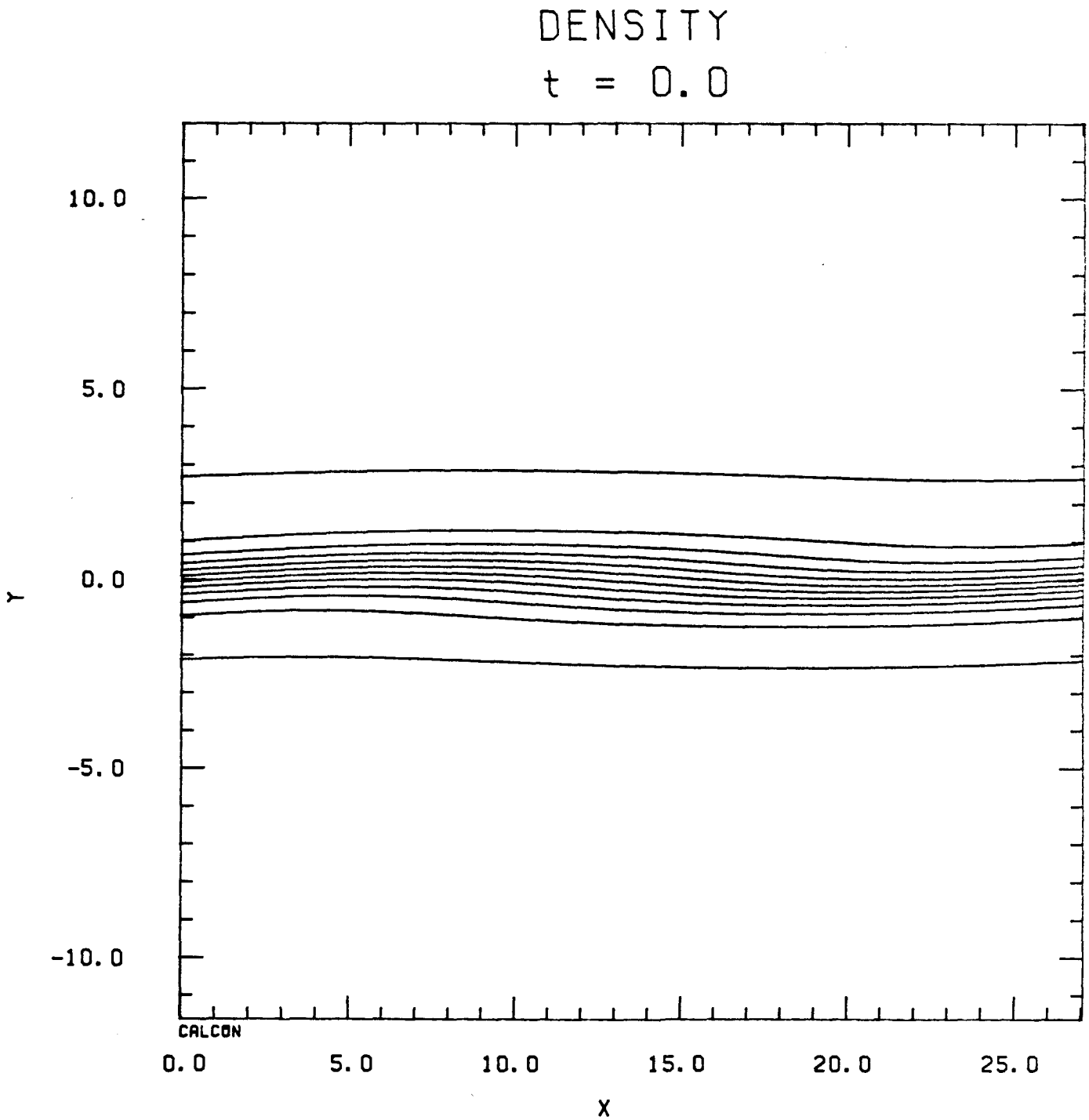

FIGURE 15A: ALPHA=.225,.45 JO=.174 RE=200 PR=.72
INITIAL RELATIVE PHASE=0.0 EPS=.004 A1(0)=3OA2(0)

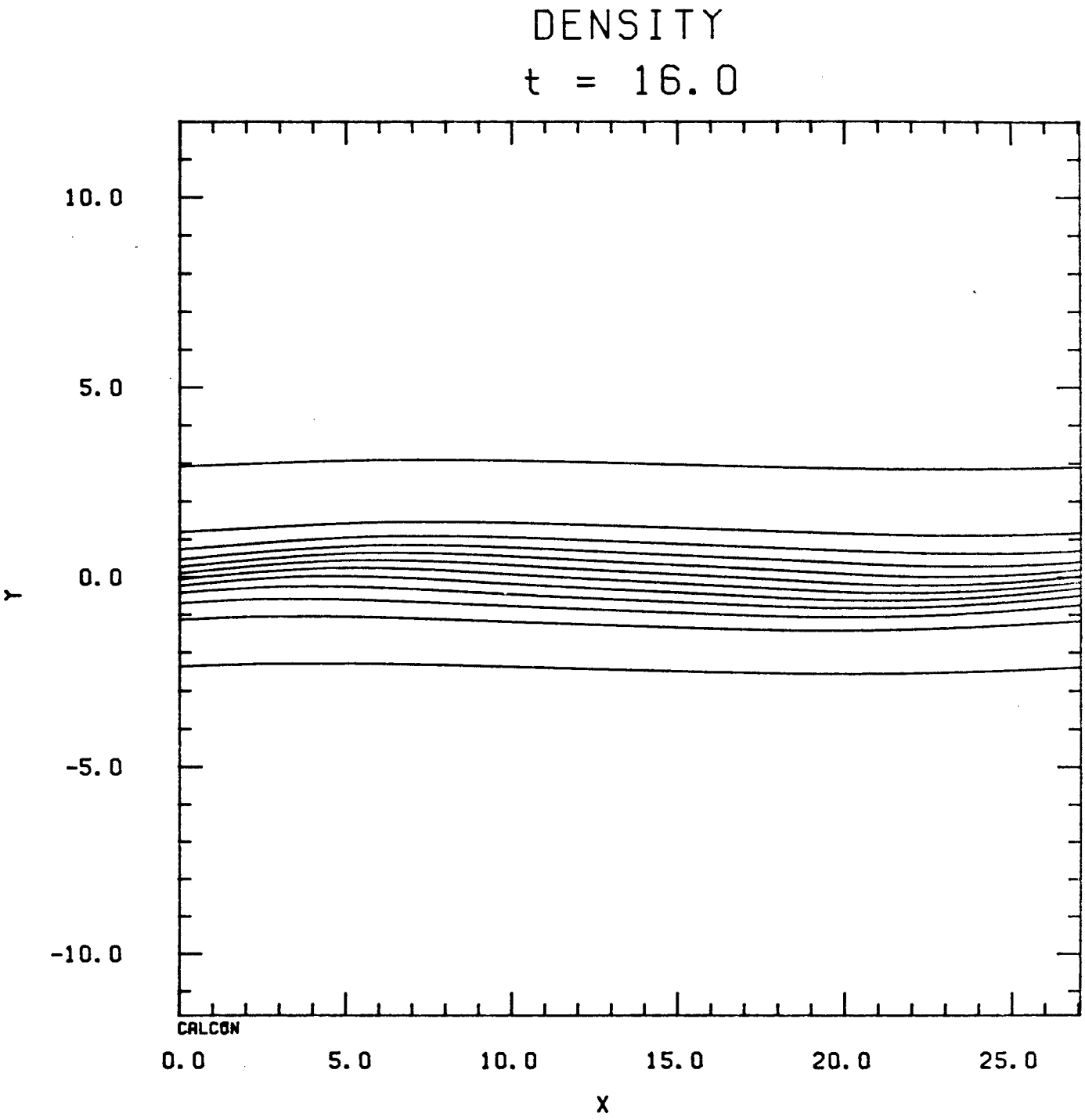

FIGURE 15B: ALPHA=.225,.45 JO=.174 RE=200 PR=.72
INITIAL RELATIVE PHASE=0.0 EPS=.004 A1(0)=30A2(0)

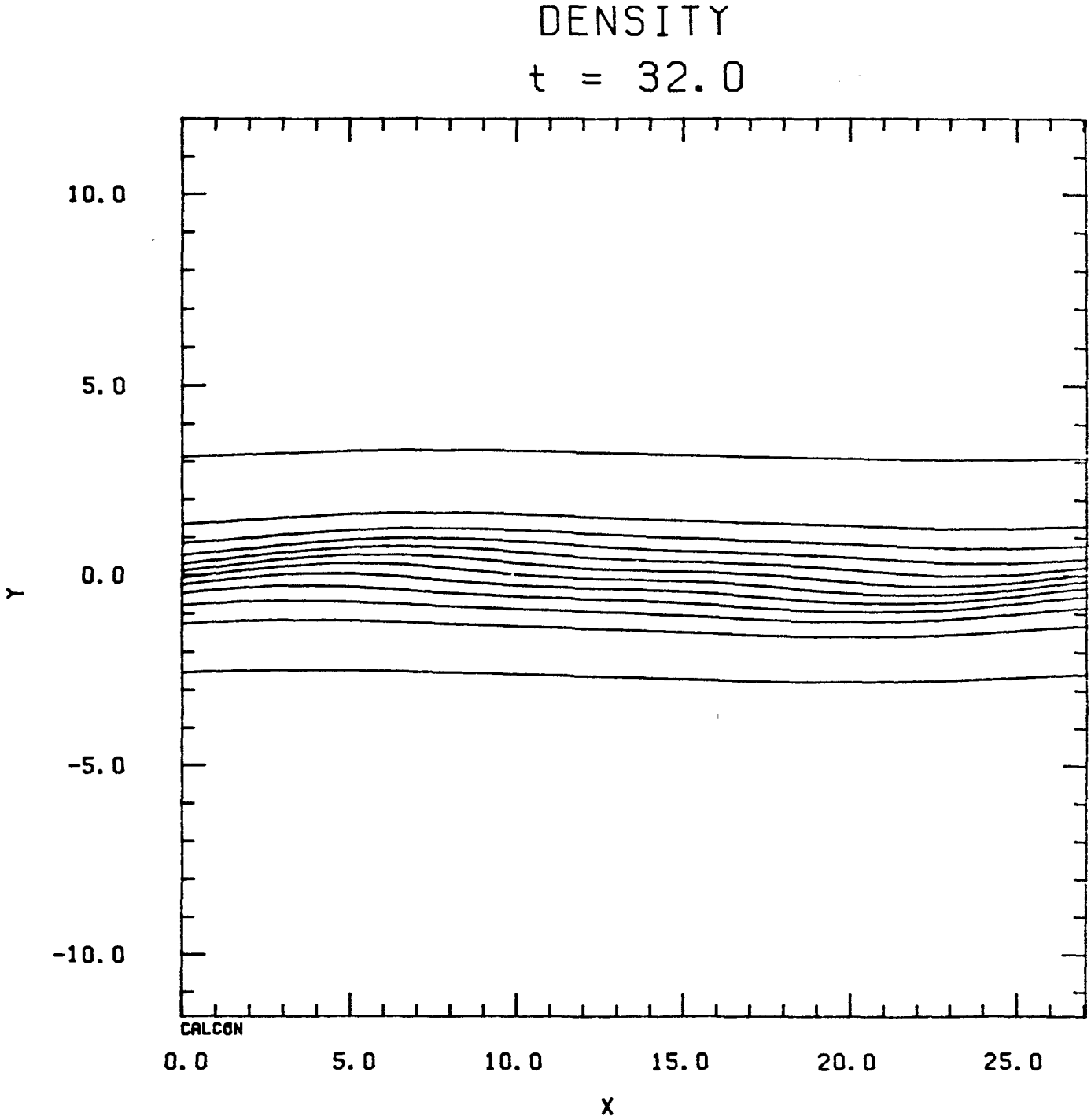

FIGURE 15C: ALPHA=.225,.45 JO=.174 RE=200 PR=.72
INITIAL RELATIVE PHASE=0.0 EPS=.004 A1(0)=30A2(0)

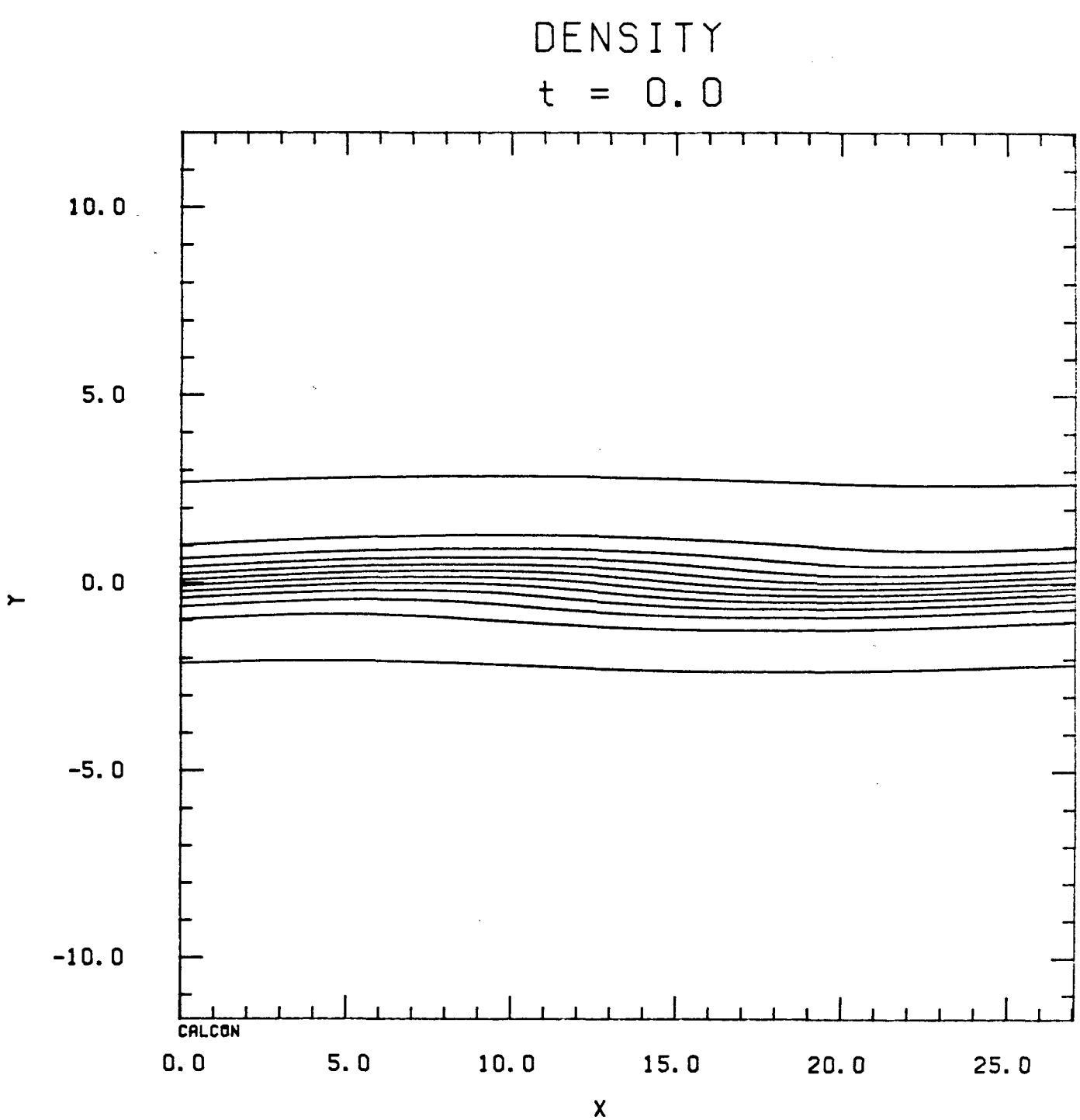

FIGURE 16A: ALPHA=.225,.45 JO=.174 RE=200 PR=.72
INITIAL RELATIVE PHASE=PI EPS=.004 A1(0)=3OA2(0)

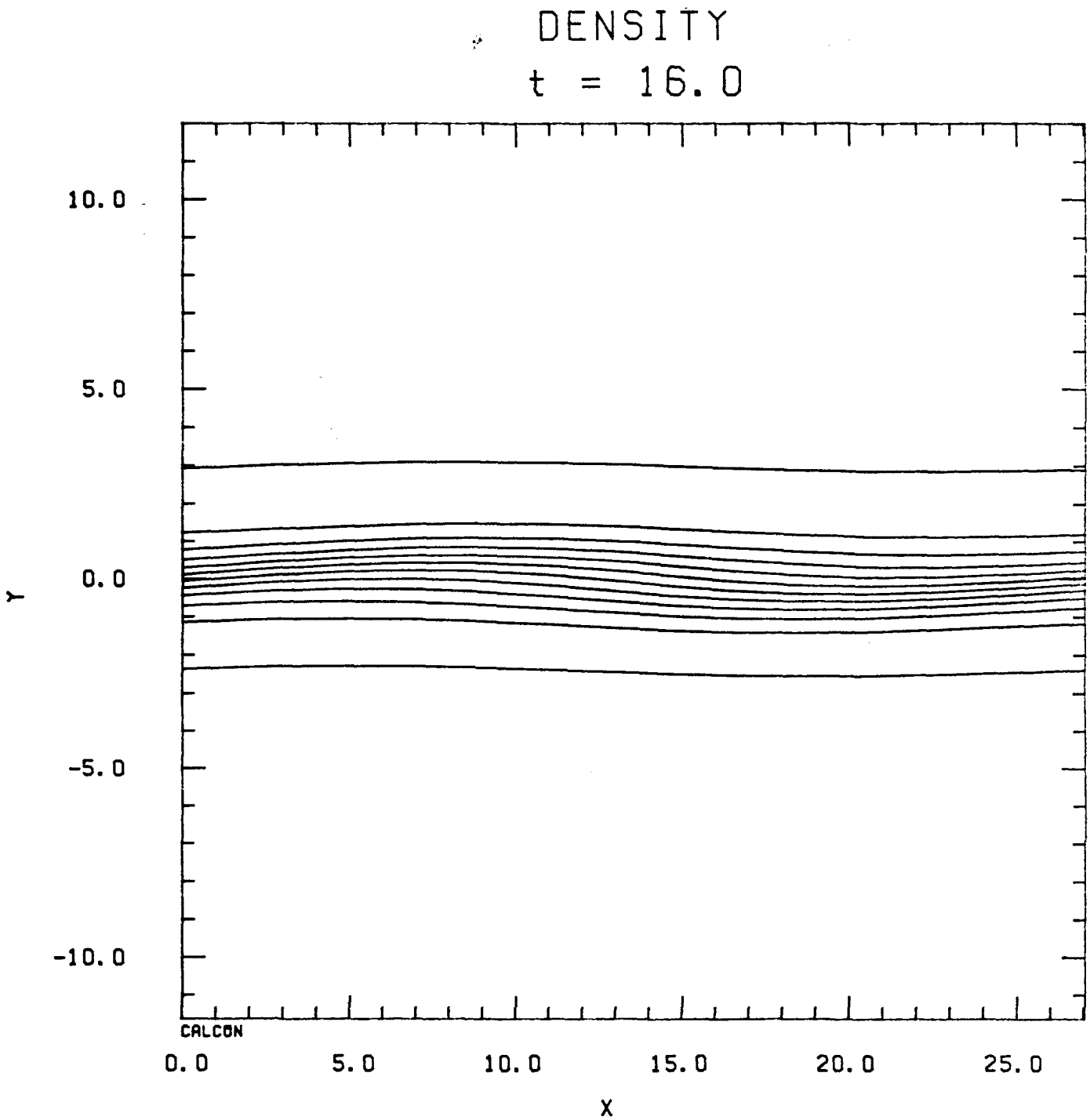

FIGURE 16B: ALPHA=.225,.45 JO=.174 RE=200 PR=.72
INITIAL RELATIVE PHASE=PI EPS=.004 A1(0)=3OA2(0)

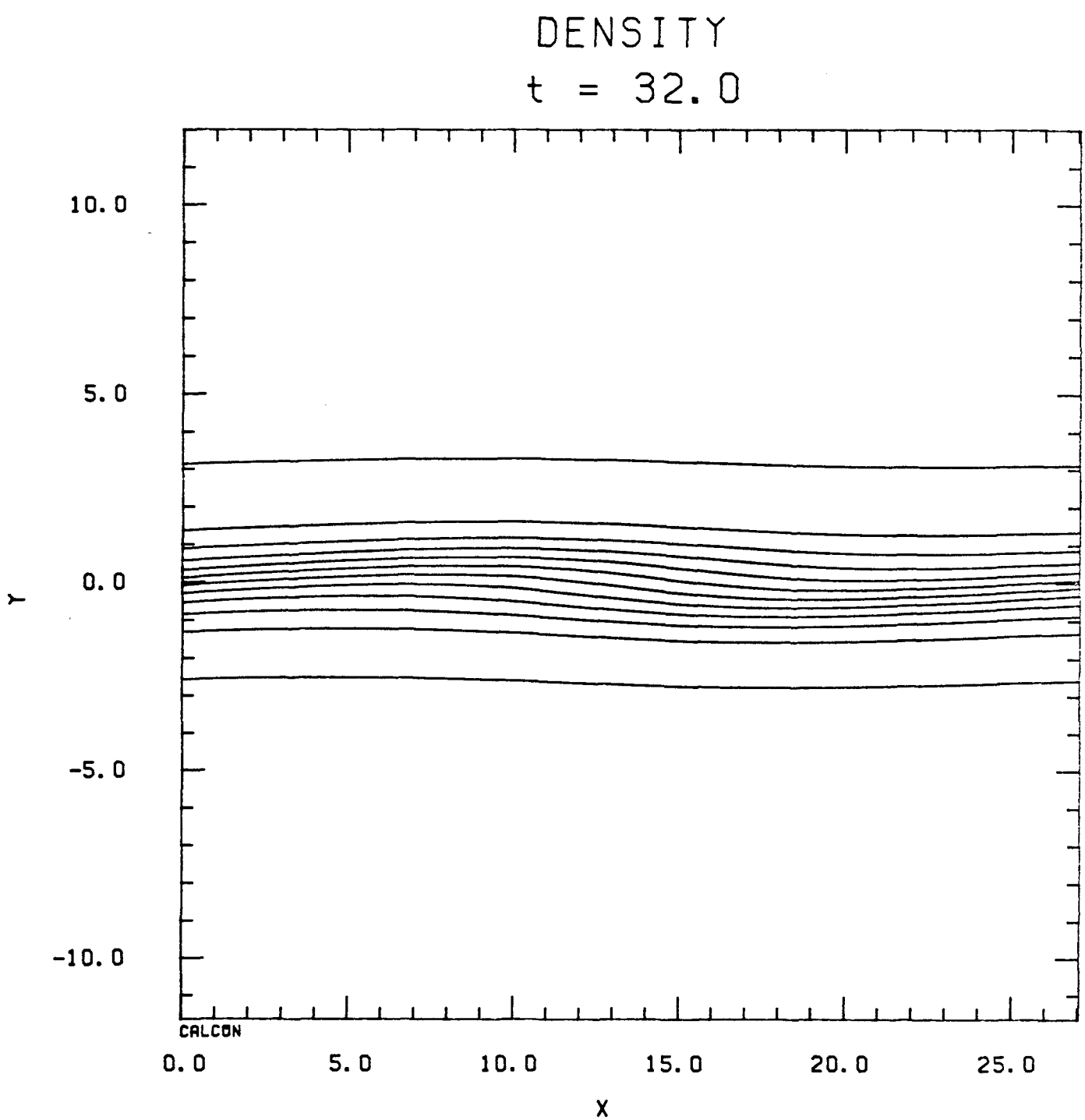

FIGURE 16C: ALPHA=.225,.45 JO=.174 RE=200 PR=.72
INITIAL RELATIVE PHASE=PI EPS=.004 A1(0)=30A2(0)

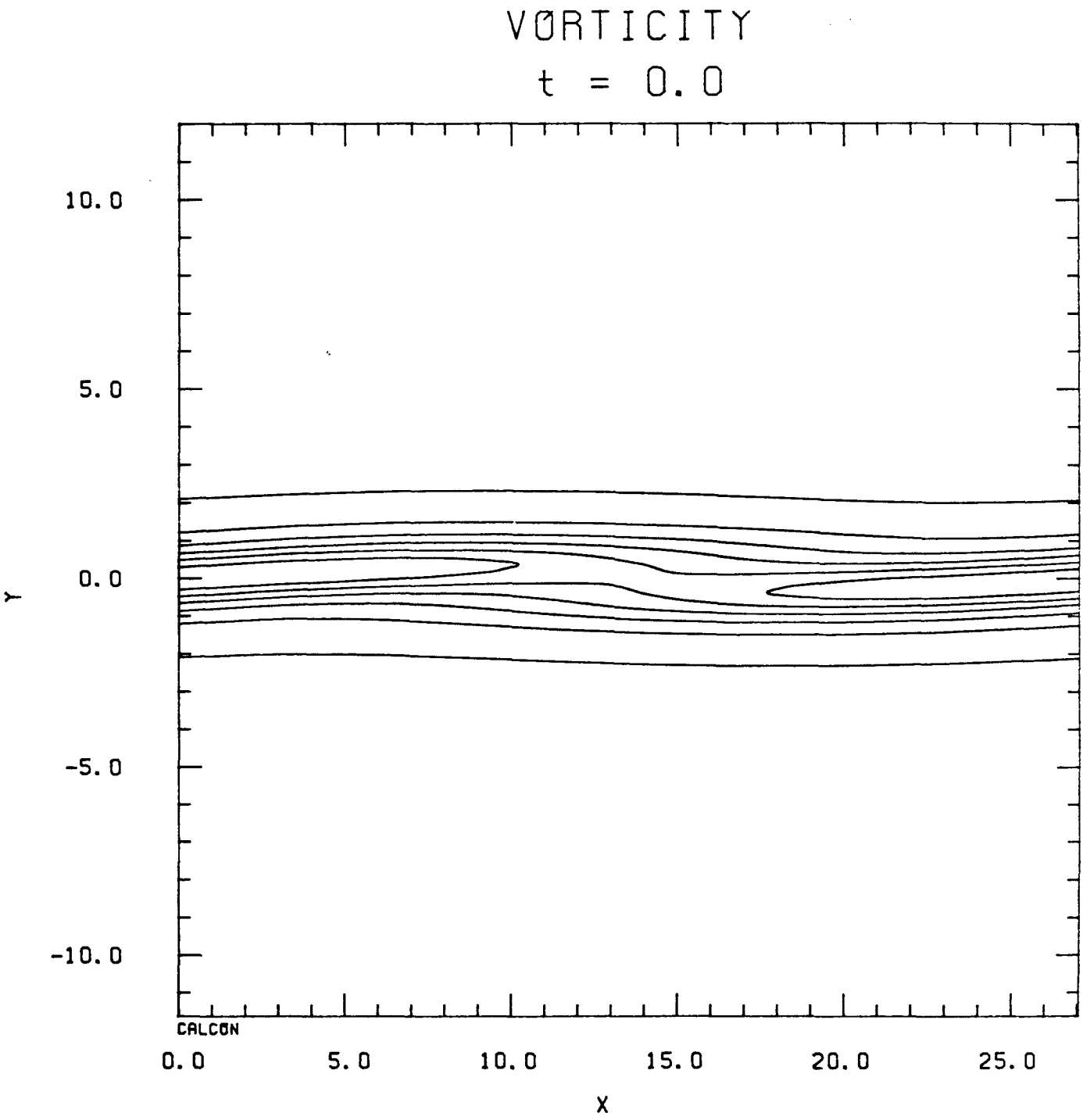

FIGURE 17A: ALPHA=.225,.45 JO=.174 RE=200 PR=.72
INITIAL RELATIVE PHASE=0.0 EPS=.004 A1(0)=30A2(0)

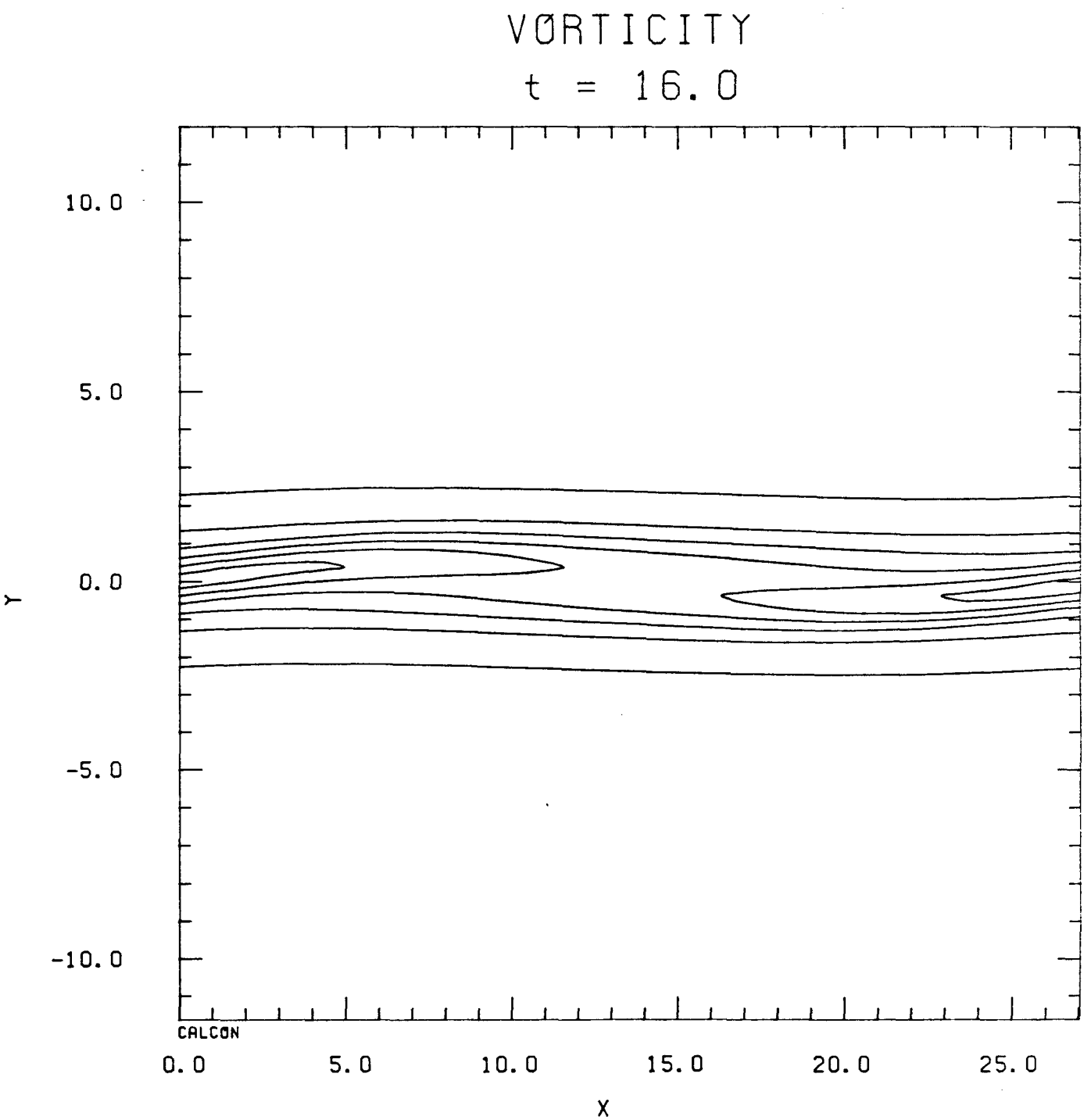

FIGURE 17B: ALPHA=.225,.45 JO=.174 RE=200 PR=.72
INITIAL RELATIVE PHASE=0.0 EPS=.004 A1(0)=30A2(0)

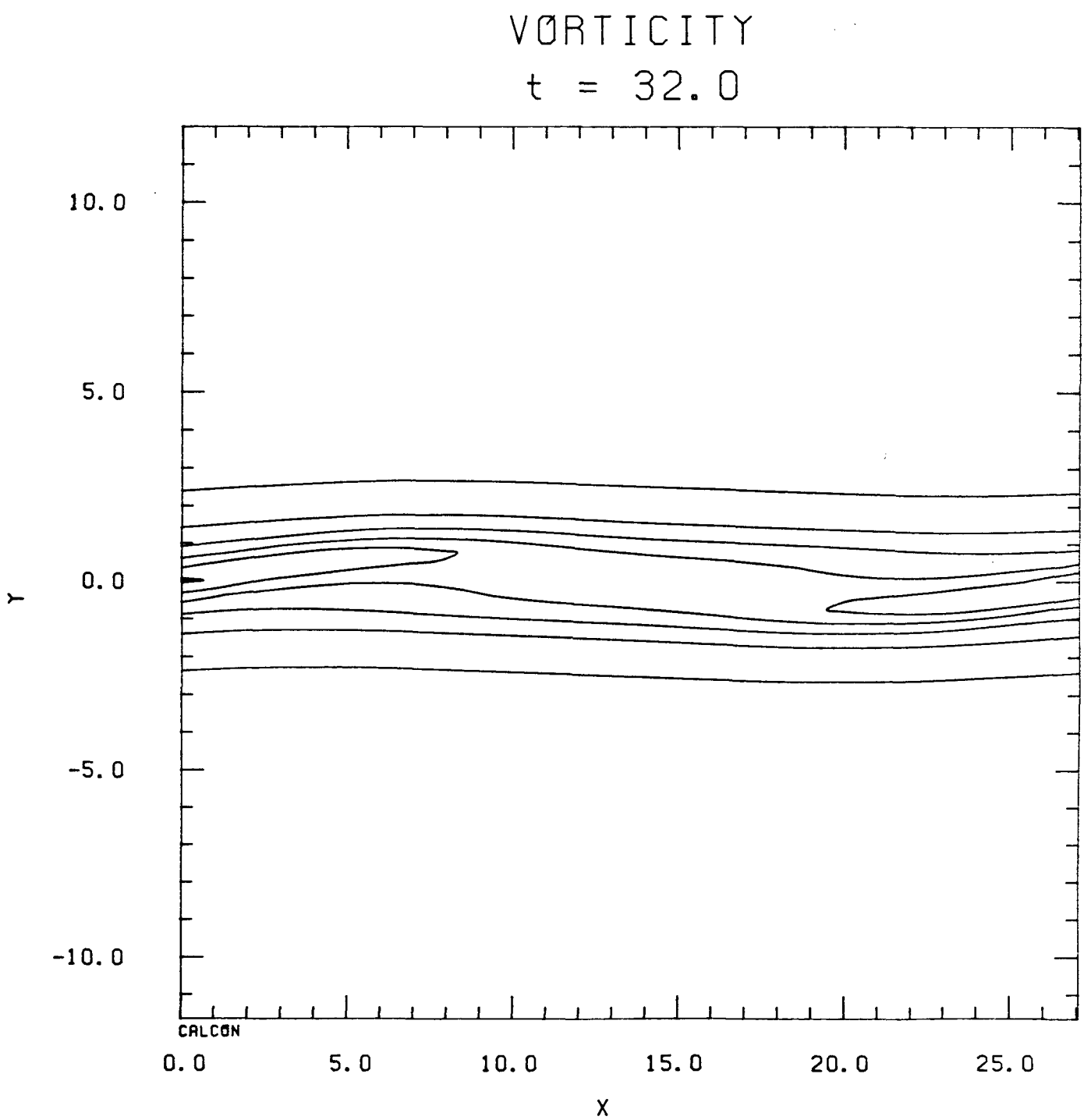

FIGURE 17C: ALPHA=.225,.45 JO=.174 RE=200 PR=.72
INITIAL RELATIVE PHASE=0.0 EPS=.004 A1(0)=3ØA2(0)

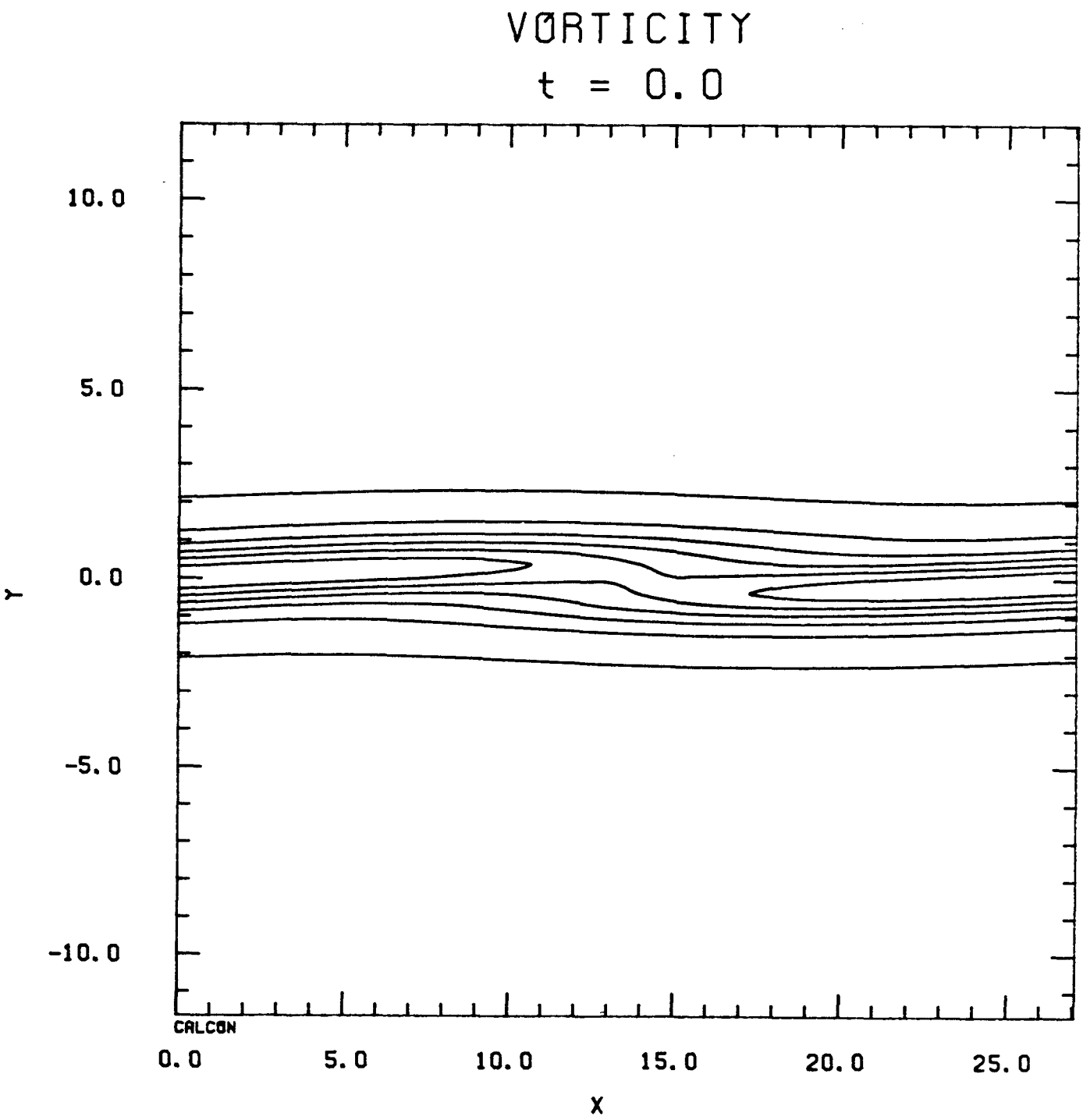

FIGURE 18A: ALPHA=.225,.45 JO=.174 RE=200 PR=.72
INITIAL RELATIVE PHASE=PI EPS=.004 A1(0)=30A2(0)

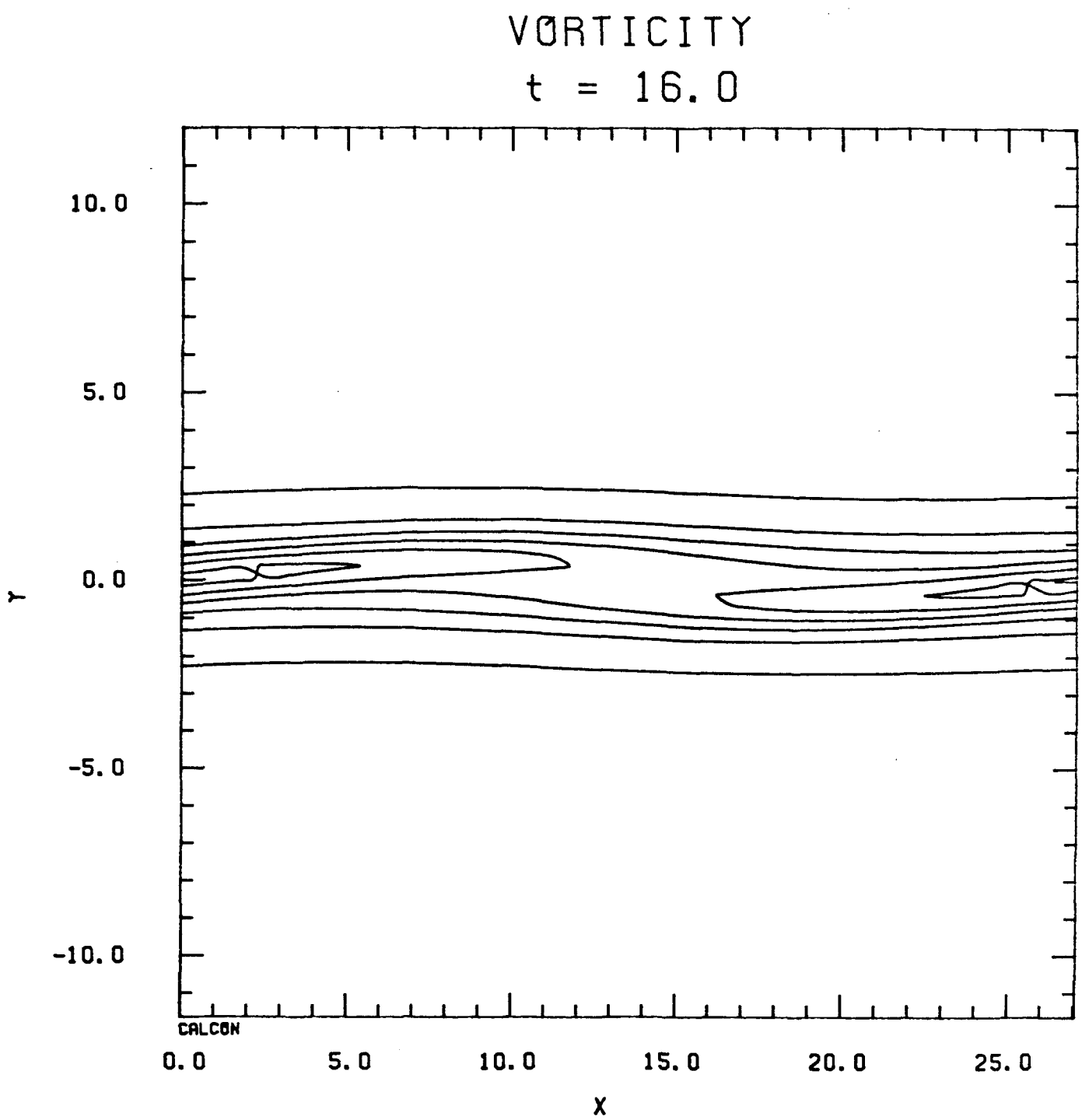

FIGURE 18B: ALPHA=.225,.45 JO=.174 RE=200 PR=.72
INITIAL RELATIVE PHASE=PI EPS=.004 A1(0)=30A2(0)

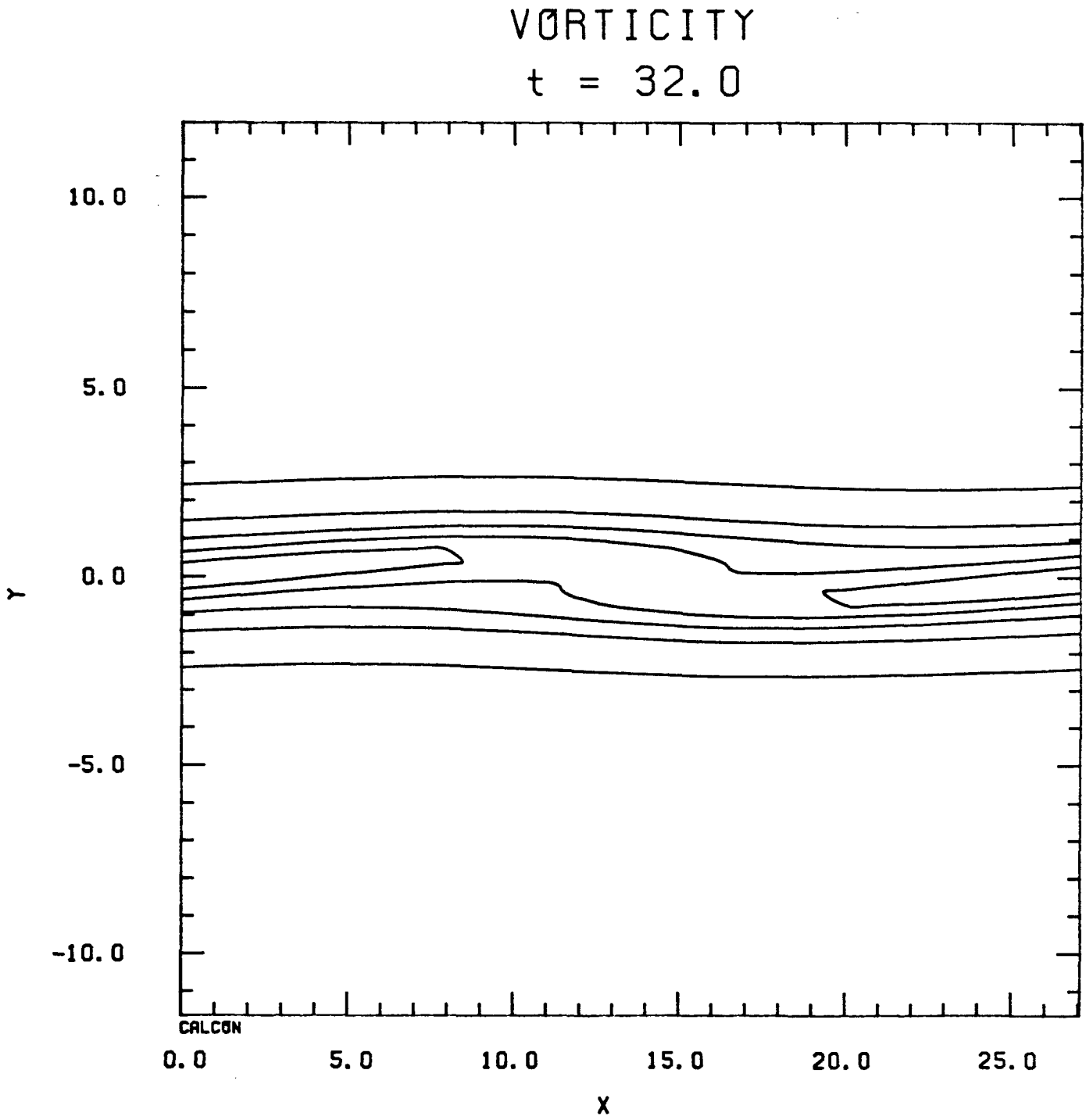

FIGURE 18C: ALPHA=.225,.45 JO=.174 RE=200 PR=.72
INITIAL RELATIVE PHASE=PI EPS=.004 A1(0)=3ØA2(0)

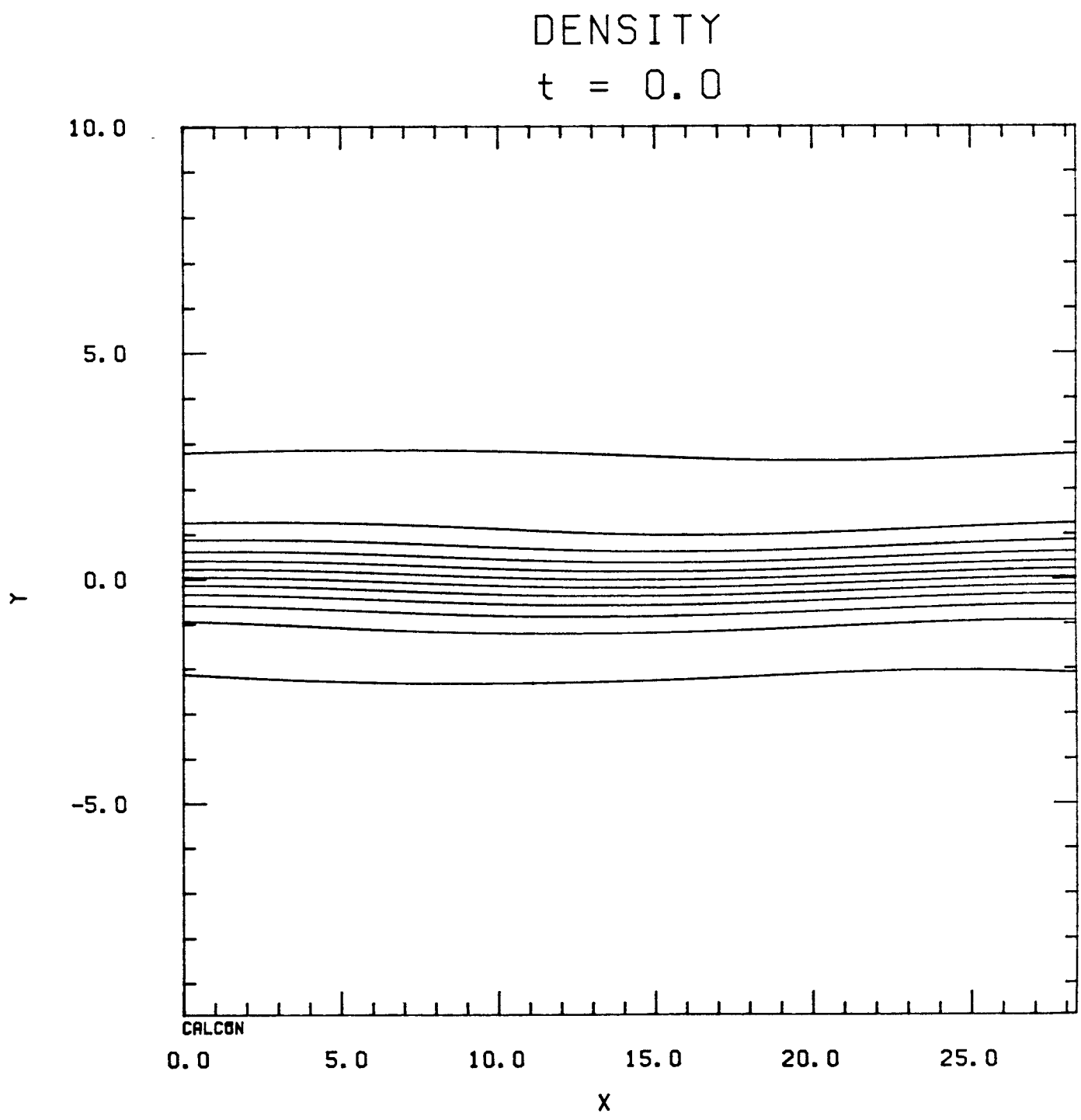

FIGURE 19A: ALPHA=.215 JO=.07 RE=50 PR=.72
EPS=.0616 INITIALLY LONG WAVE ALONE

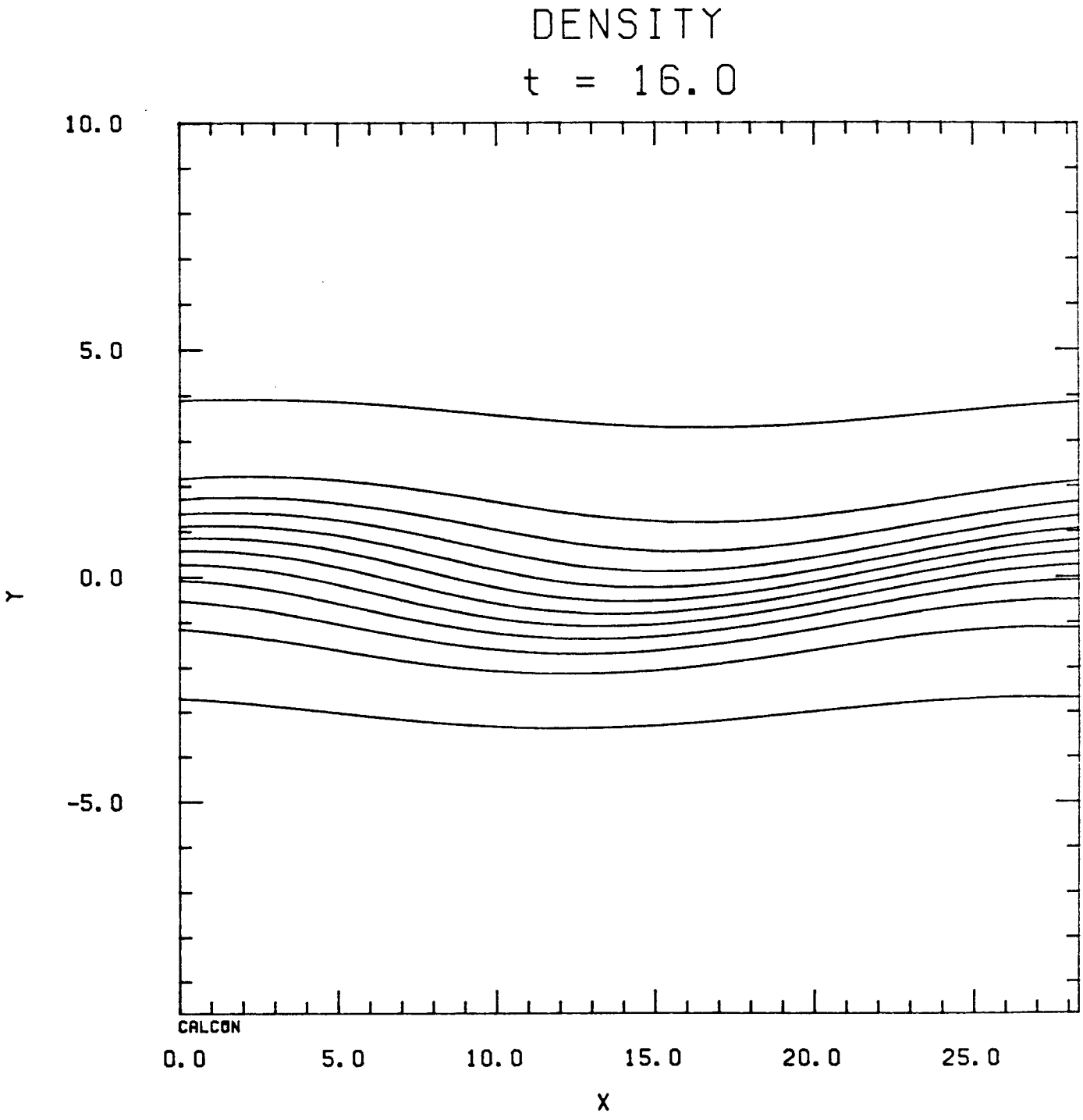

FIGURE 19B: ALPHA=.215 JO=.07 RE=50 PR=.72
EPS=.0616 INITIALLY LONG WAVE ALONE

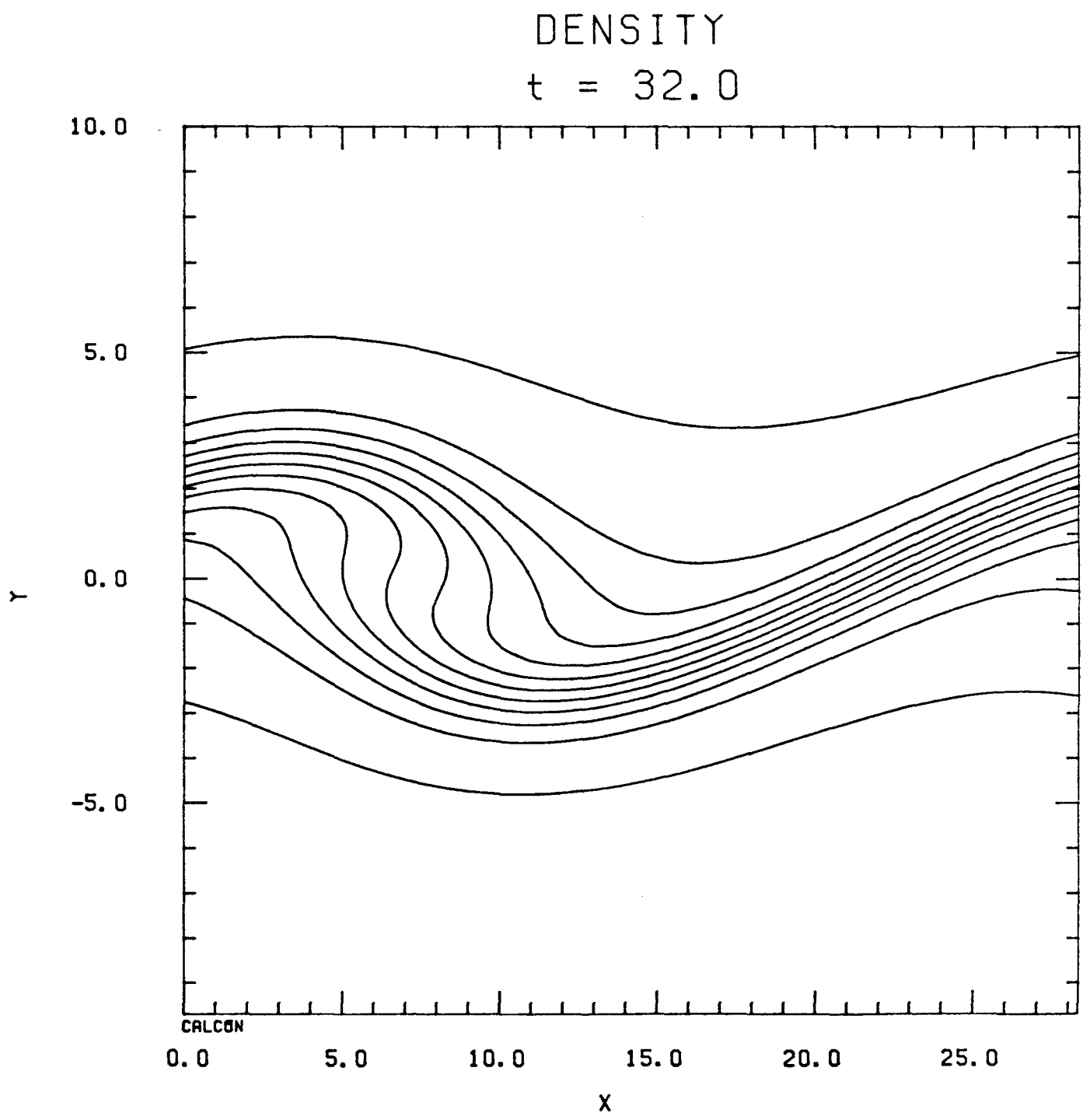

FIGURE 19C: ALPHA=.215 JO=.07 RE=50 PR=.72
EPS=.0616 INITIALLY LONG WAVE ALONE

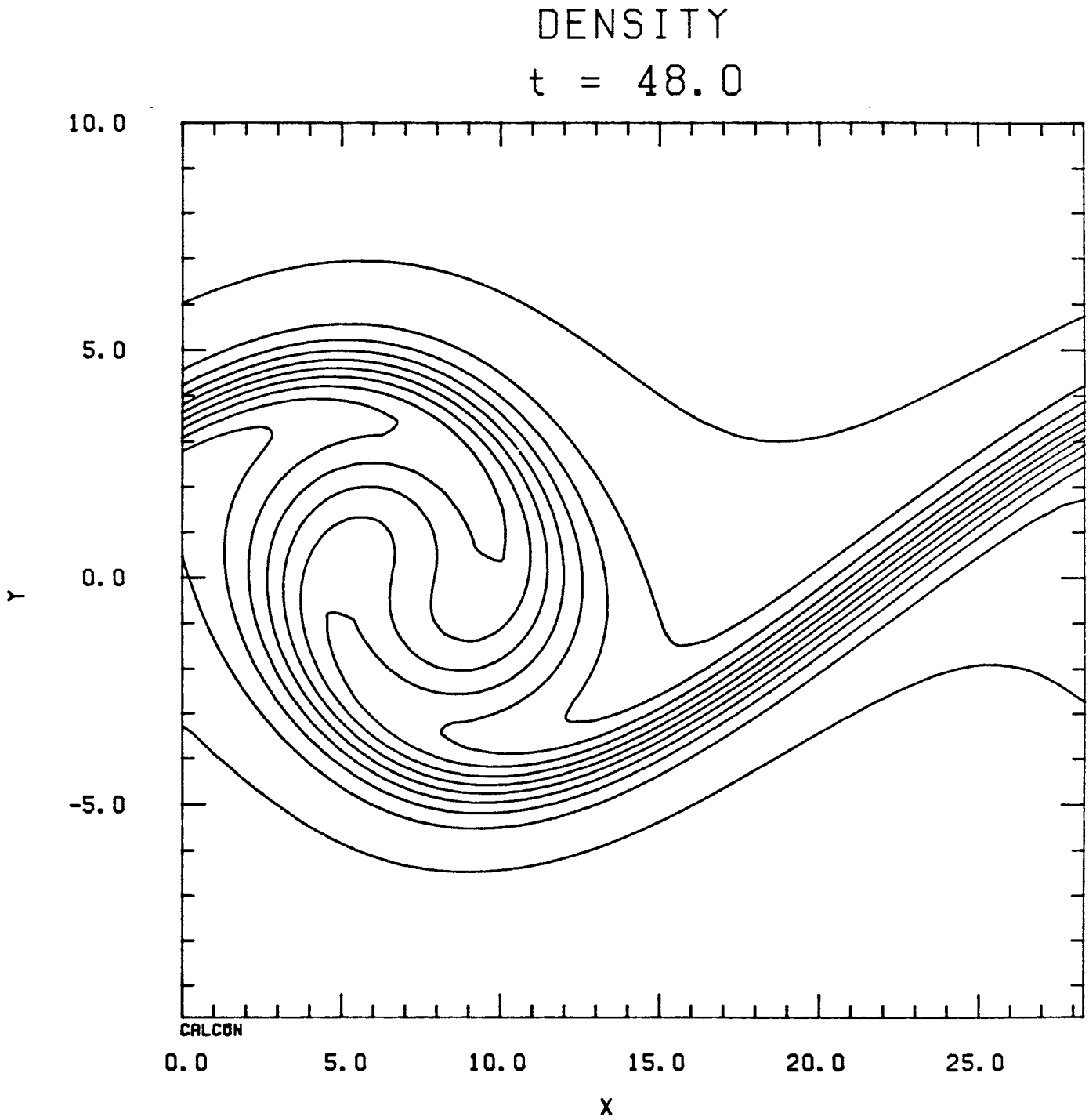

FIGURE 19D: ALPHA=.215 JO=.07 RE=50 PR=.72
EPS=.0616 INITIALLY LONG WAVE ALONE

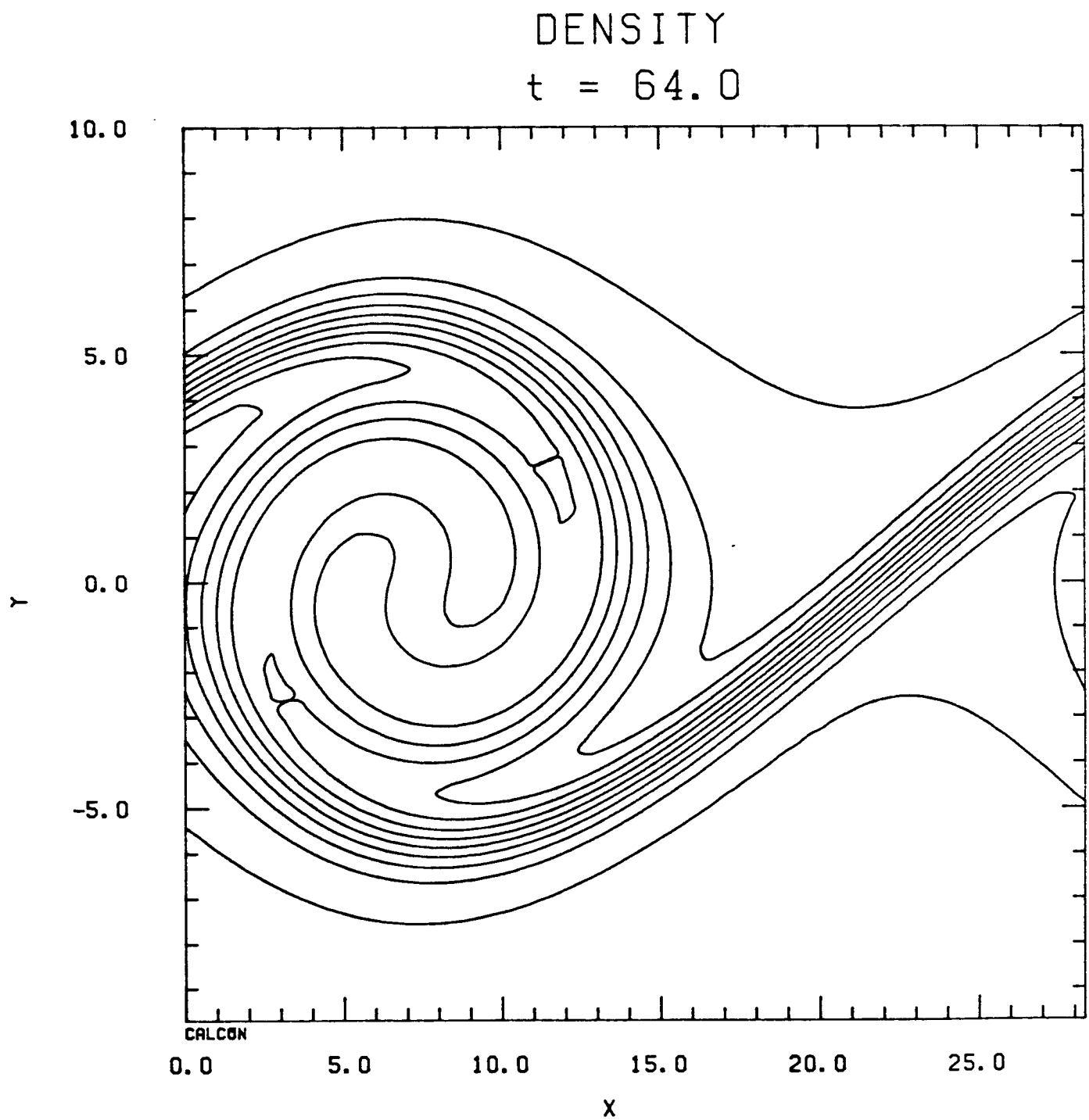

FIGURE 19E: ALPHA=.215 JO=.07 RE=50 PR=.72
EPS=.0616 INITIALLY LONG WAVE ALONE

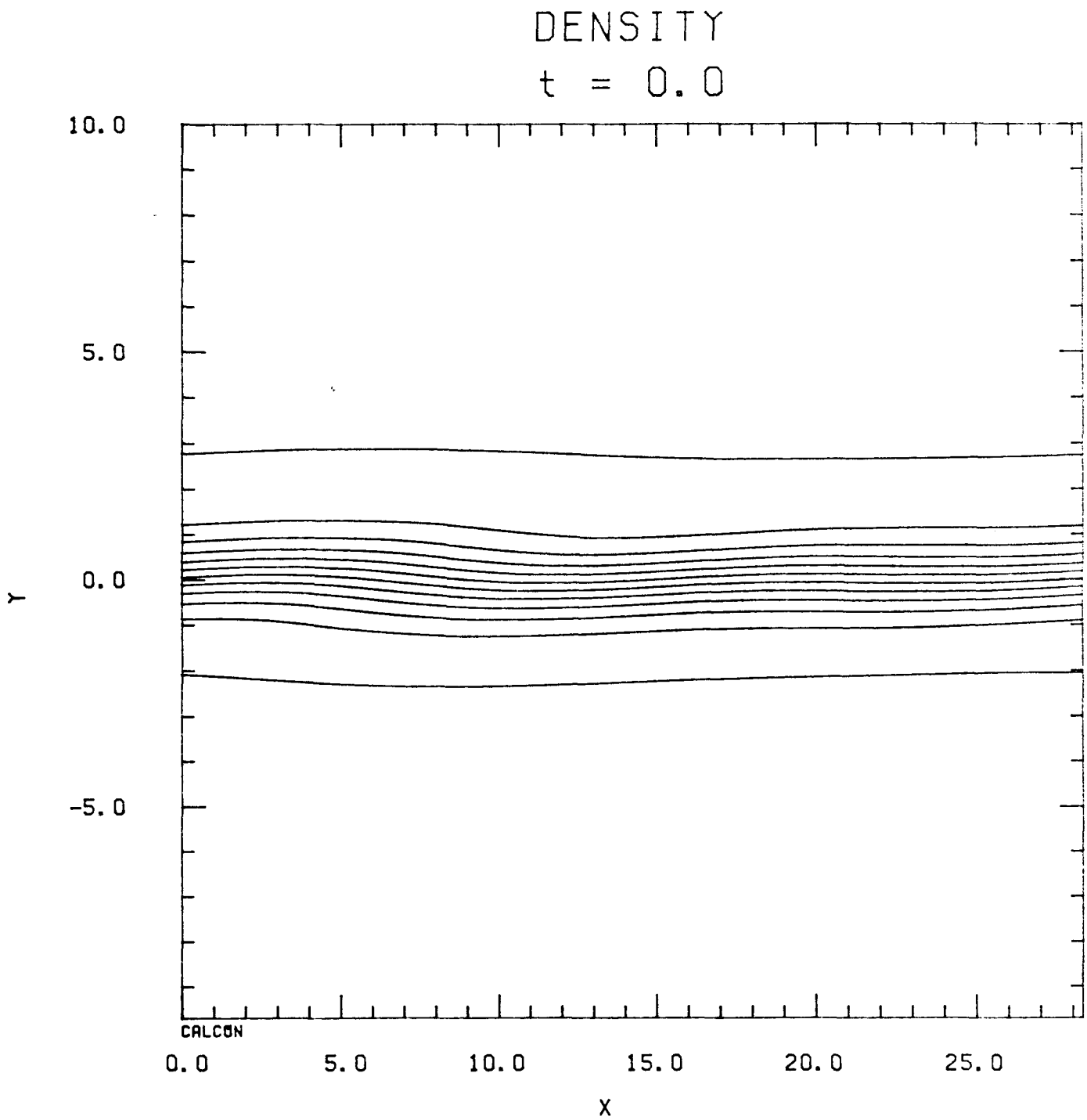

FIGURE 20A: ALPHA=.215,.43 JO=.07 RE=50 PR=.72
INITIAL RELATIVE PHASE=-PI
EPS=.0326 A1(0)=1.89A2(0)

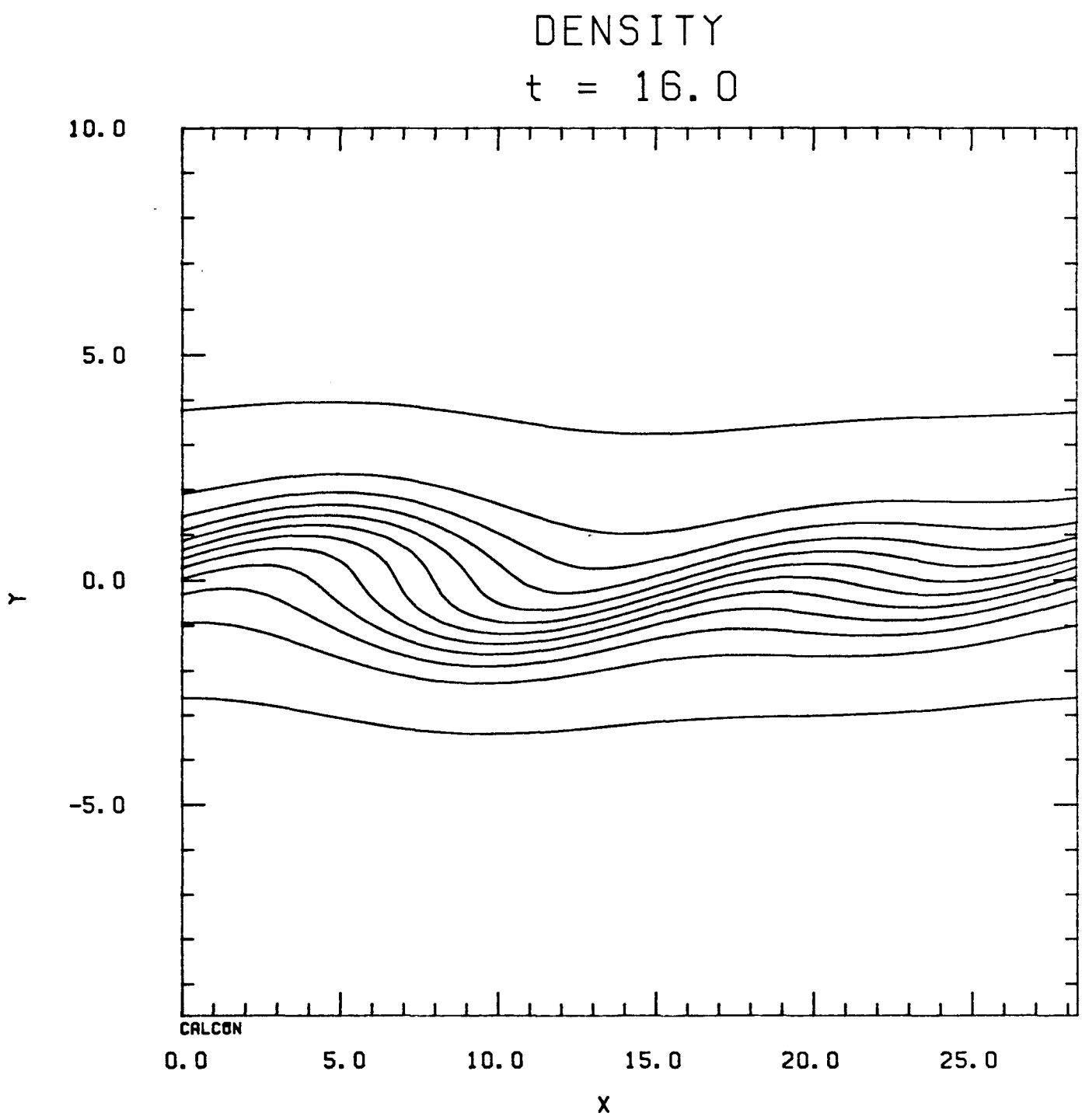

FIGURE 20B: ALPHA=.215,.43 JO=.07 RE=50 PR=.72
INITIAL RELATIVE PHASE=-PI
EPS=.0326 A1(0)=1.89A2(0)

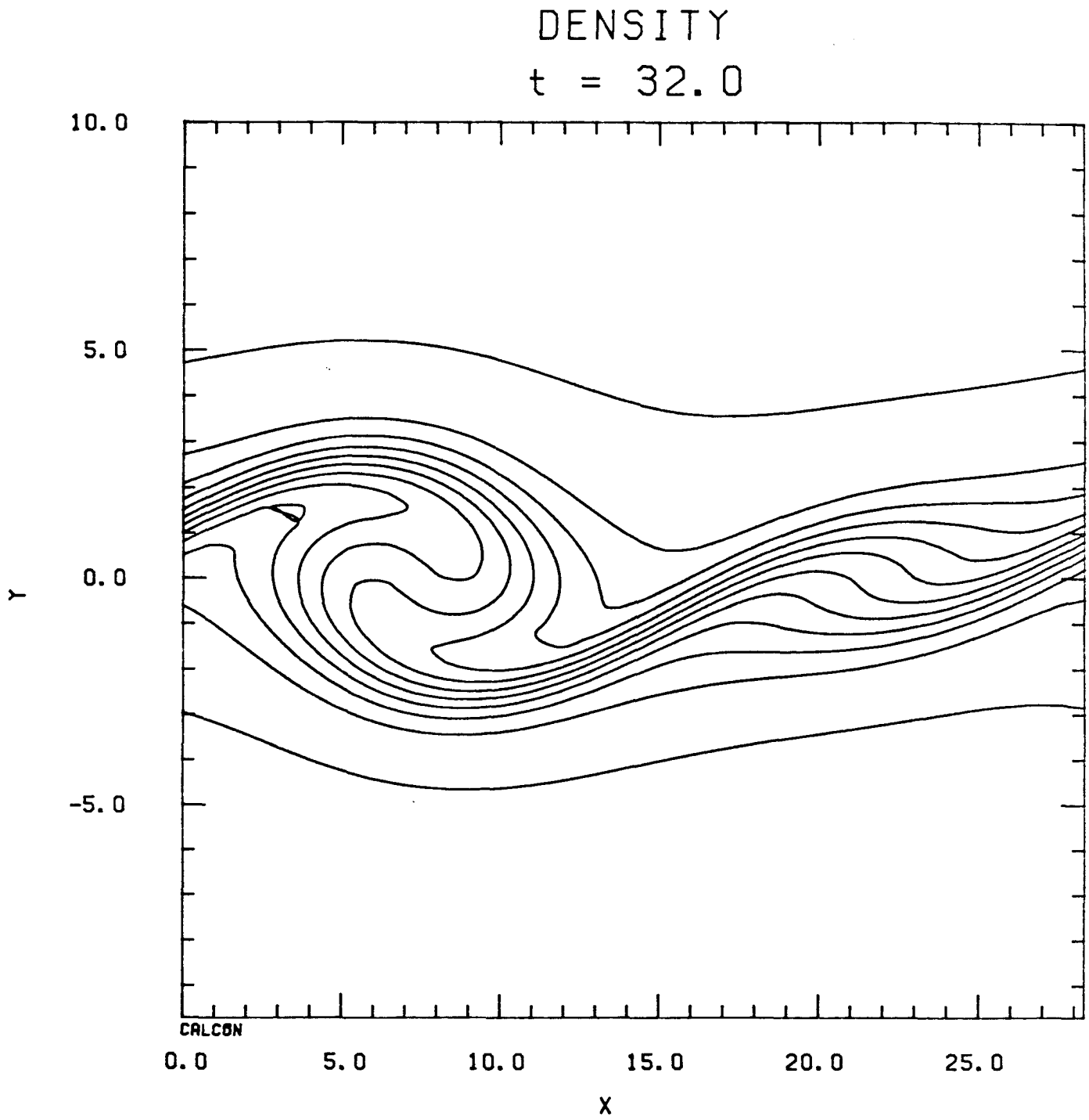

FIGURE 20C: ALPHA=.215,.43 JO=.07 RE=50 PR=.72
INITIAL RELATIVE PHASE=-PI
EPS=.0326 A1(0)=1.89A2(0)

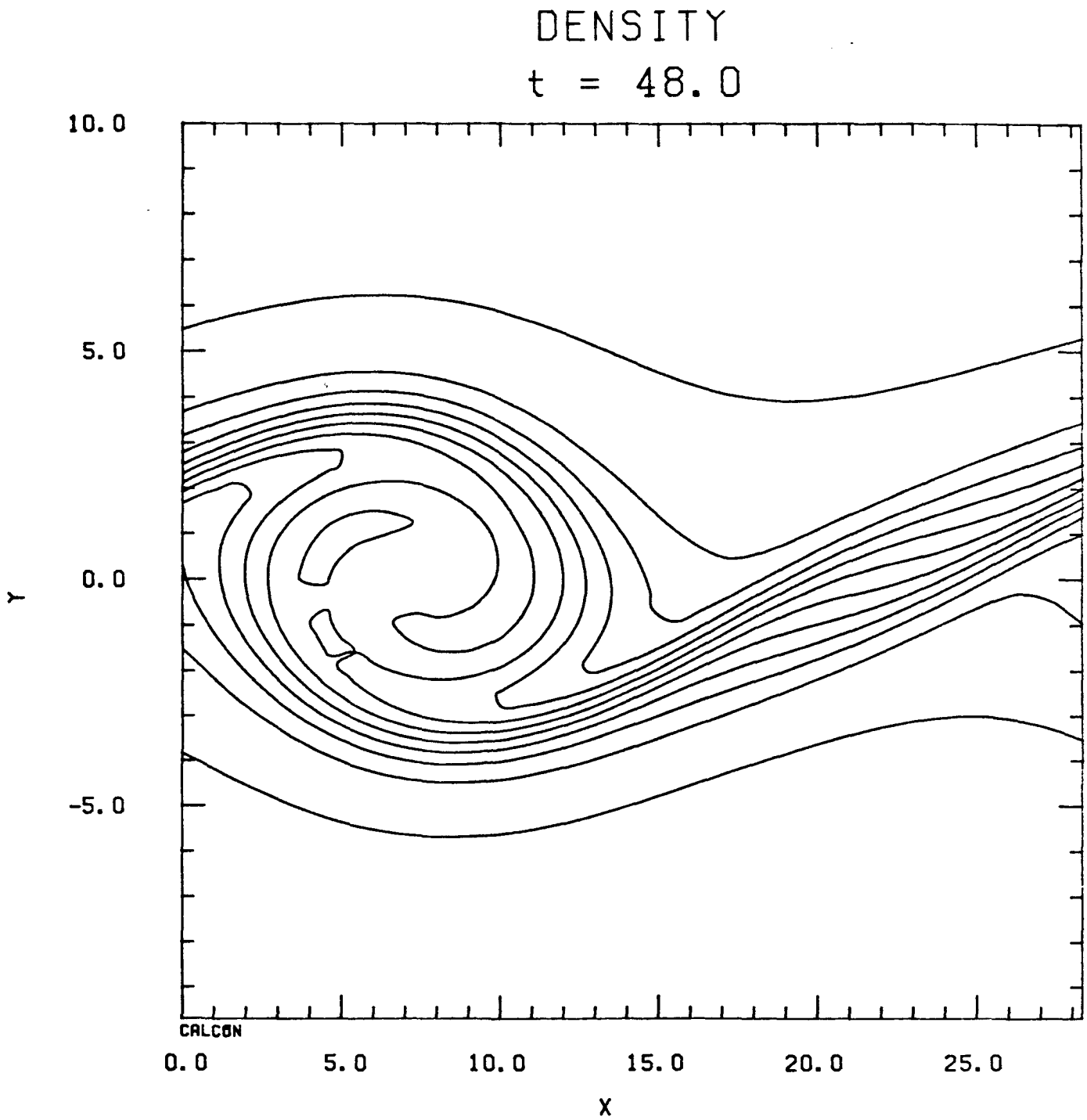

FIGURE 20D: ALPHA=.215,.43 JO=.07 RE=50 PR=.72
INITIAL RELATIVE PHASE=-PI
EPS=.0326 A1(0)=1.89A2(0)

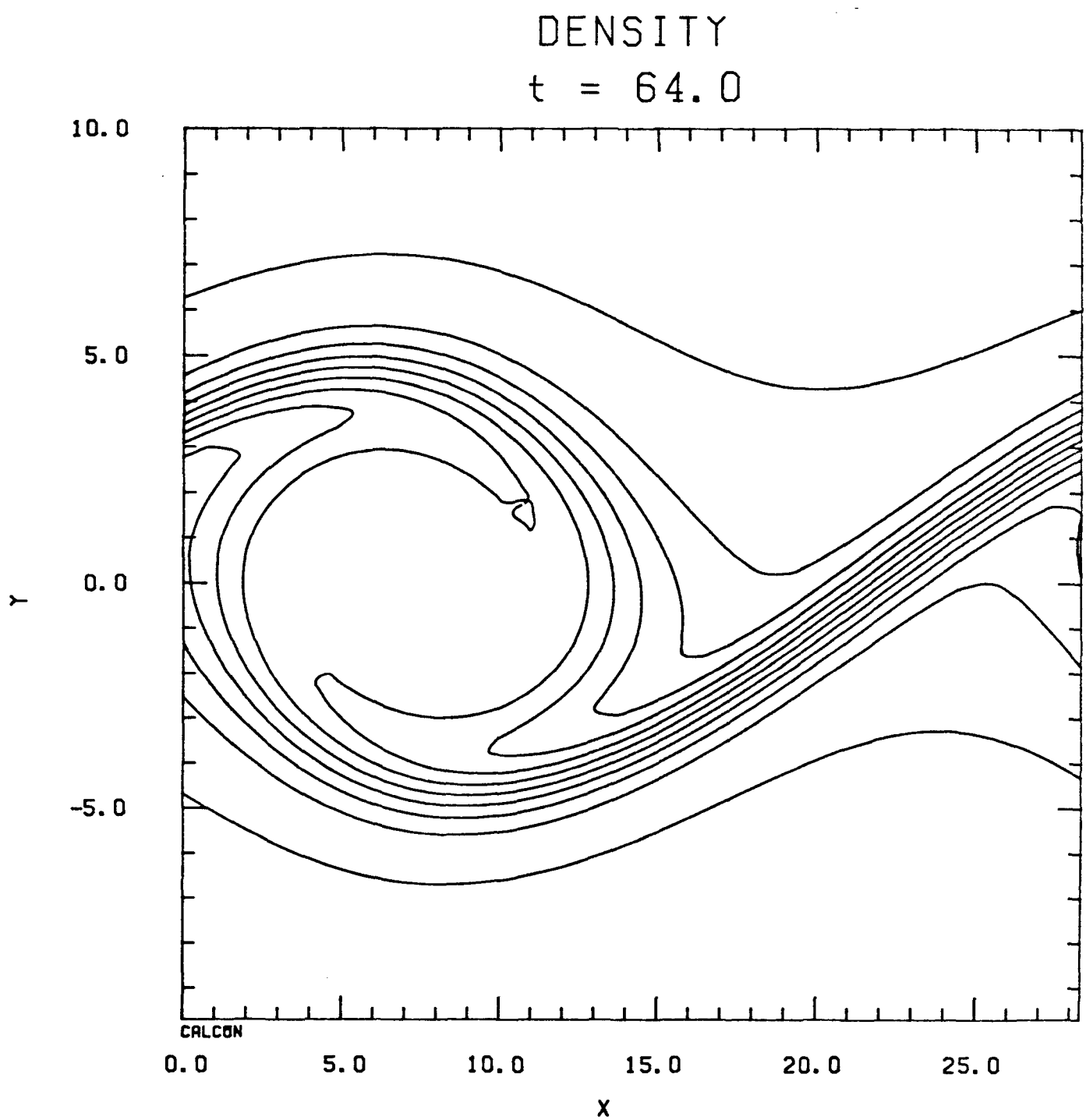

FIGURE 20E: ALPHA=.215,.43 JO=.07 RE=50 PR=.72
INITIAL RELATIVE PHASE=-PI
EPS=.0326 A1(0)=1.89A2(0)

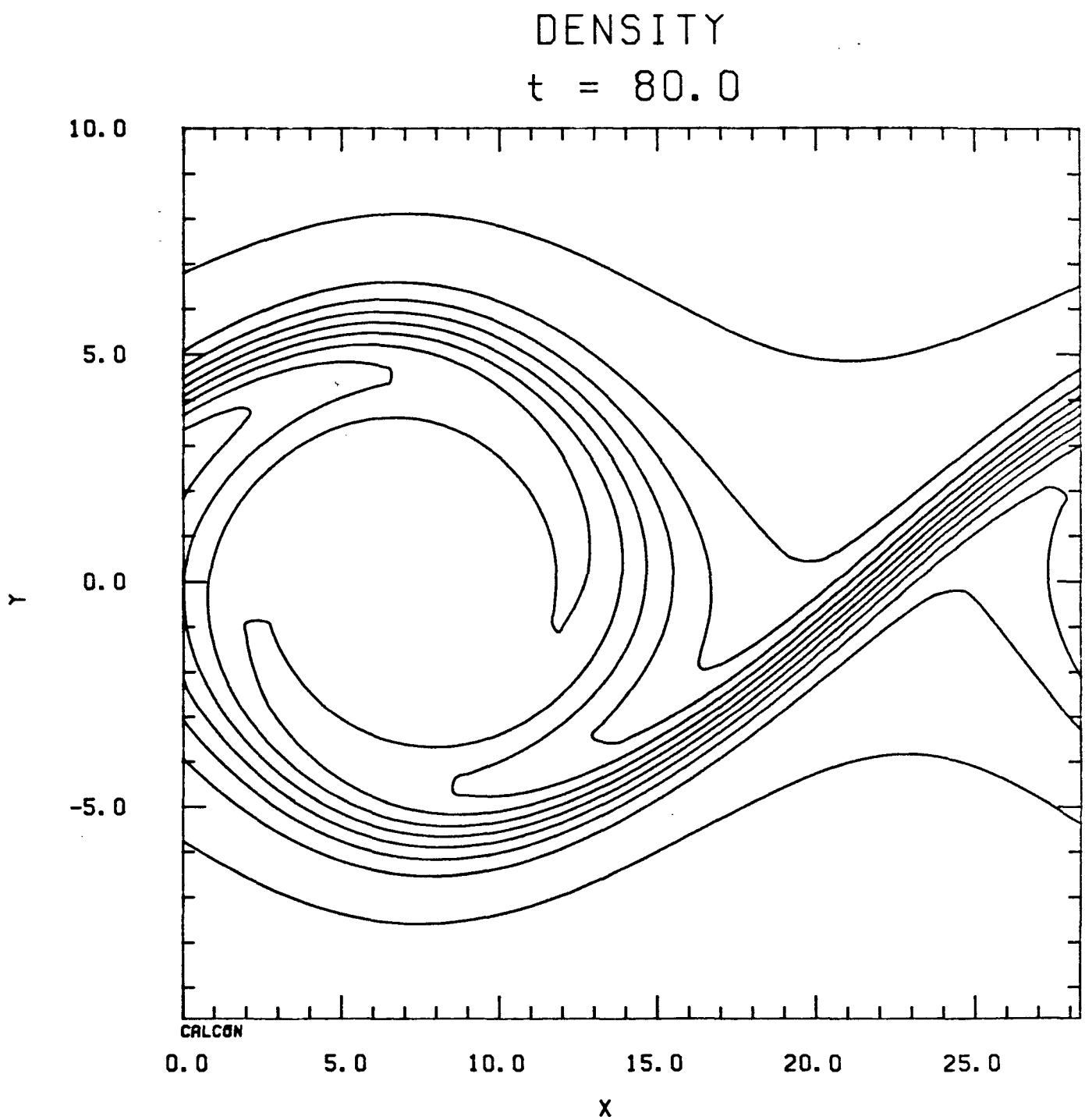

FIGURE 20F: ALPHA=.215,.43 JO=.07 RE=50 PR=.72
INITIAL RELATIVE PHASE=-PI
EPS=.0326 A1(0)=1.89A2(0)

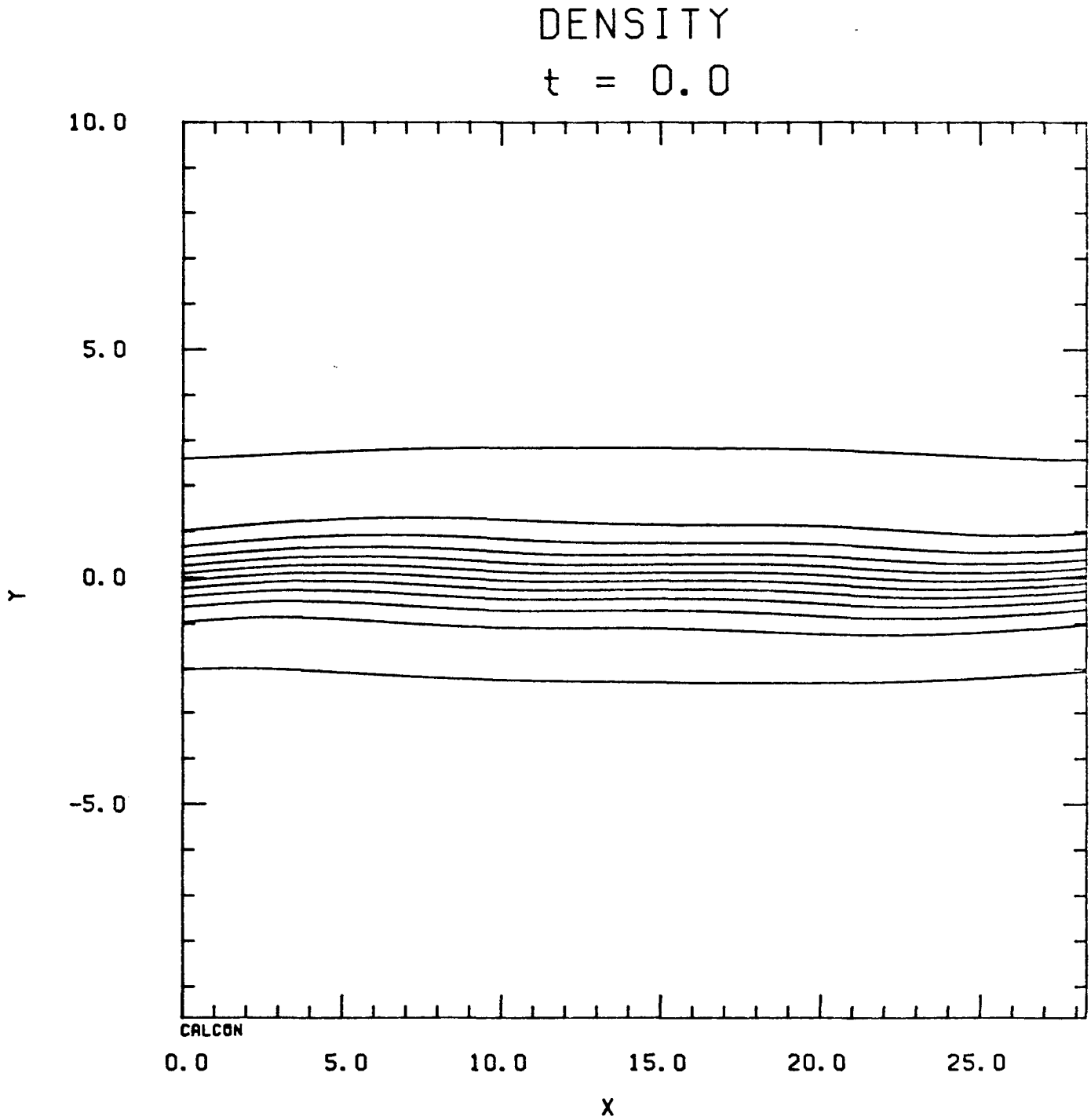

FIGURE 21A: ALPHA=.215,.43 JO=.07 RE=50 PR=.72
INITIAL RELATIVE PHASE=0.0
EPS=.0326 A1(0)=1.89A2(0)

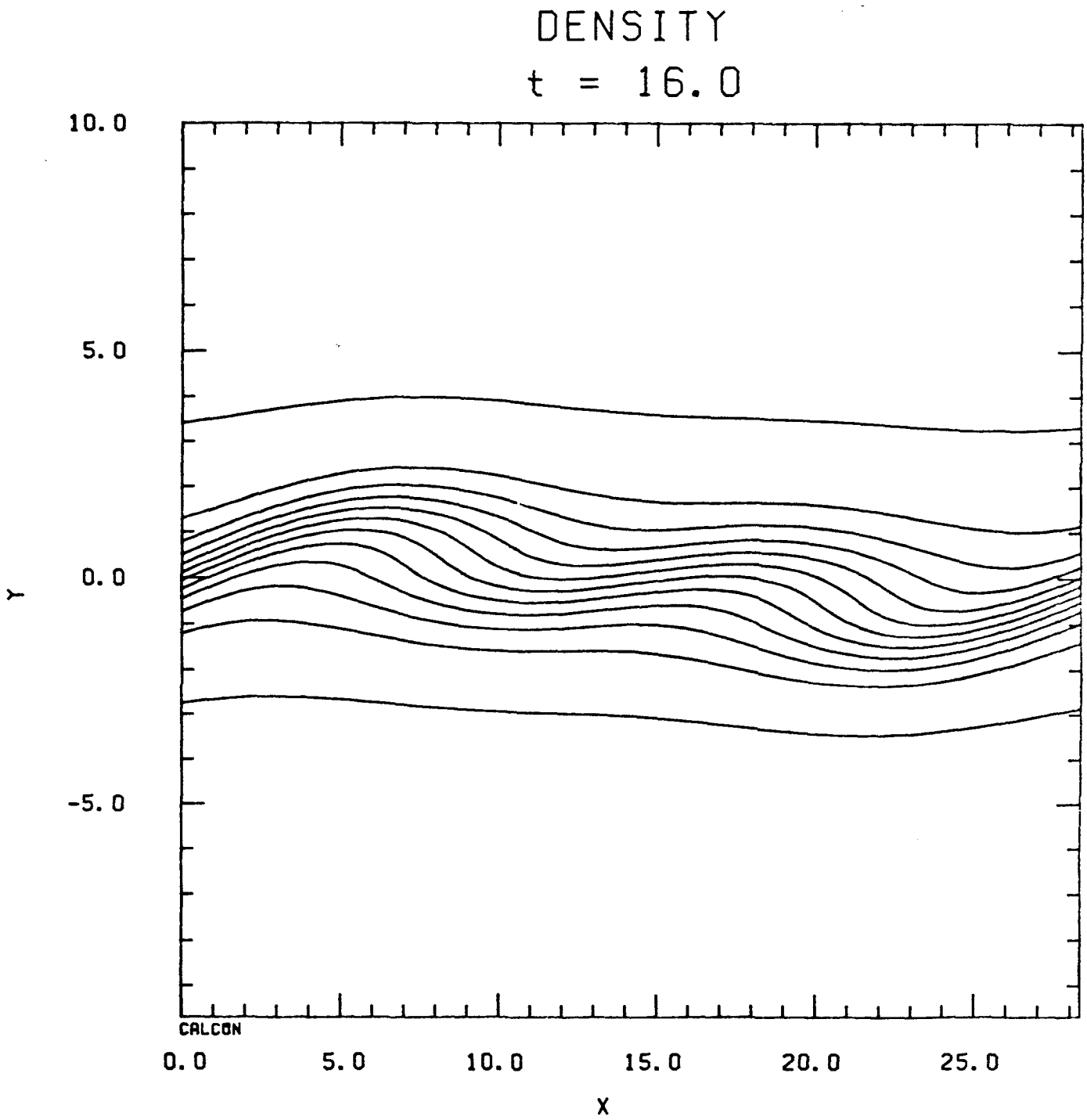

FIGURE 21B: ALPHA=.215,.43 JO=.07 RE=50 PR=.72
INITIAL RELATIVE PHASE=0.0
EPS=.0326 A1(0)=1.89A2(0)

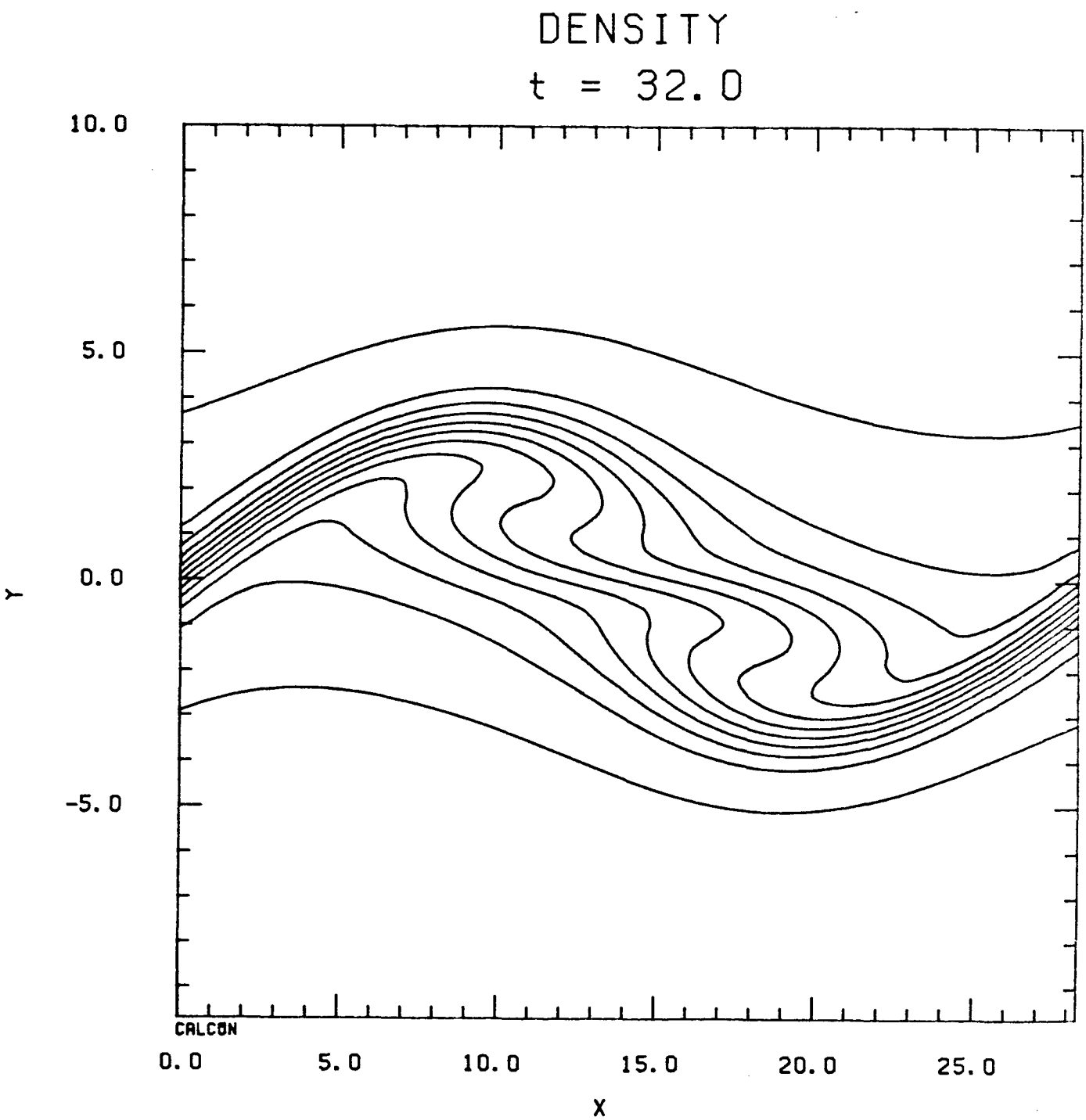

FIGURE 21C: ALPHA=.215,.43 JO=.07 RE=50 PR=.72
INITIAL RELATIVE PHASE=0.0
EPS=.0326 A1(0)=1.89A2(0)

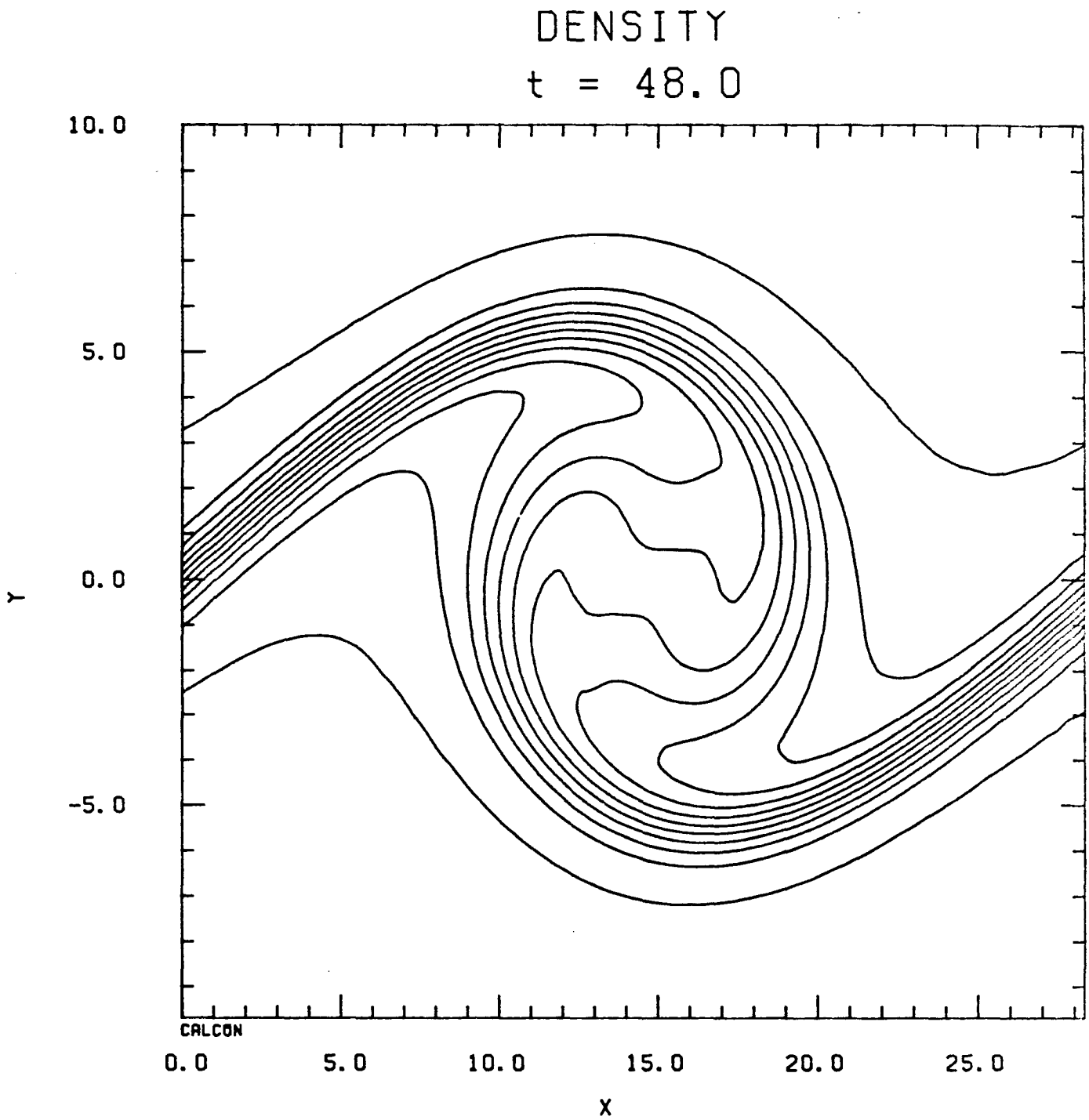

FIGURE 21D: ALPHA=.215,.43 JO=.07 RE=50 PR=.72
INITIAL RELATIVE PHASE=0.0
EPS=.0326 A1(0)=1.89A2(0)

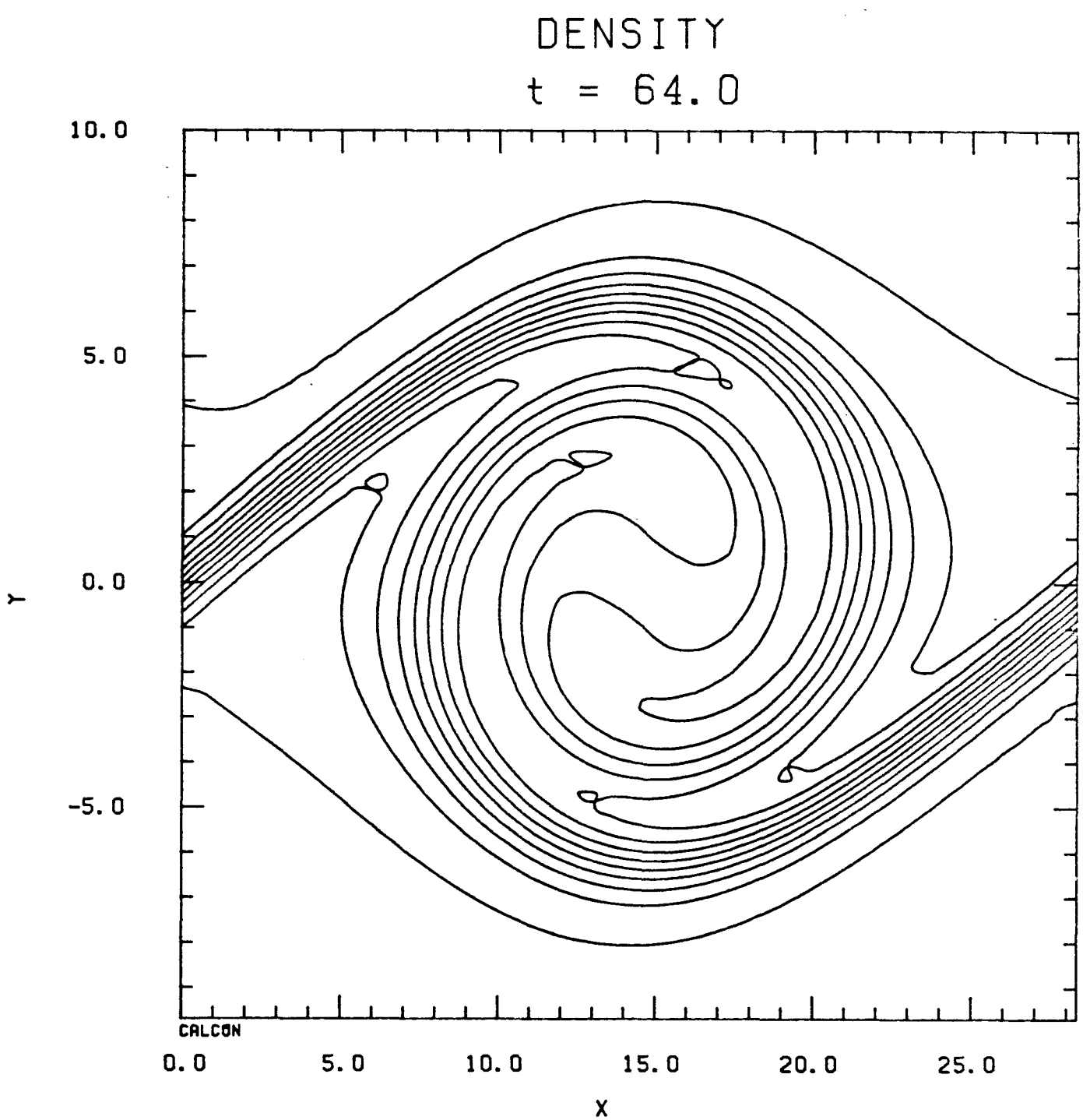

FIGURE 21E: ALPHA=.215,.43 J0=.07 RE=50 PR=.72
INITIAL RELATIVE PHASE=0.0
EPS=.0326 A1(0)=1.89A2(0)

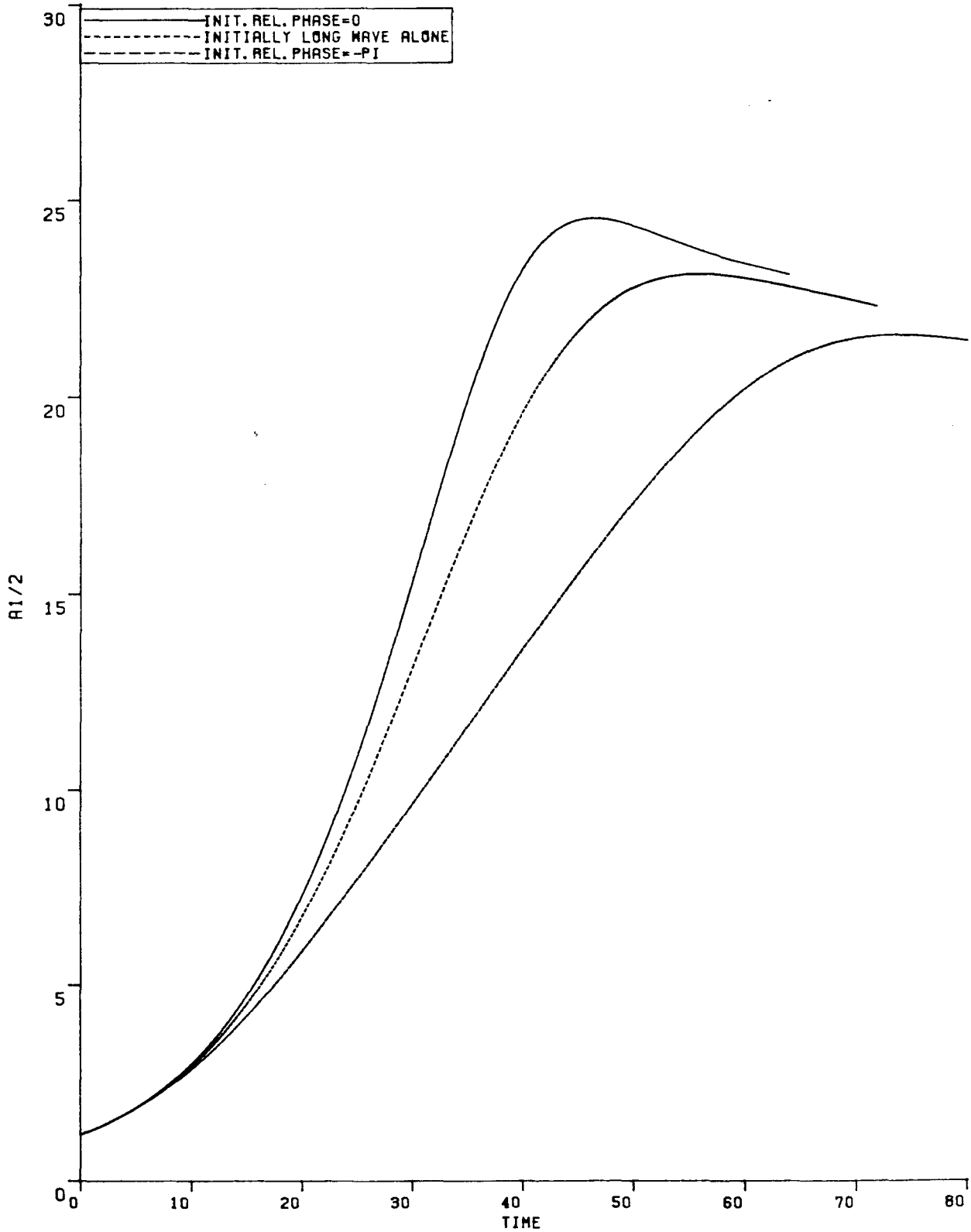

FIGURE 22: LONG WAVE OF LONG LINEARLY UNSTABLE AND FASTEST GROWING WAVES, A1(0)=1.89A2(0) RE=50 PR=.72 JO=.07 ALPHA=.215,.43 EPS=.0326

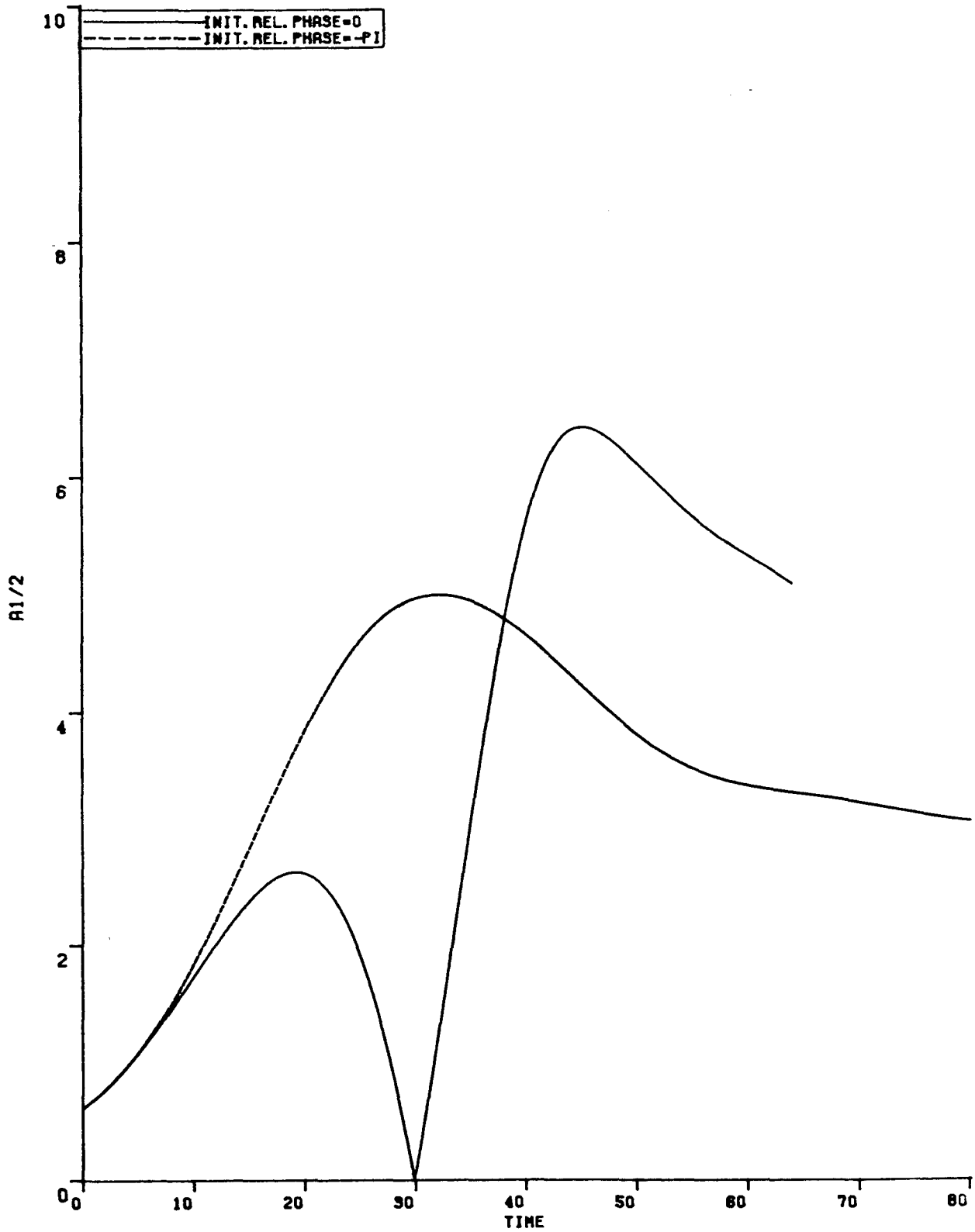

FIGURE 23: SHORT WAVE OF LONG LINEARLY UNSTABLE AND FASTEST GROWING WAVES, A1(0)=1.89A2(0) RE=50 PR=.72 JO=.07 ALPHA=.215,.43 EPS=.0326

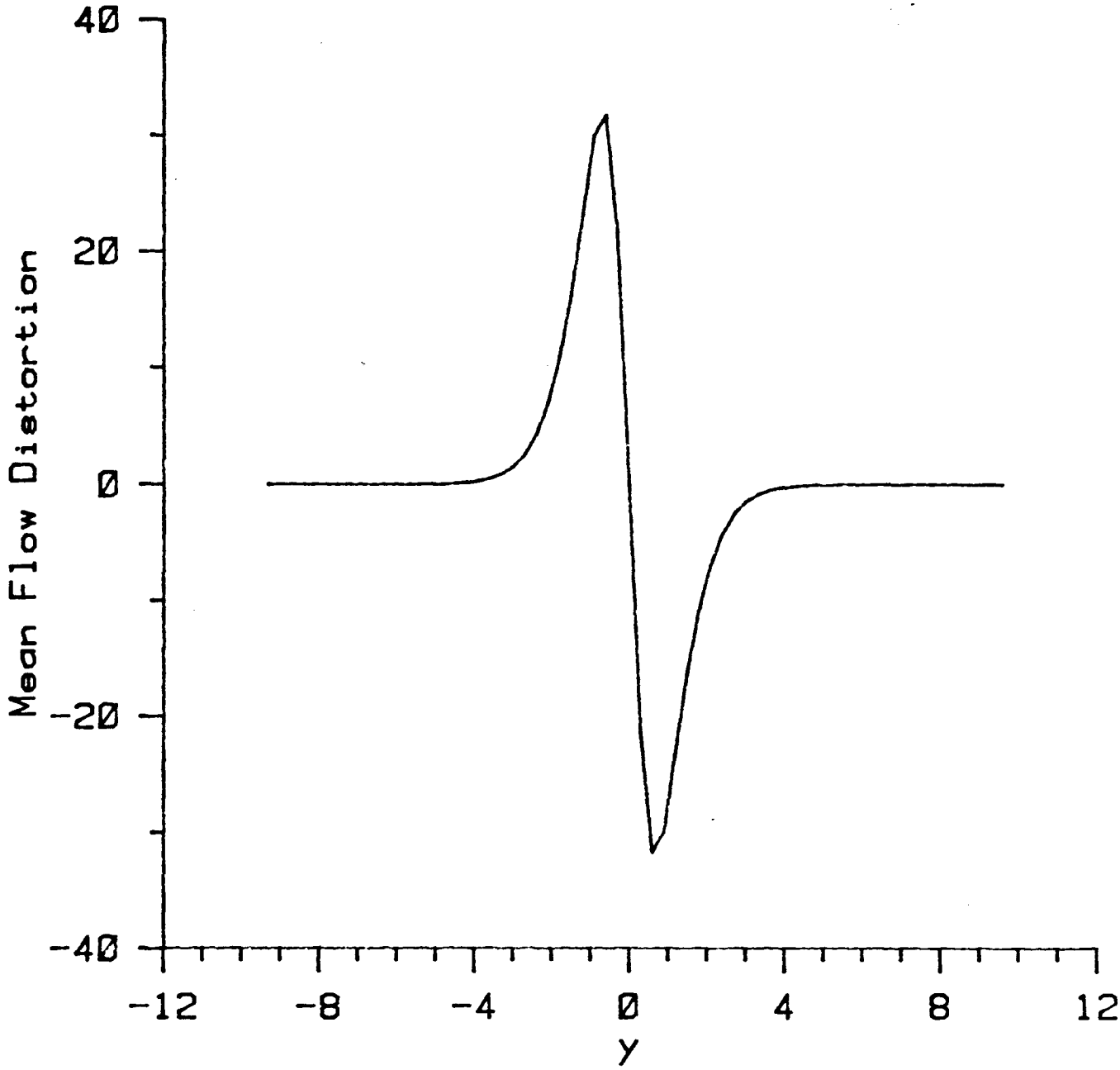

Figure 24: Mean flow distortion at t=56 for the case of two neutral waves with Re=200 Pr=0.72 eps=0.08 and a1(0)=1.5a2(0)